Gas Phase Infrared Spectroscopy of Cationic Metal Carbonyl Complexes

by

Allen M. Ricks

(Under the direction of Michael A. Duncan)

Abstract

Novel cationic metal and metal oxide ligand complexes are studied in the gas phase using infrared spectroscopy. Density functional theory calculations are preformed in support of the

Index words: Infrared Spectroscopy Mass Spectrometry

Gas Phase Infrared Spectroscopy of Cationic Metal Carbonyl Complexes

by

Allen M. Ricks

B.S., California State University Chico, 2006

A Thesis Submitted to the Graduate Faculty

of The University of Georgia in Partial Fulfillment

of the

Requirements for the Degree

Doctor of Philosophy

Athens, Georgia

2010

Gas Phase Infrared Spectroscopy of Cationic Metal Carbonyl Complexes

by

Allen M. Ricks

Approved:

Major Professor: Michael A. Duncan

Committee: Nigel Adams
Geoff Smith

Electronic Version Approved:

Maureen Grasso
Dean of the Graduate School
The University of Georgia
July 2010

Dedication

I would like to dediacte this thesis to the dream that someday I will have something to dedicate it to.

Acknowledgments

I would like to acknowledge Gary Douberly, Prosser Carnegie and Mike Duncan for their support and encouragement throughout my graduate career. I would also like to thank Mike Heaven of Emory University for letting us borrow his uranium rod.

Table of Contents

List of Figures

List of Tables

Chapter 1

Introduction

There is an abundance of knowledge on the structure and spectroscopy of stable closed shell molecules and this has allowed the development of analytical techniques for determining the presence of such species. Much of the chemistry involved in the formation of stable molecules involves ions and radicals, but these species are much harder to characterize due to their reactive nature. Organic chemsits have come up with ingenious ways to trap and study reactive radicals in the condensed phase, and they have been well studied in the gas phase using sophisticated spectroscopic techniques. Ions, the focus of this thesis, have been well studied using mass spectrometric techniques, however the low density of ions present in a mass spectrometer precludes the use of traditional spectroscopic techniques to obtain structural information. Structural information of ions in mass spectrometers can be inferred using fragmentation patterns but this is only applicable to well-behaved systems, typically organic ions and biomolecules.

It is well established that mass spectrometers are extremely sensitive instruments able to detect the presence of molecules in very small concentrations and that infrared spectrometers are capable of identifying structures and properties of molecules if present in large enough quantities. Our group strives to bring together the best of both techniques, obtaining detailed structural information by obtaining the infrared spectra of ions by utilizing the sensitivity and selectivity of a mass spectrometer. The bulk of the work presented will focus on carbonyl monoxide ligands (CO) bound to metal ions

Carbon monoxide is a common ligand in many inorganic transition metal complexes.[1,2,3] Carbonyl transition metal complexes are important in biological systems such as hemoglobin

where the carbon monoxide is known to compete with oxygen for the binding site of the iron core.[4] Metal carbonyl complexes are important in catalysis and are used in the production of single walled carbon nanotubes.[5] The carbonyl stretching frequency (ν_{CO}) has been used to diagnose binding sites in surface sciences because the carbonyl binds strongly to metallic surfaces and the ν_{CO} stretch occurs at a frequency where few other molecules absorb.[6] The shift of ν_{CO} relative to the gas phase value (2143 cm^{-1}) is indicative of the type of interactions occurring in the system being probed. By studying complexes of only one metal atom and one or more carbonyl molecules, we reduce the complexity of the system which can allow us to better understand the fundamental metal ligand interactions taking place.

Transition metal carbonyl complexes have been studied extensively using infrared spectroscopy in the condensed phase[7,8,9,10,11] and in the gas phase[12,13,10,14,8] most recently by photoelectron spectroscopy of the corresponding anions.[15,16,17,18,19] The frequency of the CO stretch (ν_{CO}) has been shown to change based on the type and extent of metal-ligand interactions in an inorganic complex. This shift correlates well with the electron donating ability of the metal, with electron rich metals causing a large ν_{CO} red shift and electron poor metals causing a smaller red shift, or in extreme cases a blue shift.[1,19] This effect is traditionally attributed to the extent of σ-bonding and π-back bonding in the metal carbonyl system. Sigma bonding is thought to reduce the electron density in the partially anti-bonding CO σ molecular orbital and thus increases the C-O bond strength leading to a ν_{CO} blue shift. Conversely π-back bonding from the metal to the purely antibonding π^* LUMO of CO results in a ν_{CO} red shift. This effect is evident in the isoelectronic series $Ni(CO)_4$, $Co(CO)_4^-$ and $Fe(CO)_4^{2-}$ in which ν_{CO} stretching frequencies are (respectively) 2094, 1946 and 1799 cm^{-1}.[7,9,9,19] The covalent π and σ interactions are historically thought to dominate the nature of the metal carbonyl bond, however recently it has been proposed that in cationic carbonyl systems electrostatic interactions play an important role in the ν_{CO} frequency.[20,21] This new avenue of thought is due to recent *ab initio* calculations that show the CO σ HOMO is slightly bonding,[20,21] not antibonding as was previously thought.[22,23] To confirm this exper-

imentally we need to investigate systems where the electrostatic interaction is the dominate bonding force, and to date there are few examples of this.

Ionic metal carbonyl complexes are interesting to study because by varying the charge on the core metal one can change the extent of the π interaction. The dissociation energies of several cationic metal carbonyl systems have been measured.[24,25,26,27,28] These studies have determined the metal-carbonyl binding energy is generall greater than 0.5 eV, indicating a strong bonding interaction. Infrared spectra of metal cluster-carbonyl ionic complexes have been obtained using free electron lasers[29,30,31,32] and several ionic systems with a single metal have been studied in the condensed phase[7,8,9,11] and in rare gas matrices.[33,34,35,36,37,38,39,40] However there is little gas phase spectroscopy of atomic cationic metal carbonyl systems. Recently we have developed methods which allow the infrared spectra of various metal carbonyl cations to be probed in the gas phase using infrared photodissociation spectroscopy (IRPDS).[41,42,43] This technique uses new infrared laser technology to probe ionic systems spectroscopically by fragmenting them on resonance and measuring this fragmentation using a mass spectrometer. We have recently applied IRPDS in the study of the $Pt(CO)_n^+$ and $Au(CO)_n^+$ systems,[44,45] but to date it has not been applied to any first row transition metal carbonyl complexes.

Chapter 2

Experimental

2.1 The Mass Spectrometer

A schematic of the UGA ion spectrometer is shown in Figure 2.1 and a brief description will be given. Ions are generated using a laser ablation/ionization source which consists of the third harmonic of a Nd:YAG laser (355 nm) loosely focused onto a rotating and translating metal rod.[42,43,46] Perpendicular to the laser vaporization, gas is pulsed through a Series 9 General Valve. Cooling in the supersonic gas pulse generates large neutral clusters of the expanding gas. Ions generated in the laser vaporization process embed themselves in these clusters and both collisional and evaporative cooling leads to efficient ion-molecule and ion-molecule-rare gas complex formation.

A collimated beam is formed from the gas expansion using a Beam Dynamics 5 mm skimmer and sent into a second differentially pumped chamber where cations are pulse extracted into a Wiley-McLaren Time-Of-Flight (TOF) mass spectrometer[47] equipped with a reflectron. A home built "mass gate" situated at the end of the first flight tube can be held at a high positive potential (+900V) which deflects all ions into the wall of the TOF. The mass gate can be pulsed to ground for a tunable period of time to allow a selected mass/charge ratio of ions into the reflectron region where they are intersected with the tunable output of an infrared Optical Parametric Oscillator/Optical Parametric Amplifier (OPO/OPA) laser system. On resonant absorption the ion can fragment provided it has a bond weaker than that of the infrared photon. If dissociation occurs it produces a lighter "daughter" ion which travels down the second tube of the time-of-flight and arrives earlier

than any unfragmented "parent" ion. By monitoring the appearance of the lighter daughter ion as a function of infrared laser frequency an infrared spectrum is generated.

2.2 The LaserVision OPO/OPA System

The infrared optical parametric oscillation/optical parametric amplification (OPO/OPA) system used in these experiments was developed and sold by Dean Guyer through his company LaserVision. The system is pumped using 500 mJ/pulse of 1064 nm light from a Spectra Physics Pro 230 Nd:YAG laser operating at 10 Hz. The pump beam is split into two beams, one of which is sent through a KDP doubling crystal to generate 532 nm photons. This is coupled into the OPO cavity where optical parametric conversion generates two different beams whose frequency sum to equal that of the 532 nm pump beam. Traditionally the higher frequency beam is called the "signal" and the lower frequency beam is the "idler".

A schematic of the OPO/OPA system is shown in Figure 2.2 and a brief description of its operation will follow. The 1064 nm pump beam (9398.5 cm^{-1}, blue line in Figure 2.2) is split into two beams by BS1, one beam is doubled to 532 nm light (18,797 cm^{-1}, green line) in a KDP crystal. The doubled beam is separated from residual 1064 light by DC1 and sent into the OPA crystal where optical parametric conversion splits the light into two beams, signal and idler. Conservation of energy dictates that the frequency of the signal and idler beams add to equal the frequency of the pump beam ($\nu_{signal} + \nu_{idler} = \nu_{532}$) and that the number of signal and idler photons be equal. By varying the angle of the OPO crystal the phase-matching conditions are changed allowing the frequencies generated to change. The signal beam (red line) is tunable from 710-880 nm (14084.5-11363 cm^{-1}), the idler beam (yellow) from 4748.5-7453.5 cm^{-1}. In the current configuration the signal beam is disposed of by DC4 into BD2 and the idler travels through the four crystals that comprise the OPA. In the OPA difference frequency mixing with 1064 nm light amplifies the idler beam and generates a second lower frequency beam (termed mid IR, purple) which is tunable from 4748-2000

cm^{-1}. The mid IR and idler beams are orthogonally polarized and can be separated using a polarizer.

The wavelength region of this system can be extended by preforming Difference Frequency Mixing of the idler and mid IR beams in a $AgGaSe_2$ crystal. This affords wavelength coverage in the ∼600-2200 cm^{-1} range, allowing access to the fingerprint region of the infrared spectrum. This tabletop system can cover the entire infrared region with fairly narrow linewidth (∼1 cm^{-1}).

2.3 Computational

Advances in computing power (see Moore's Law) coupled with the ever expanding capability of Density Functional Theory (DFT) and *ab initio* techniques allow us to calculate structural, energetic, and spectroscopic information for a variety of systems. These techniques have proven useful in previous studies in our lab and in certain cases to be discussed later are helpful in interpreting the present experimental data. Over the past four years I have built and maintained several computational computers and clusters, the workhorse of which is a single node 64-bit Dell Precision 690 workstation. Despite the advanced age of this system (4 years, an eternity for computers) it still has impressive hardware specs: two dual core Intel Xeon processors (each core running at 3.73 GHz), 16Gb of DDR2 RAM and a 750 Gb SATA hard drive. The system currently runs Ubuntu Server 8.04 (Hardy Heron) and utilizes the Simple Queueieng System (http://sqs.sourceforge.net/) to queue up Bash scripts which can be configured to run computational jobs. The system is currently configured to use the GAMESS, pcGAMESS, Firefly, NWChem, Orca and CFOUR computational packages which allows us to use the preferred code for a particular task. All the calculations presented in this thesis were done using the pcGAMESS program.[48]

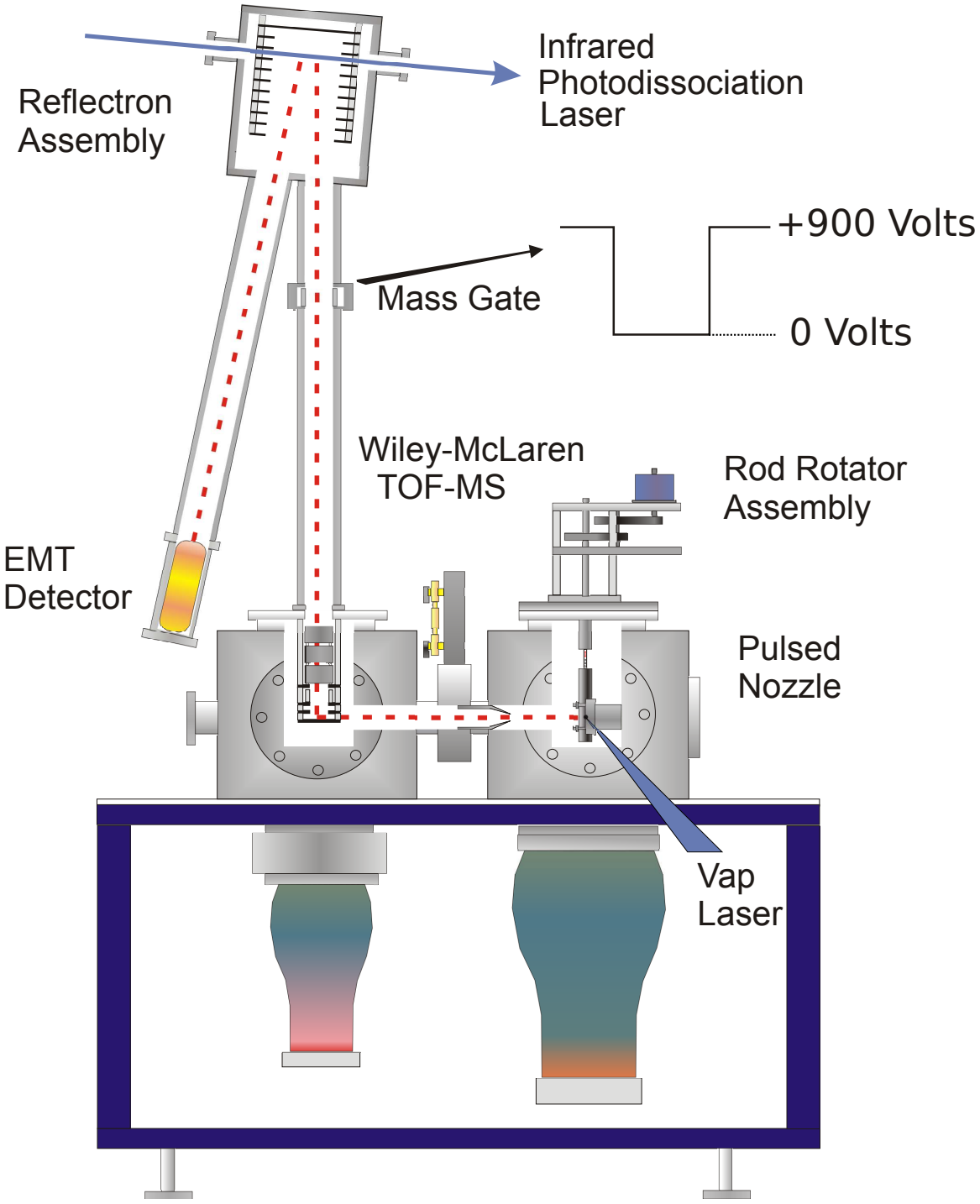

Figure 2.1: Diagram of the UGA ion spectrometer.

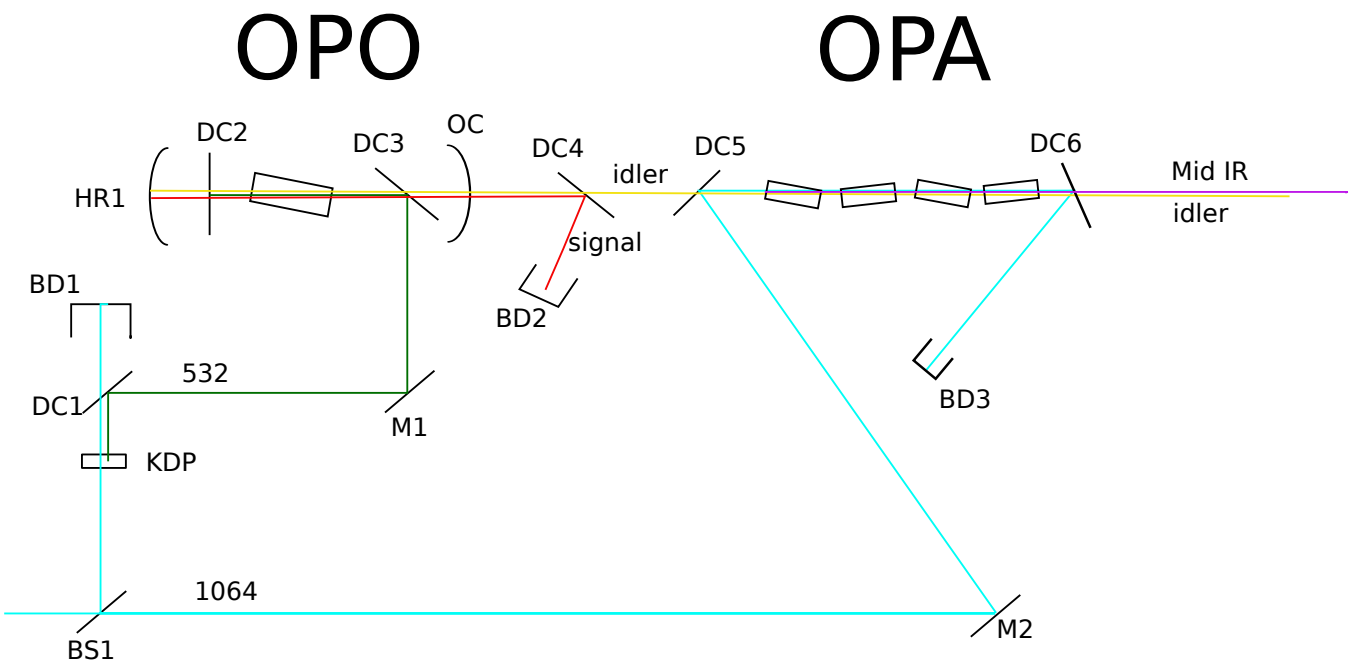

Figure 2.2: Diagram of the Optical Parametric Oscillation/Optical Parametric Amplification (OPO/OPA) system used for infrared experiments.

Chapter 3

Cobalt Carbonyl Complexes

3.1 Introduction

Ionic metal carbonyl complexes are interesting to study because by varying the charge on the core metal one can change the extent of the σ and π interactions. Infrared spectra of multi metal-carbonyl ionic complexes has been obtained using free electron lasers[29,30,31,32] and several ionic systems with a single metal have been studied in the condensed phase[7,8,9,11] and in rare gas matrices.[33,34,35,36,37,38,39,40] However there is little gas phase spectroscopy of cationic metal carbonyl systems. Recently we have developed methods which allow the infrared spectra of various metal carbonyl cations to be probed in the gas phase using infrared photodissociation spectroscopy (IRPDS).[41,42,43] This technique uses new infrared laser technology to probe ionic systems spectroscopically by fragmenting them on resonance and measuring this fragmentation using a mass spectrometer. We have recently applied IRPDS in the study of the $Pt(CO)_n^+$ and $Au(CO)_n^+$ systems,[44,45] but to date it has not been applied to any first row transition metal carbonyl complexes. For this work we have used IRPDS to study cationic cobalt carbonyl complexes $Co(CO)_n^+$ for n=5-9.

The $Co(CO)_5^+$ complex is predicted to be intrinsically stable because it satisfies the so-called 18-electron rule and is isoelectronic to $Fe(CO)_5$ which is stable at room temperature. Recently the salt $Co(CO)_5^+(CF_3)_3BF^-$ was synthesized and characterized using infrared and Raman spectroscopy and x-ray crystallography.[49] This study concluded that in the salt the $Co(CO)_5^+$ cation has D_{3h} symmetry with two infrared active bands at 2146 and 2120 cm^{-1}. In gas phase studies the $Co(CO)_n^+$ - CO (n=0-4) bond dissociation energies have been previously measured by Armentrout,[50] and the $Co(CO)_4^+$ - CO bond energy was determined

to be 0.68 eV (6291 cm^{-1}). Additional CO molecules beyond the first coordination sphere of Co^+ would be expected to be weakly bound such that they could be eliminated with a single mid-infrared photon (∼2100 cm^{-1}), making them suitable for study using the IRPDS method.[41,42,43] The infrared spectral signatures of $Co(CO)_n^+$ can give insights into the nature of the bonding between the carbonyls and the ionic metal core. In the larger clusters (n>6) it is not likely that all the carbonyls will be directly coordinated to the metal center and we can investigate the bonding between the surface carbonyls and the fully coordinated cationic core, an interaction that is likely to be mostly electrostatic.

3.2 Experimental

$Co(CO)_n^+$ ions are produced in a pulsed laser vaporization ionization source which consists of the third harmonic of a pulsed Nd:YAG laser (355 nm; Spectra-Physics Indi) focused onto a rotating and translating $\frac{1}{4}$ inch cobalt rod mounted on the front of a pulsed nozzle (Series 9 General Valve) in the cutaway configuration which has been described previously.[42] The pulsed nozzle is backed by pure CO gas (National Specialty Gas) or a mixture of CO and Ar gases at stagnation pressures of 3-10 atm. The gas expansion is skimmed into a second chamber where positive ions are pulse extracted into a home made Wiley-McLaren time-of-flight mass spectrometer equipped with a reflectron. Using pulsed deflection plates situated at the end of the first flight tube, only the ion of interest is allowed into the reflectron where it is intersected with the tunable output of an infrared Optical Parametric Oscillator (LaserVision) pumped by the fundamental of a Nd:YAG laser (1064 nm; Spectra Physics Pro 230) which affords continuous tuning in the region 2000-4000 cm^{-1} with a linewidth of 1 cm^{-1}. When the infrared laser is on resonance with a vibration of the cationic complex, absorption, and intramolecular vibrational energy redistribution leading to predissociation of the complex occurs on a time-scale much less than that of the ion residency time in the reflectron (∼1 μS). Infrared spectra are obtained by monitoring the appearance of the lighter fragment ion as a function of infrared laser wavelength.

In support of the experimental work, Density Functional Theory (DFT) calculations were carried out to determine the structures and relative energetics of several possible isomers of $Co(CO)_n^+$ (n=5-7) considering the singlet, triplet and quintet states of each cluster size. The calculations were performed using the B3LYP functional[51,52] as implemented in the pcGAMESS computational code.[48] The Watchers+f basis set[53] was used on the Co atom while the DZP basis set[54] was used for the carbon and oxygen atoms. The same functional and a similar basis set was used to calculate the structure and infrared frequencies for the neutral $Fe(CO)_5$ which is isoelectronic to $Co(CO)_5^+$.[55] The calculated structure and infrared frequencies of $Fe(CO)_5$ gave good agreement with the known gas-phase data.[13] Symmetry was used for the several input geometries but not rigorously enforced during the calculation and the symmetry of the complexes reported is that which the various structures converged to without any constraint.

3.3 Results and Discussion

A mass spectrum is shown in 3.1. The largest $Co(CO)_n^+$ peak corresponds to $Co(CO)_5^+$, suggesting that the first coordination sphere of the $Co(CO)_n^+$ cluster consists of five CO molecules bound to the central Co^+ cation. The so-called infrared breakdown mass spectra of the $Co(CO)_n^+$ (n=5-9) complexes are shown in Figure 3.2. These spectra are obtained by taking the difference between the mass spectrum of a mass selected complex with the infrared laser on and off. The number of carbonyls in the fragment ions is listed above the corresponding peak and the negative going peak is depletion of the parent complex due to photodissociation caused by the laser. For each cluster size the infrared breakdown spectrum was obtained with the laser set to the maximum absorbance of that particular cluster. The lower signal to noise obtained for the for the n=5 cluster size indicates a poor fragmentation yield. A low fragmentation yield usually arises because the binding energy of the complex is greater than the energy of the photon absorbed. This means the fragmentation process is multiphoton and therefore inefficient, or that we are only able to fragment the "hot" fraction

of the ions whose internal energy is sufficiently close to the dissociation threshold that a single photon causes photodissociation. The breakdown for clusters with n>5 terminates at n=5, which is again suggestive of the intrinsic stability of this cluster.

The infrared spectra of the $Co(CO)_n^+$ (n=5-9) complexes are shown in Figure 3.3. We were unable to directly photodissociate cluster sizes n=1-4 and were only able to dissociate a small fraction of the n=5 complex. The spectrum for n=5 is broad and featureless with a signal to noise ratio much lower than that of the larger cluster sizes. The spectrum of the D_{3h} $Co(CO)_5^+$ ion in the experimentally measured region should consist of two peaks, one attributed to a doubly degenerate e′ stretch and a a_2'' mode at higher frequency, similar to that seen for the $Fe(CO)_5$ complex[13] and what was observed in the $Co(CO)_5^+(CF_3)_3BF^-$ salt.[49] However, if the n=5 species is the fully coordinated complex, we would not expect to be able to measure its spectrum using IRPDS. The $Co(CO)_4^+$-CO binding energy has been experimentally determined to be 6291 cm^{-1},[50] meaning this cluster will not dissociate by absorbing a single photon, so the measured IRPD must come from some other process. It is possible that the photodissociation observed is a three photon process or that we are only able to dissociate complexes that already have ∼4000 cm^{-1} of internal energy. It is not uncommon in laser vaporization experiments to produce a small subset of clusters that survive the supersonic expansion without complete collisional quenching of their internal energy. In these hot complexes many excited vibrational modes would be populated and anharmonic coupling between modes would lead to broad absorbtions and shifted vibrational resonances. In larger complexes with ligands outside the core coordination, this effect would not be observed because any significant internal energy would lead to elimination of these weakly bound "surface" molecules before the complex reached the laser interaction region. If the fragmentation process observed were due to a cold complex absorbing multiple photons, the result would be similar because the first few photons absorbed could be thought of as "heating" the complex before the final photon caused fragmentation. Broadening of spectral features near in frequency and red shifting of vibrational bands has been

observed in experiments where multiple infrared photons are used to dissociate a covalently bound molecule.[56] This would explain the broad spectrum for the $Co(CO)_5^+$ complex shown in 3.3. Because of the broad spectrum, the n=5 species itself does not provide clear insight into the structure of this complex.

Beginning with the spectrum for the n=6 complex the dissociation efficiency is much greater, consistent with a one-photon process. This greater dissociation yield for n>5 also supports the five-ligand coordination suggested earlier. In the n=6 spectrum, two main peaks are present at 2135 and 2146 cm^{-1} while a third much weaker peak is located at 2163 cm^{-1}. As the cluster size increases from n=6-9 the relative intensities of the 2135 and 2146 cm^{-1} peaks stay fairly constant, while the peak at 2163 cm^{-1} grows in intensity. This indicates that the 2163 cm^{-1} peak is due to CO molecules bound to a core $Co(CO)_n^+$ ion, and the presence of this peak in the $Co(CO)_6^+$ spectrum means the core ion is $Co(CO)_5^+$.

To further elucidate these spectra, we have performed DFT calculations on $Co(CO)_n^+$ n=1-6. The calculated structure of $Co(CO)_5^+$ is in agreement with the structure measured in the $Co(CO)_5^+(CF_3)_3BF^-$ salt using x-ray crystallography.[49] For all complexes with n>5 the singlet was found to be lowest in energy. A minimum on the singlet potential energy surface was not found for the singlet $Co(CO)_6^+$ complex where all six CO molecules are coordinated to the central cobalt atom. All input structures where the six CO molecules were coordinated to the central cobalt atom converged to structures which consist of a central D_{3h} $Co(CO)_5^+$ complex with a second sphere CO molecule. This is consistent with the conclusion drawn from the mass spectrum that five CO molecules complete the first coordination sphere around the cobalt cation. The triplet $Co(CO)_6^+$ did converge to a hexacoordinate O_h structure. At the level of theory employed, the singlet D_{3h} $Co(CO)_5^+$ with a single surface CO is predicted to be lower in energy than the hexacoordinate triplet O_h $Co(CO)_6^+$, but only by 2.3 kcal/mol. For all cluster sizes considered the quintet was always significantly higher in energy is ruled out as the carrier of any of the bands seen in Figure 3.3.

The calculated and experimental infrared spectra for the $Co(CO)_n^+$ (n=5-7) cluster sizes is shown in Figure 3.6. The calculated frequencies are scaled by 0.97 and are given a 10 cm^{-1} FWHM Lorentzian lineshape for comparison to the experimental spectra. The scaling factor was chosen to make the calculated and experimental $Co(CO)_5^+$ 2146 cm^{-1} bands agree, and is in line with scaling factors recommended for the B3LYP functional.[57] Calculations for the singlet $Co(CO)_n^+$ faithfully reproduce the measured spectra and support the assignment of the infrared spectra of the larger clusters to a core $Co(CO)_5^+$ ion with surface carbonyls. The frequency of the surface carbonyl band is calculated to be further to the red than experimentally measured. The calculated infrared spectra for the triplet complexes are sufficiently different from the observed spectra that we can rule these out as possibilities.

The peak at 2135 cm^{-1} in the $Co(CO)_6^+$ spectrum (Figure 3.6) we assign to the doubly degenerate e' in plane asymmetric CO stretch of the $Co(CO)_5^+$ core which represents a 15 cm^{-1} blue-shift from the value in the salt.[49] The addition of a sixth CO to the $Co(CO)_5^+$ core formally splits the double degenerate e' modes into two nondegenerate a' and a'' modes, however this splitting is calculated to be $\sim$3 cm^{-1} and we are not able to resolve it. The peak at 2146 cm^{-1} in the $Co(CO)_6^+$ spectrum we assign to the a_2'' out of phase CO stretching of the axial carbonyls on the core $Co(CO)_5^+$ ion, which is exactly the same value obtained in the $Co(CO)_5^+(CF_3)_3BF^-$ salt.[49] The iron pentacarbonyl complex, $Fe(CO)_5$ is isoelectronic to $Co(CO)_5^+$ and also has D_{3h} symmetry[13]. The e' and a_2'' modes of $Fe(CO)_5$ are centered at and 2013 and 2034 cm^{-1}.[13] The red shift of the vibrational frequencies for the neutral relative to the isoelectronic cation is due to the difference in π back bonding from the metal d orbitals into the antibonding π^* LUMO of the CO ligands. The high signal to noise ratios achieved in this experiment are attributed to the extremely efficient fragmentation of the $Co(CO)_n^+$ (n>5) cluster ions. This is in line with the calculated intensities of the IR active modes probed, which are generally >500 km/mol, as well as the low binding energy of the surface CO. As the $Co(CO)_n^+$ cluster size increases the two main peaks located at 2135 and 2146 cm^{-1} in the $Co(CO)_6^+$ spectrum gradually split further apart and shift to the red until

they are located at 2129 and 2143 cm^{-1} in the $Co(CO)_9^+$ spectrum. The shift and splitting is attributed to surface carbonyls crowding and shifting the vibrational frequencies of the modes associated with the core $Co(CO)_5^+$ ion.

As we have discussed for other systems, in a complex where there are more ligands than binding sites on the metal the excess molecules bind to the surface of the fully coordinated complex and have spectra similar to the free molecule.[42,43] In the $Co(CO)_6^+$ spectrum (Figure 3.3) the surface CO ν_{CO} stretch is located at 2163 cm^{-1}, a ~20 cm^{-1} to the blue from the gas phase value of 2143 cm^{-1}. The large surface CO blue shift is in contrast to the much smaller (~5 cm^{-1}) shifts we have observed for surface CO_2 molecules in metal CO_2 systems.[43,58] In a fully coordinated complex the surface carbonyls cannot interact with the core metal d orbitals, so the interaction between the surface CO molecules and the core $Co(CO)_5^+$ ion can be described as a combination σ-donation and electrostatic interaction. The interaction of a CO molecule with a spherically symmetrical point charge has been explored computationally by Goldman and Krogh-Jespersen by placing a proton with only single diffuse s basis function near the carbon end of a CO molecule.[20] The only types of interaction possible in such a complex is σ donation and electrostatic interaction as the π^* orbital of CO does not have the correct symmetry to bond with the spherically symmetric point charge. The authors determined that the interactions in these types of systems is dominated by electrostatic interactions and that σ bonding was quite small. By varying the proton-carbon distance, Goldman and Krogh-Jespersen investigated the effects of the mostly electrostatic interaction as a function of point charge-carbonyl distance. Interpolating from the authors published results to the $Co(CO)_5^+$-CO distance of 4.1 Å calculated in this work the surface ν_{CO} is predicted to be blue shifted 17 cm^{-1} from the gas phase value, which is close to the experimentally determined blue shift of 20 cm^{-1} . Although the $Co(CO)_5^+$ cation is not a point charge, this model appears to work well to a first approximation. To our knowledge this is the first published gas phase data on the interaction of a surface CO molecule with a fully coordinated metal carbonyl core cation.

As discussed previously we were unable to directly photodissociate the small $Co(CO)_n^+$ (n<5) complexes presumably because they are too tightly bound. By modifying the laser vaporization source to move the metal rod out of the expansion by ∼1 in we were able to generate cobalt carbonyl-argon complexes. In these systems the argon atom is sufficently weakly bound such that it can be eliminated with a single infrared photon. The infrared spectra of the $Co(CO)_n^+$ ions obtained in this manner are shown in Figure 3.4. The spectrum of the n=5 cation obtained via elimination of a single CO from $Co(CO)_6^+$ and via elimination of Ar from $Co(CO)_5^+Ar$ are the top two traces in Figure 3.4. These spectra are similar with the exception of the weak peak at 2163 cm^{-1} in the $Co(CO)_6^+$ spectrum which is consistent with our assignment of this band to a weakly bound "surface" carbonyl. For n=4 the spectrum consists of two peaks blue shifted from those observed for the n=5 spectrum with different relative intensities. This is indicative of a structural change between the n=5 and 4 ions, possibly due to a change in spin state on the central metal atom. For n=1-3 there is a single infrared band observed and the comparisions of these bands and DFT calculations will be shown in the next section.

The calculated vibrational frequencies and intensities of the small cobalt carbonyl cations were given a 10 cm^{-1} FWHM lineshape for comparison to the experimental spectra and are shown in Figure 3.6. For n=6 the measured spectrum matches well with that calculated for the five coordinate singlet isomer with a surface CO and not the six coordinate triplet species, lending further credence to our previous conclusions. The n=4 spectrum matches well with that calculated for the triplet species and is assigned as such. This indicates that there is a "spin flip" between the n=4 and 5 complexes with the triplet isomer being observed for the n=4 complex and the singlet isomer for n=5 and larger.

Infrared spectra of smaller cobalt carbonyl clusters and their calculated IR spectra are shown in Figure 3.5. For the n=3 complex the experimental spectrum consists of a single broad peak centered at 2158 cm^{-1}, the calculated triplet spectrum displays a single peak while the singlet has two peaks. Because a single peak is observed this band is assigned to

the singlet isomer. For the n=2 ion the singlet state is sufficently high in energy that it is not considered here and the spectrum is asssigned to the triplet isomer. Similarly the singlet state for the n=1 ion is calculated to be sufficently higher in energy than the triplet state so the observed spectrum is assigned to the triplet state.

In conclusion, we have presented the first gas phase infrared spectra of any kind for the 18-electron complex $Co(CO)_5^+$ as well as identified it as the core of the $Co(CO)_6^+$ ion and in larger clusters. In addition we have the first spectral evidence for the presence of a CO molecule bound to a fully coordinated carbonyl cationic complex in the gas phase, and that the ν_{CO} of the surface CO is blue shifted in agreement with theoretical predictions.[20]

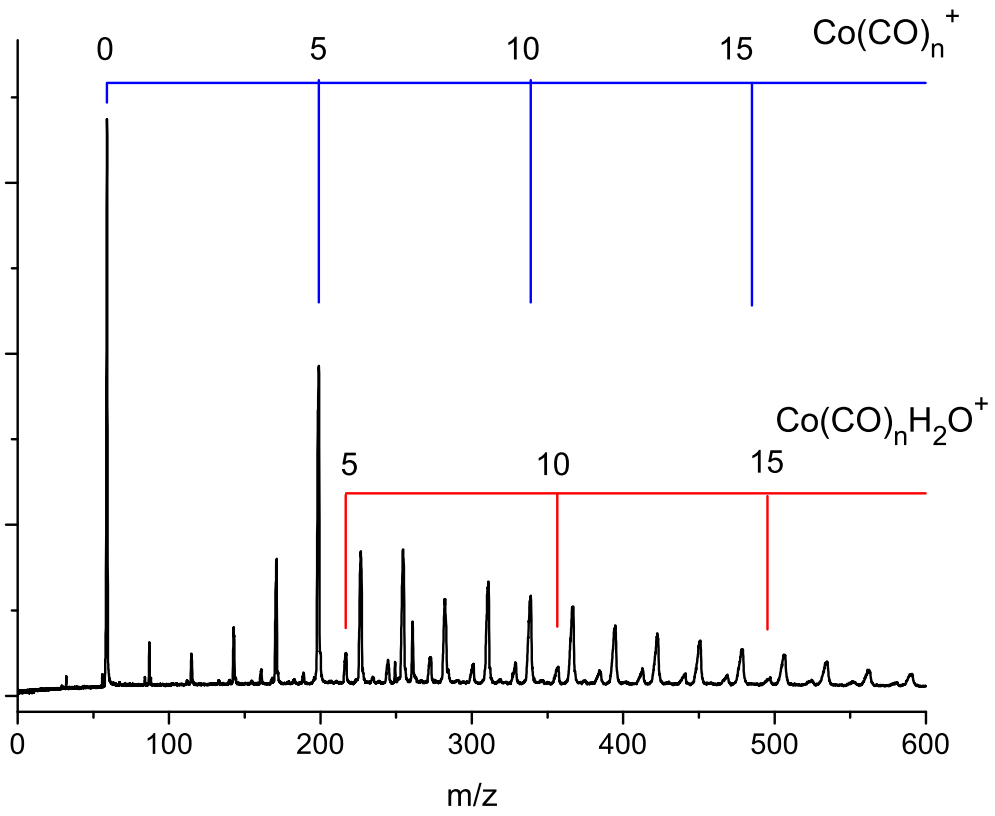

Figure 3.1: Mass spectrum of cobalt carbonyl cations $Co(CO)_n^+$ n=1-20. The minor distribution of peaks are complexes with a single water molecule, water is added to the gas expansion to facilitate ion formation.

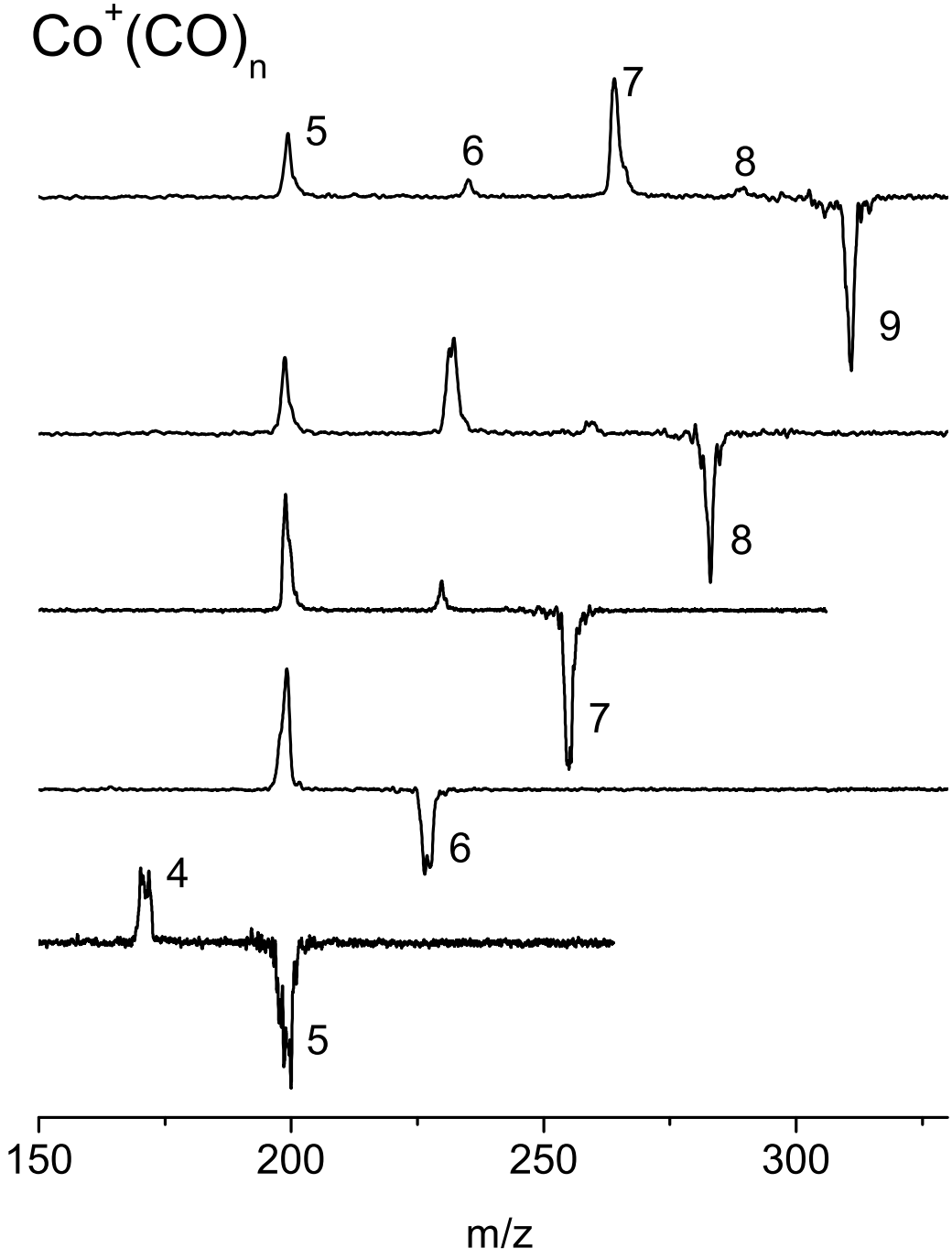

Figure 3.2: Photodissociation breakdown spectra of the larger cobalt carbonyl complexes ($Co(CO)_n^+$ n>4). For the clusters begining with n=6 the breakdown terminates with n=5, indicative of the stability of this complex. The n=5 complex was found to have weak fragmentation consistent with a strongly bound complex.

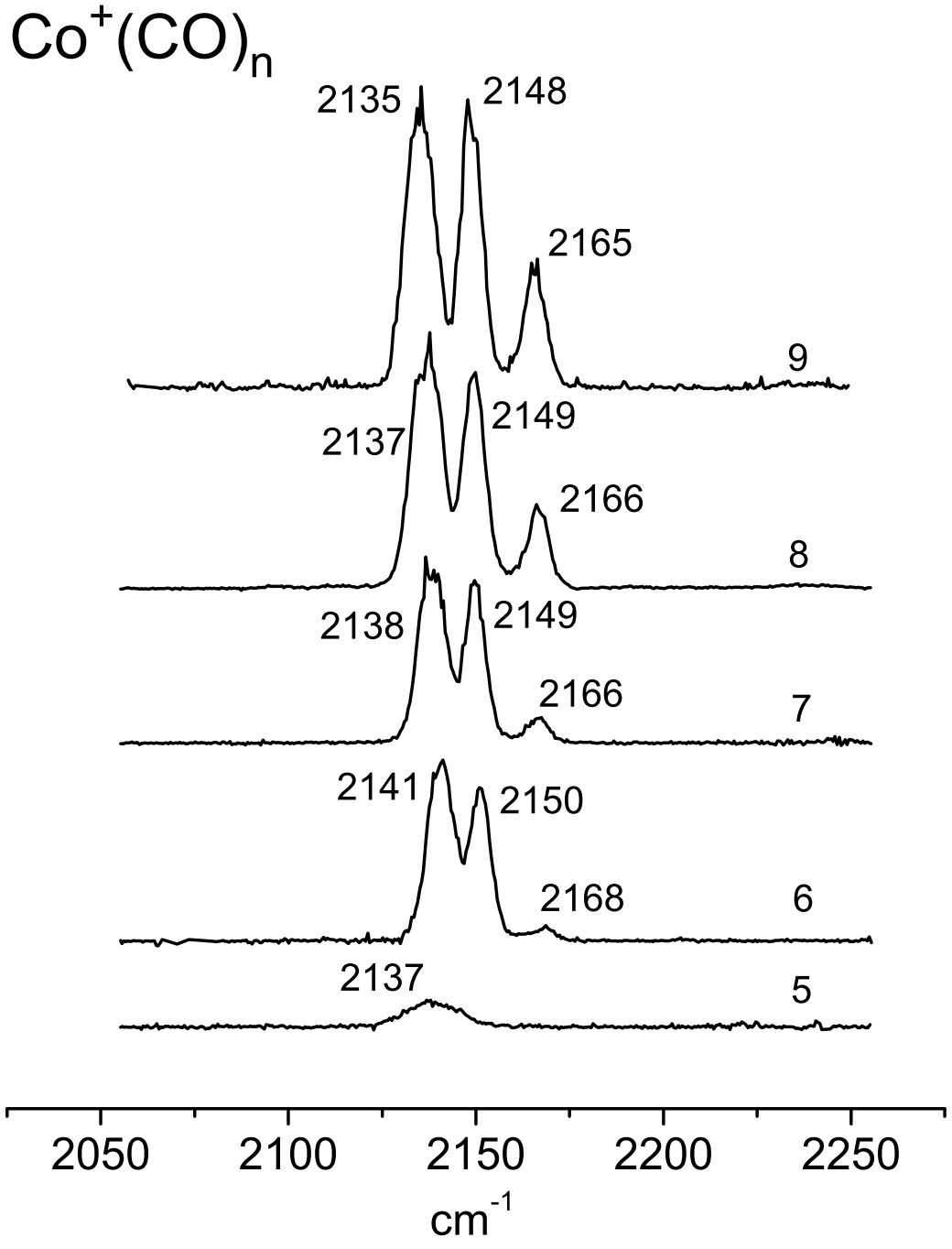

Figure 3.3: Infrared spectra of larger cobalt carbonyl cations. All spectra were obtained by monitoring loss of CO from the parent complex.

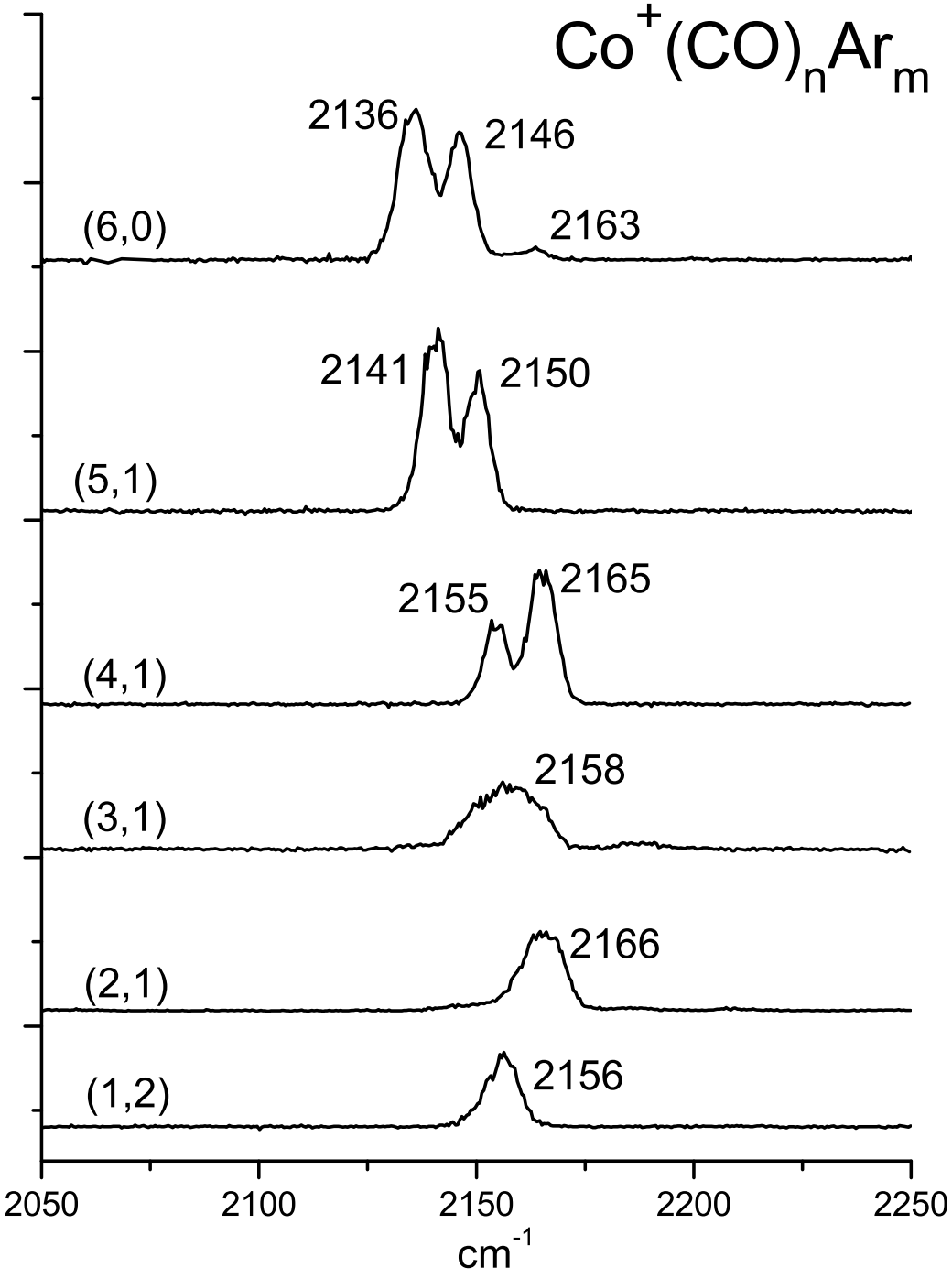

Figure 3.4: Infrared spectra of small cobalt carbonyl cations. The spectrum at the top was obtained via elimination of CO from the $Co(CO)_6^+$ while the others were obtained using argon tagging.

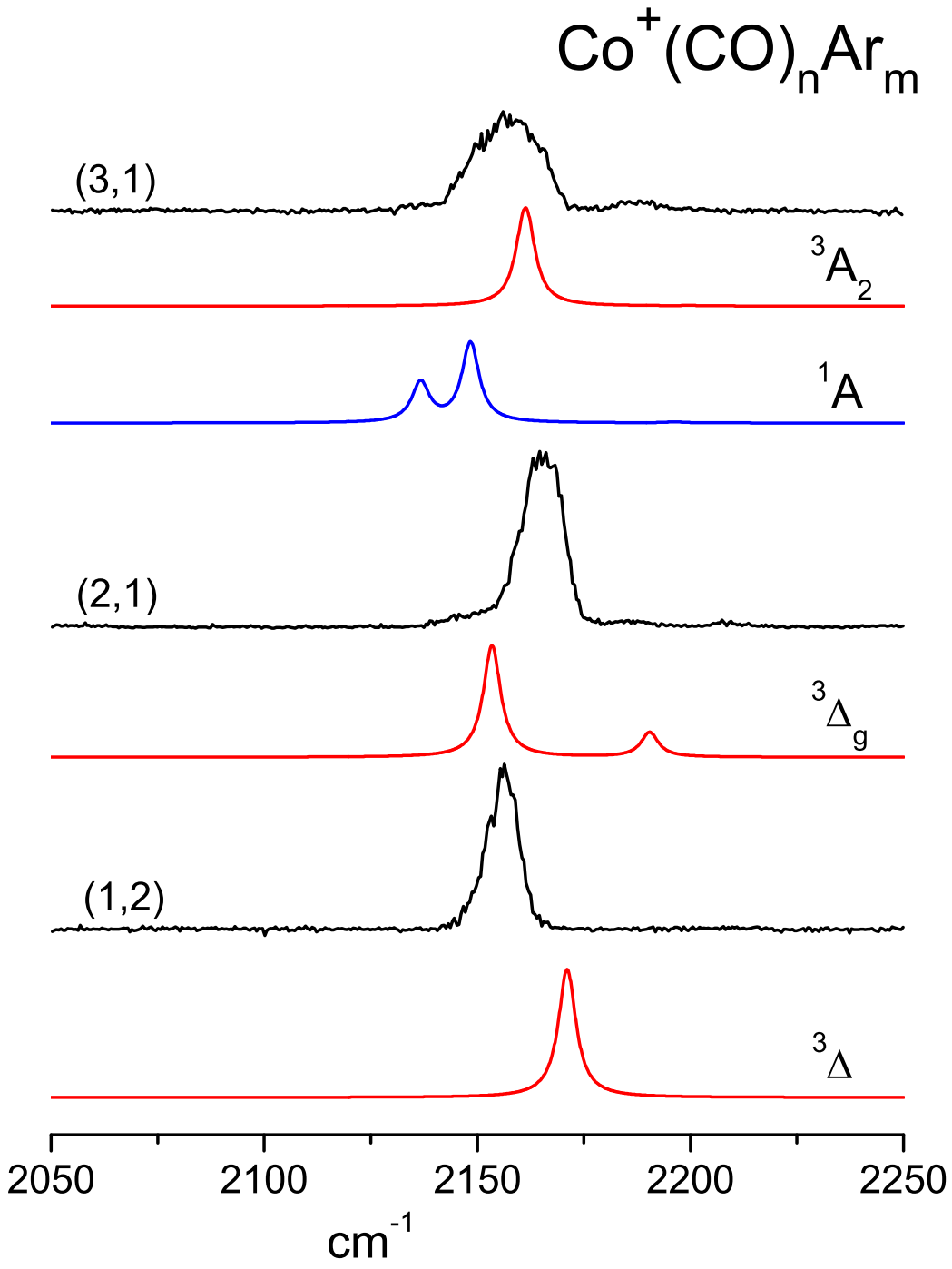

Figure 3.5: infrared spectra of small cobalt carbonyl cations. the spectrum at the top was obtained via elimination of Co from the $Co(CO)_6^+$ while the others were obtained using argon tagging.

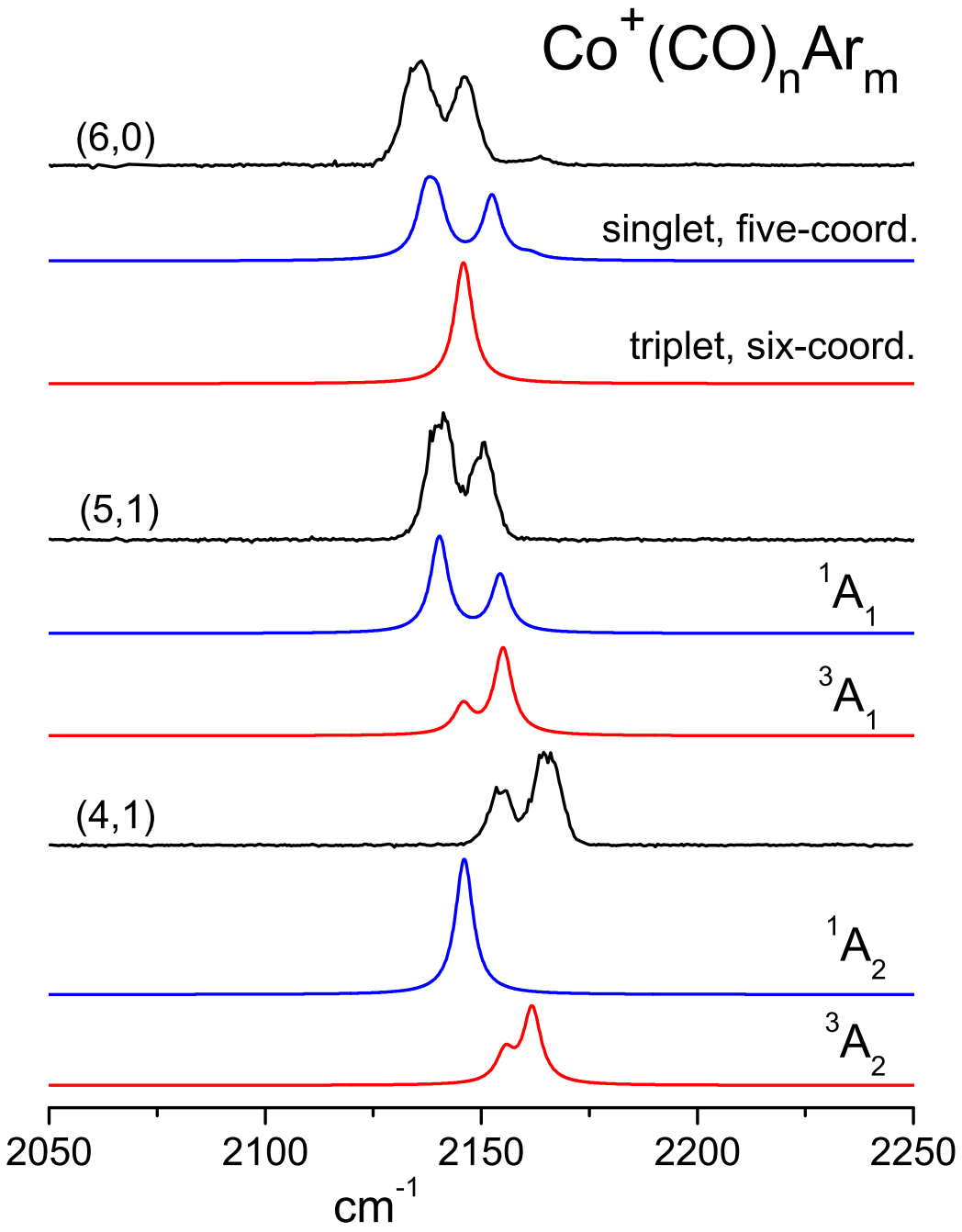

Figure 3.6: Infrared spectra of larger cobalt carbonyl cations. the spectrum at the top was obtained via elimination of Co from the $Co(CO)_6^+$ while the others were obtained using argon tagging.

Chapter 4

Vanadium Carbonyl Complexes

Vanadium is a first row transition metal atom which has five valence electrons, therefore its cation has four. The electronic structure of the ground state is known to be a quintet while in complexes it is generally a quintet or triplet.[59,60,61] The binding energies of carbonyl ligands to vanadium carbonyl ionic complexes have been studied previously by the group of Peter Armentrout at the University of Utah.[25] These authors found that the $V(CO)_n^+$-CO binding energies decreased from n=1-3 then rose again for n=4-6, which the authors attributed to changes in the electronic structure of the central metal ion beginning at n=4. Binding of CO to $V(CO)_6^+$ was found to be much higher than would be expected if the seventh CO were loosely associated with a fully coordinated metal carbonyl complex. This indicates that the seventh ligand is directly coordinated to the central metal ion. Because the vanadium cation has four valence electrons, the seven coordinate carbonyl complex would form an 18-electron complex and would thus is expected to be stable in spite of the steric crowding which results with seven ligands. A more recent Density Functional Theory and *ab initio* study of the $V(CO)_7^+$ ion came to the conclusion that it is a singlet seven coordinate species with C_{3v} symmetry.[62] To date there have been no spectroscopic investigations of cationic vanadium carbonyl complexes of any size. Presented here is a through experimental study of cationic vanadium carbonyl cations beginning with one carbonyl and up to and beyond the first coordination sphere, done in conjunction with Density Functional Theory (DFT) calculations. The DFT work was done using the B3LYP functional as implemented in the pcGAMESS computational package. The def2-qzvp basis set was used for vanadium, the DZP basis for carbon and oxygen and the 6-311G(d) basis set for argon and neon.

The infrared spectrum of the VCO^+ ion has been obtained using argon tagging as well as neon tagging and is shown in Figure 4.1. Neon has a lower polarizability and presumably a lower binding energy to VCO^+ than argon. This is confirmed by the experimental observation that a single 2100 cm^{-1} photon was not enough to fragment a single argon from VCO^+. When two argon atoms are attached to VCO^+ an infrared spectrum was obtained by monitoring the loss of a single argon. This spectrum consists of a single peak at 2130 cm^{-1}, while the infrared spectrum obtained by tagging with a single neon atom yields a single peak at 2150 cm^{-1}. For both the neon and argon tagged complexes, the quintet isomer is predicted to be lowest in energy by about 22 kcal/mol (see Table 4.2) and have a single carbonyl stretch at about 2200 cm^{-1}. Based on the calculated relative energetics this band is assigned to the quintet isomer. The neon tagged spectrum displays a weak feature at 2145 cm^{-1} which we can only assign to the presence of a higher energy metastable spin state, probably the triplet.

The infrared spectrum of the $V(CO)_2^+$ ion was obtained using argon and neon tagging. The spectrum is shown in Figure 4.2 and consists of two peaks with similar positions in both spectra. DFT calculations predict the $V(CO)_2^+$ ion to be linear. The rare gas tags bind on the metal ion to give a C_{2v} structure. Binding of the rare gas causes a slight distortion of the C-V-C bind angle away from linearity, so there is the possibility that both the in-phase (A_1) and out-of-phase (B_1) CO stretches are IR active thus giving rise to two peaks. The deviation from linearity should be less as the distortion introduced by the rare gas tag decreases, therefore as we go from argon tagging to neon tagging the complex should become more linear and the IR intensity of the in-phase mode should decrease. However the relative intensity of the two peaks is the same in the neon and argon spectra which indicates that either tag is not inducing much of a distortion. Another possibility for the observation of two peaks is a combination band. The 23 cm^{-1} splitting between the two peaks it too small to be a combination with a fundamental of the core $V(CO)_2^+$ ion (lowest calculated frequency 262 cm^{-1}). It could also be due to a combination with a mode involving the rare gas tag, however as we go from argon to neon the splitting should also change, which is not observed.

There is also the possibility that we have trapped electronic isomers differing in the spin state on the central vanadium cation. The high energy metastable spin states would be long lived and could conceivably be observed in this experiment. Previous work on bare vanadium cations generated using laser vaporization and studied using ion mobility have identified ions trapped in excited electronic states assigned to the triplet and quintet.[63] Therefore we assign the two peaks in the $V(CO)_2^+$Ne and $V(CO)_2^+$Ar spectra to ions with quintet and triplet multiplicity. The calculated vibrational frequencies of the spin isomers (Table 4.2) show that the quintet state has a higher CO stretching frequency than the triplet state, therefore we assign the high frequency peak in both spectra to a quintet isomer and the lower frequency peak to the triplet isomer. Calculations show that when the neon tag is switched to argon the intensity of the CO stretch is only slightly perturbed, and the relative intensities of the two peaks in the neon and argon spectra are very similar indicating that the same amount of the two isomers is produced using neon and argon tagging.

The spectrum of $V(CO)_3^+$ was obtained using argon and neon tagging (shown in Figure 4.3) and consists of two peaks similar to the previous spectrum of $V(CO)_2^+$. In contrast to the $V(CO)_2^+$ system, the calculated vibrational spectrum of the lowest energy isomer (see Table 4.4) has two infrared peaks with intensity ratios in agreement with the experimental spectrum. Thus the simplest assignment of this spectrum is to the quintet isomer. It is interesting that no other isomers are observed for this system when two isomers were apparently found for the $V(CO)_2^+$ system.

The infrared spectrum of the $V(CO)_4^+$ ion obtained using argon tagging is shown in Figure 4.4 and consists of a single intense peak at 2076 cm^{-1}, with a minor feature at 2112 cm^{-1}. Previously the Armentrout group observed a marked change in the carbonyl binding energies at n=4 which they interpreted as a change in the electronic state of the central ion[25], however in our experiment we often observe isomers that are not the lowest energy structures. The quintet $V(CO)_4^+$ ion is calculated to have a nearly planar structure which gives rise to a single infrared active CO stretching mode. The triplet isomer is calculated to be 1.6 kcal/mol

higher in energy and has a C_{2v} structure giving rise to multiple vibrational bands, while the singlet isomer has a tetrahedral structure giving rise to a single infrared active band. The experimental spectrum are consistent with either the quintet or singlet isomer. The quintet isomer is calculated to be 17.5 kcal/mol lower in energy than the singlet but the observed band is $\sim$50 cm^{-1} to the red of the bands observed in the $V(CO)_3^+$ spectrum which we assigned to the quintet state. Calculations have shown that the lower the spin state on the central metal ion the larger the red shift. It is tempting to assign this band to the triplet state based on the large red shift however the number of bands predicted does not match with the experimental observation, therefore we believe more theoretical work is necessary to elucidate the structure of this ion.

The infrared spectrum of the $V(CO)_5^+$ ion obtained using argon tagging is shown at the top of Figure 4.5 and consists of a single intense peak at 2075 cm^{-1}. This spectrum matches well with that predicted for the triplet isomer, which is also calculated to be the lowest energy isomer. This makes assignment fairly straight forward. The observed vibrational band of this ion is near that observed for the $V(CO)_4^+$ ion which lends support to the assignment of that spectrum to the triplet isomer.

The infrared spectrum of the $V(CO)_6^+$ ion obtained using argon tagging has a single peak at 2097 cm^{-1} and is shown at the top of Figure 4.6. Calculations show that the triplet $V(CO)_6^+$ ion is the lowest energy isomer and has a D_{3d} structure, distorted from O_h symmetry due to Jahn-Teller effects. In this ion the distortion is small enough that the splitting of the vibrational bands cannot be resolved in this experiment. The observed spectrum is assigned to this triplet state.

The group of Peter Armentrout at Utah measured the $V(CO)_6^+$-CO binding energy to be 4436 cm^{-1}, much higher than would be expected if the seventh CO were bound to a fully coordinated $V(CO)_6^+$ ion through electrostatic interactions. Therefore the authors concluded the ion was the seven coordinate 18-electron complex as discussed in the introduction to this chapter. In our experiment the $V(CO)_7^+$ ion was found to fragment efficiently by loss of a

single CO molecule and the spectrum obtained by monitoring CO loss is shown in Figure 4.7. This spectrum is similar to that observed for $V(CO)_6^+Ar$ ion with the primary difference being the width of the peak at 2097 cm^{-1} and the appearance of a weak feature at 2156 cm^{-1}. The 2156 band is similar in position to the bands observed at 2163 in the $Co(CO)_n^+$ (n > 5) systems which were assigned to carbonyl ligands loosely associated with the fully coordinated core ion. Therefore this spectrum is assigned to a "6+1" structure, that is a six coordinate core ion with one surface carbonyl ligand. As discussed for the $V(CO)_6^+$ system the core ion is Jahn-Teller distorted from octahedral symmetry however the splitting of the vibrational bands is not large enough to be observed in the current experimental configuration.

Below the experimental spectrum are calculated spectra of the three spin states. The lowest energy isomer is the 18-electron singlet seven coordinate ion which has a calculated spectrum markedly different from that observed. Therefore we believe that the spectrum is attributable exclusively to the triplet 6+1 isomer. Previous work has shown that the binding energy of the seventh carbonyl ligand is > 4000 cm^{-1} which is more than the energy of the infrared photon. However it is possible that we are forming a mixture of isomers and can only fragment one. In order to investigate this we generated the argon tagged $V(CO)_7^+$ ion and found it to only fragment via elimination of CO and Ar to generate a spectrum similar to that observed in Figure 4.7. We must conclude that the ion generation techniques utilized by ourselves and the Armentrout group are sufficiently different so that they are efficient at producing one ion over another. This is perhaps not too surprising as the Armentrout group must model their experimental data to extract binding energies and this model is dependent on accurate knowledge of the ions internal temperature. Therefore they let the ions equilibrate to room temperature so the internal energy of the ions is well defined. At room temperature, weakly bound ions would not survive. We rely on generation of weakly bound complexes so they can be fragmented with a single infrared photon so the system is not always able to equilibrate to the lowest energy configuration. This may explain why the strongly bound $V(CO)_7^+$ ion observed in the Armentrout experiment is not observed here.

In conclusion we have obtained the infrared spectra of $V(CO)_n^+$ (n=1-7) ions. We find evidence for structures and for spin changes in small clusters. We were also unable to observe the 18-electron seven-coordinate $V(CO)_7^+$ ion previously observed by the Armentrout group.

Table 4.1: Calculated and Experimental Energetics of V^+ ions. Experimental energies were retrieved from the online NIST Handbook of Atomic Spectroscopic Data.

Species	Calculated Energy kcal/mol (absolute)	Experimental
$^5V^+$ ^{5}D J=0 ($3d^4$)	+0.0 (-943.6746600)	+0.0
$^3V^+$ ^{3}F J=2 ($3d^34s$)	+36.1 (-943.6171752)	+24.6
$^1V^+$ ^{1}G J=4 ($3d^4$)	+57.8 (-943.5824980)	+51.2

Table 4.2: Calculated relative energies and IR active carbonyl stretching frequencies of $V(CO)_1^+$ ions

Species	Relative Energy kcal/mol (absolute)	IR frequencies cm^{-1} (int. km/mol)
$^5V(CO)_1^+$	+0.0 (-1057.0581454)	2216(414)
$^3V(CO)_1^+$	+23.5 (-1057.0206614)	2117(511)
$^1V(CO)_1^+$	+28.8 (-1057.0123179)	2193(482)
$^5V(CO)_1^+Ne$	+0.0 (-1186.0240069)	2197(418)
$^3V(CO)_1^+Ne$	+22.8 (-1185.9877076)	2119(537)
$^1V(CO)_1^+Ne$	+52.4 (-1185.9404490)	2110(528)
$^5V(CO)_1^+Ar$	+0.0 (-1584.6230252)	2190(486)
$^3V(CO)_1^+Ar$	+22.1(-1584.5877988)	2178(530)
$^1V(CO)_1^+Ar$	+52.9 (-1584.5387905)	2101(583)
$^5V(CO)_1^+Ar_2$	+0.0 (-2112.1805361)	2202(482)
$^3V(CO)_1^+Ar_2$	+17.9(-2112.1520895)	2088(579)
$^1V(CO)_1^+Ar_2$	+50.3 (-2112.1003015)	2167(554)

Table 4.3: Calculated relative energies and IR active carbonyl stretching frequencies of $V(CO)_2^+$ ions

Species	Relative Energy kcal/mol (absolute)	IR frequencies cm^{-1} (int. km/mol)
$^5V(CO)_2^+$	+0.0 (-1170.4346095)	2191(1237)
$^3V(CO)_2^+$	+25.8 (-1170.3934856)	2102(2231)
$^1V(CO)_2^+$	+40.9 (-1170.3694216)	2124(1745)
$^5V(CO)_2^+Ne$	+0.0 (-1299.3974729)	2213(1010)
$^3V(CO)_2^+Ne$	+14.8(-1299.3739597)	2126(1999)
$^1V(CO)_2^+Ne$	+39.2 (-1299.3350166)	2120(1771)
$^5V(CO)_2^+Ar$	+0.0 (-1697.9975802)	2187(1335)
$^3V(CO)_2^+Ar$	+15.7 (-1697.9724927)	2117(2054)
$^1V(CO)_2^+Ar$	+35.8 (-1697.9405794)	2125(1741)

Table 4.4: Calculated relative energies and IR active carbonyl stretching frequencies of $V(CO)_3^+$ ions

Species	Relative Energy kcal/mol (absolute)	Ir frequencies cm^{-1} (int. km/mol)
$^5V(CO)_3^+$	+0.0 (-1283.8130619)	2197 (549), 2198 (1177)
$^3V(CO)_3^+$	+14.0 (-1283.7908219)	2149(1669), 2170(355), 2219(135)
$^1V(CO)_3^+$	+18.7 (-1283.7833028)	2154(562), 2166(1428), 2124(27)
$^5V(CO)_3^+Ne$	+0.0 (-1412.7778467)	2179(541), 2195(1183)
$^3V(CO)_3^+Ne$	+7.6(-1412.7657352)	2100(2125), 2190(165)
$^1V(CO)_3^+Ne$	+28.1 (-1412.7330208)	2153(2282), 2203(63)
$^5V(CO)_3^+Ar$	+0.0 (-1811.3747725)	2174(554), 2190(1204)
$^3V(CO)_3^+Ar$	+6.9 (-1811.3638263)	2128(600), 2145(1534)
$^1V(CO)_3^+Ar$	+30.5(-1811.3261596)	2134(2282), 2201(46)

Table 4.5: Calculated relative energies and IR active carbonyl stretching frequencies of $V(CO)_4^+$ ions

Species	Relative Energy kcal/mol (absolute)	Ir frequencies cm^{-1} (int. km/mol)
$^5V(CO)_4^+$	+0.0 (-1397.1842375)	2184(2240), 2195(65)
$^3V(CO)_4^+$	+1.6 (-1397.1817491)	2129(1291), 2147(1513), 2162(241)
$^1V(CO)_4^+$	+17.5 (-1397.1563941)	2146(3338)

Table 4.6: Calculated relative energies and IR active carbonyl stretching frequencies of $V(CO)_5^+$ ions

Species	Relative Energy kcal/mol (absolute)	Ir frequencies cm^{-1} (int. km/mol)
$^5V(CO)_5^+$	+5.5 (-1510.5527607)	2169(1690), 2203(803)
$^3V(CO)_5^+$	+0.0 (-1510.5614842)	2151(2620), 2203(270), 2231(72)
$^1V(CO)_5^+$	+16.7 (-1510.5349461)	2138(1225), 2161(1859), 2222(17)

Table 4.7: Calculated relative energies and IR active carbonyl stretching frequencies of $V(CO)_6^+$ ions

Species	Relative Energy kcal/mol (absolute)	Ir frequencies cm^{-1} (int. km/mol)
$^5V(CO)_6^+$	+29.8 (-1623.8882393)	2165(1690), 2201(803), 2222(68)
$^3V(CO)_6^+$	+0.0 (-1623.9357771)	2166(1272), 2169(1986),
$^1V(CO)_6^+$	+16.9 (-1623.9088240)	2154(2535), 2162(751)

Table 4.8: Calculated relative energies and IR active carbonyl stretching frequencies of $V(CO)_7^+$ ions

Species	Relative Energy kcal/mol (E_h)	IR frequencies cm^{-1} (int. km/mol)
$^5V(CO)_7^+$	+35.5 (-1737.2219163) check on iso2	2157(944), 2161(769), 2197(807), 2222(127)
$^3V(CO)_7^+$	+7.2 (-1737.2669338)	2141(1259), 2170(1116), 2173(887), 2224(63)
$^1V(CO)_7^+$	+0.0 (-1737.2784133)	2120(634), 2130(20280, 2153(592), 2178(355), 2219(101)

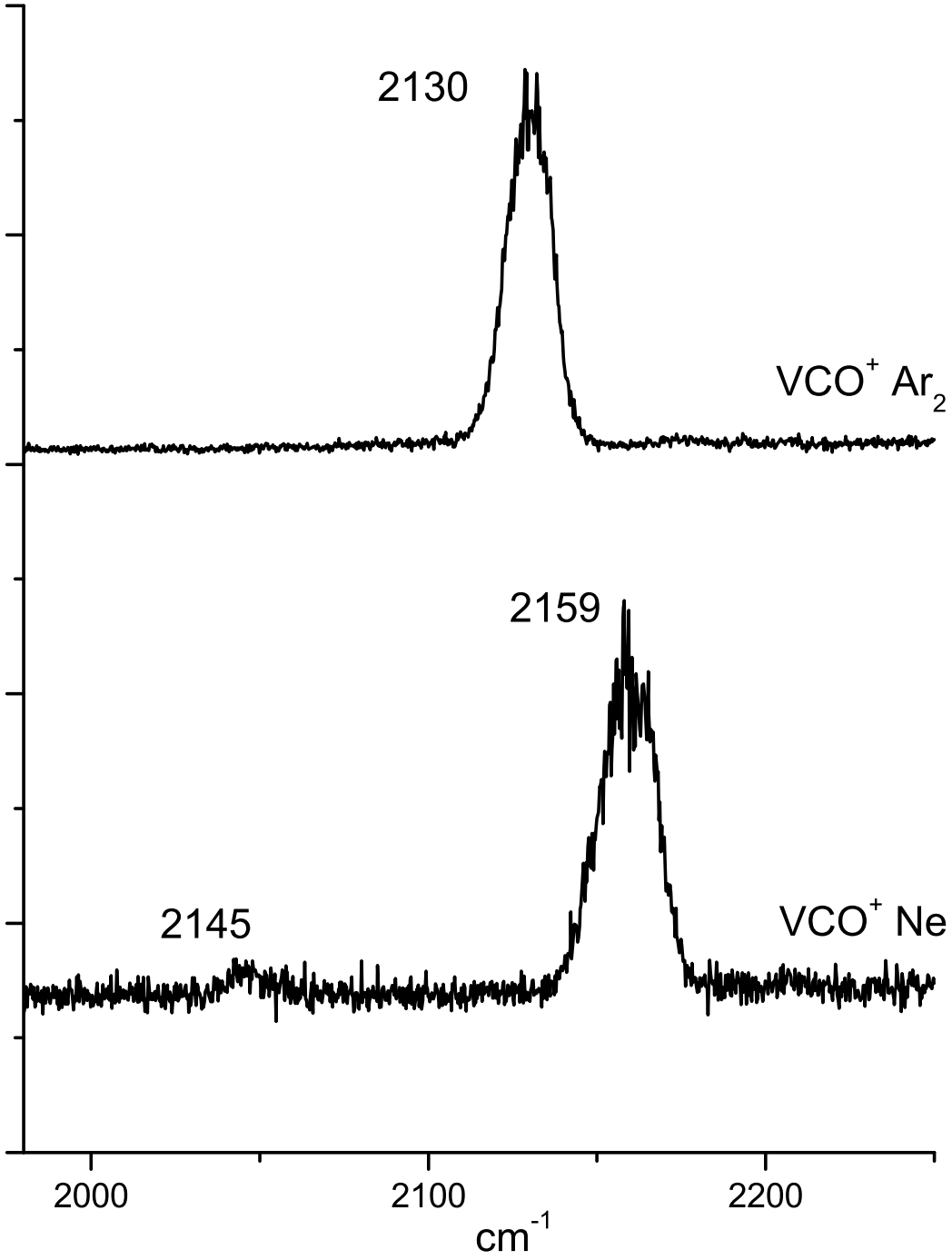

Figure 4.1: Infrared spectrum of the $V(CO)_1^+$ ion obtained using neon and argon tagging.

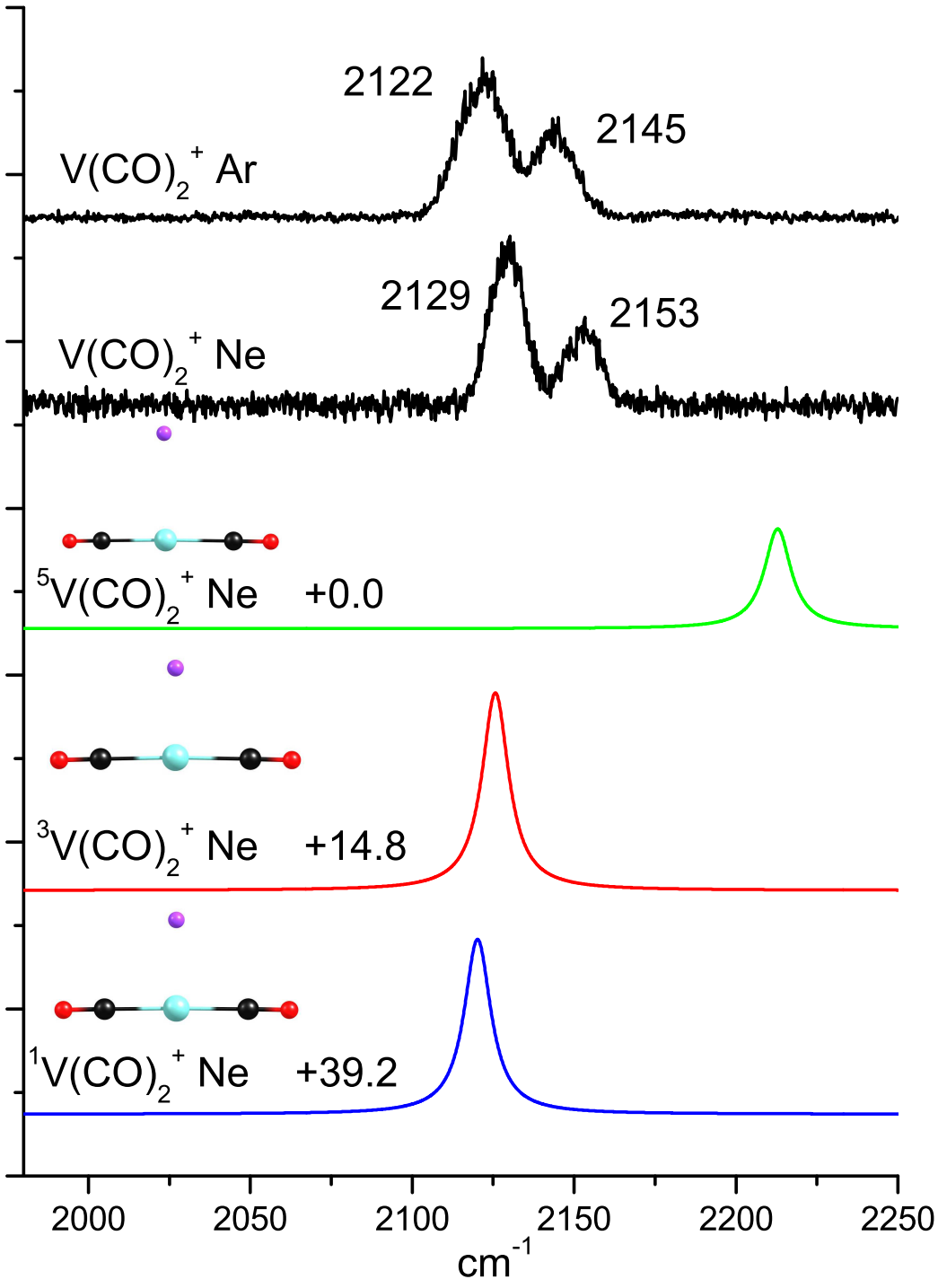

Figure 4.2: Infrared spectrum of the $V(CO)_2^+$ ion obtained using neon and argon tagging. Calculated spectra are unscaled and given a 10 cm^{-1} FWHM Lorentzian lineshape. Calculated relative energetics of the isomers is given in kcal/mol.

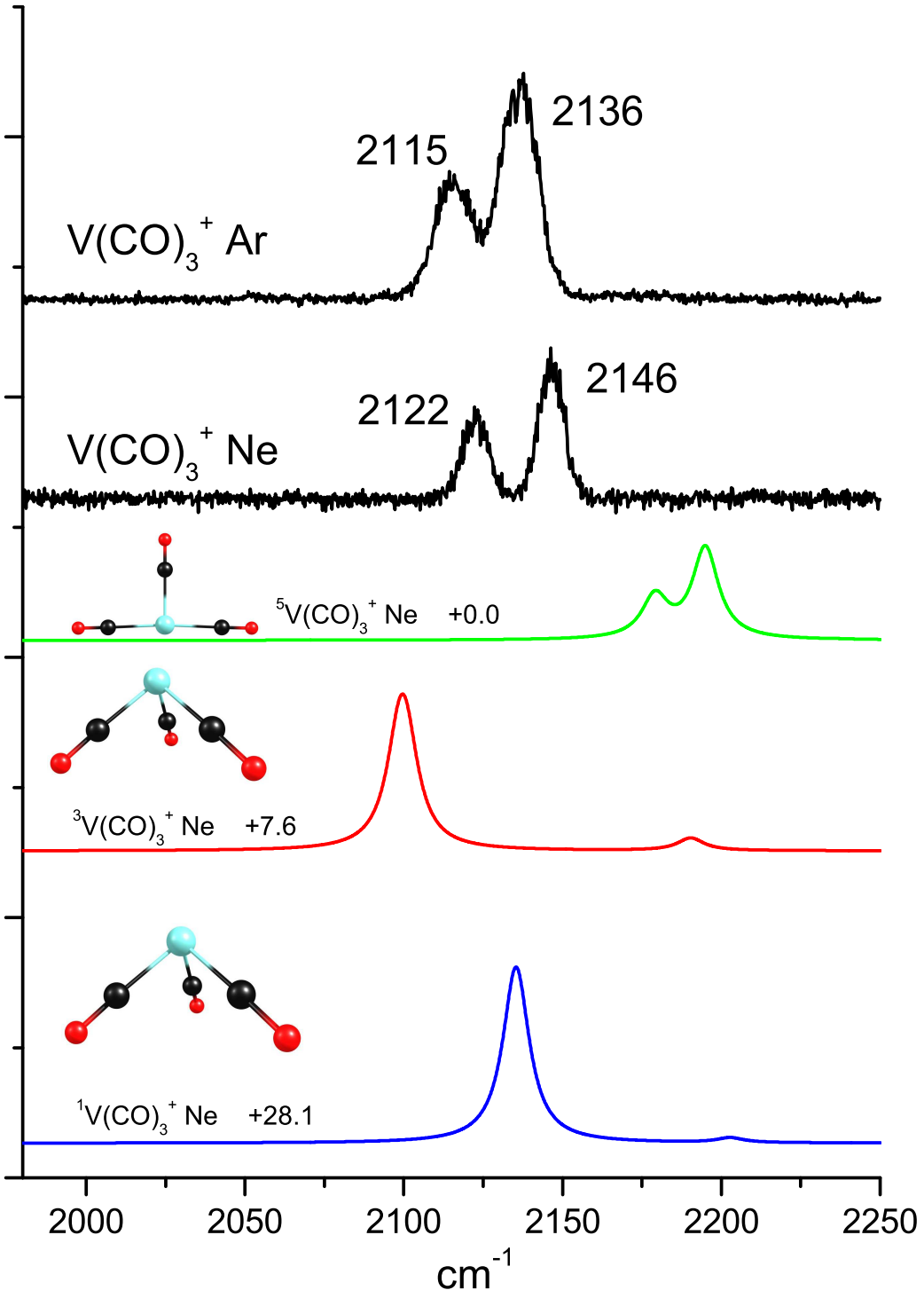

Figure 4.3: Infrared spectrum of the $V(CO)_3^+$ ion obtained using neon and argon tagging. Calculated spectra are unscaled and given a 10 cm^{-1} FWHM Lorentzian lineshape. Calculated relative energetics of the isomers is given in kcal/mol.

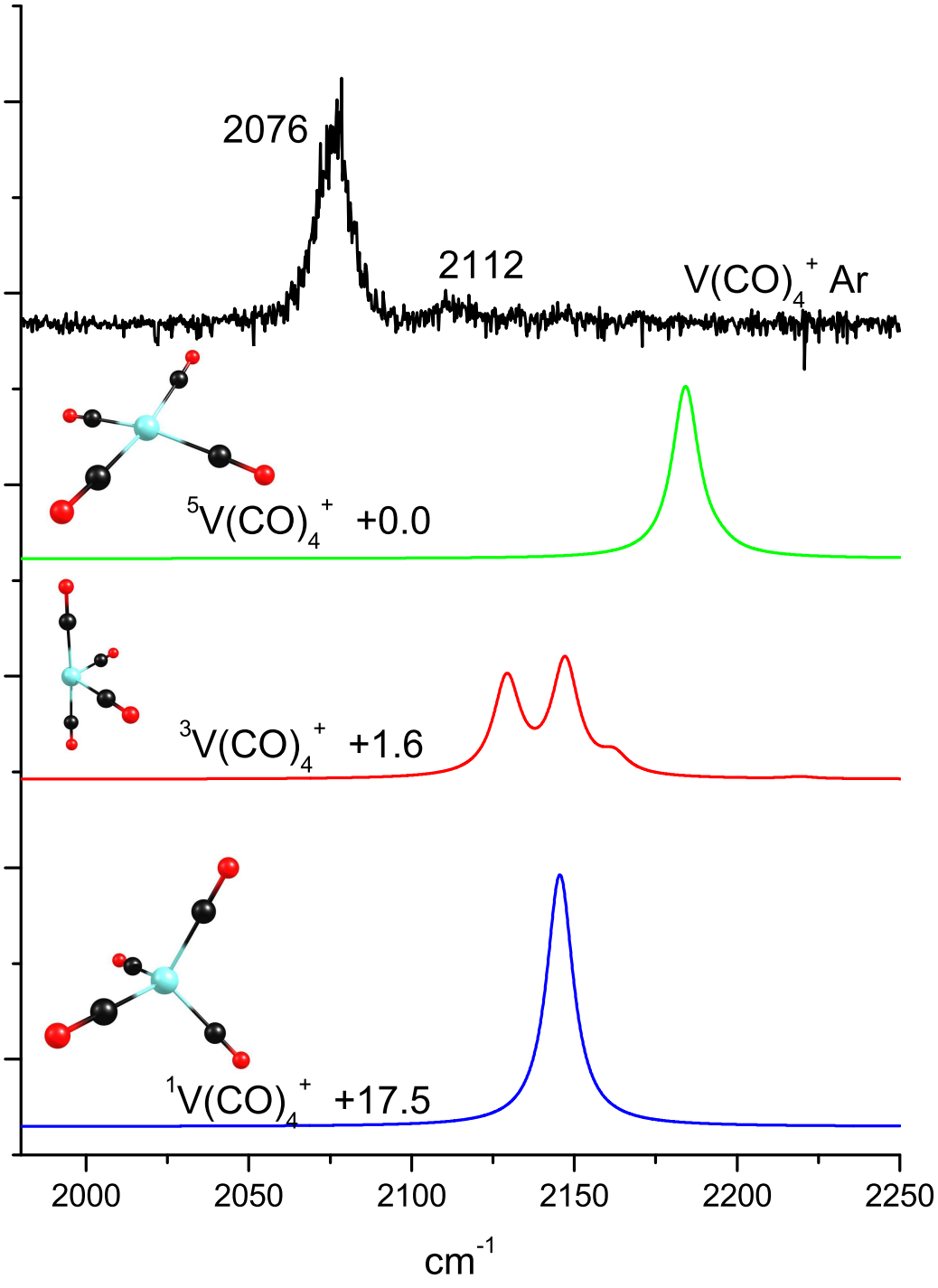

Figure 4.4: Infrared spectrum of the $V(CO)_4^+$ ion obtained using argon tagging. The calculated spectra are unscaled and given a 10 cm^{-1} FWHM Lorentzian lineshape. Calculated relative energetics of the isomers is given in kcal/mol.

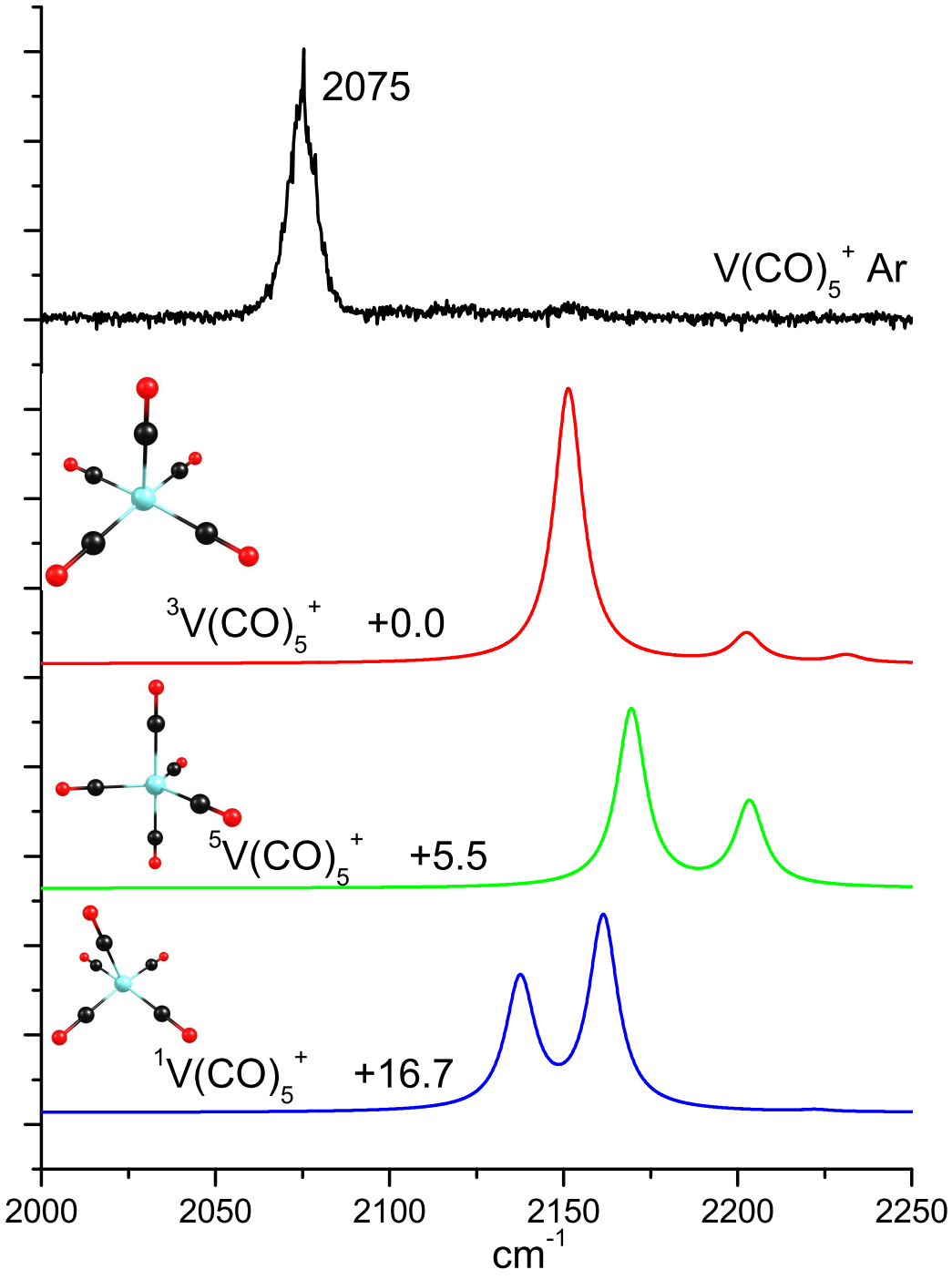

Figure 4.5: Infrared spectrum of the $V(CO)_5^+$ ion obtained using argon tagging. The calculated spectra are unscaled and given a 10 cm^{-1} FWHM Lorentzian lineshape. Calculated relative energetics of the isomers is given in kcal/mol.

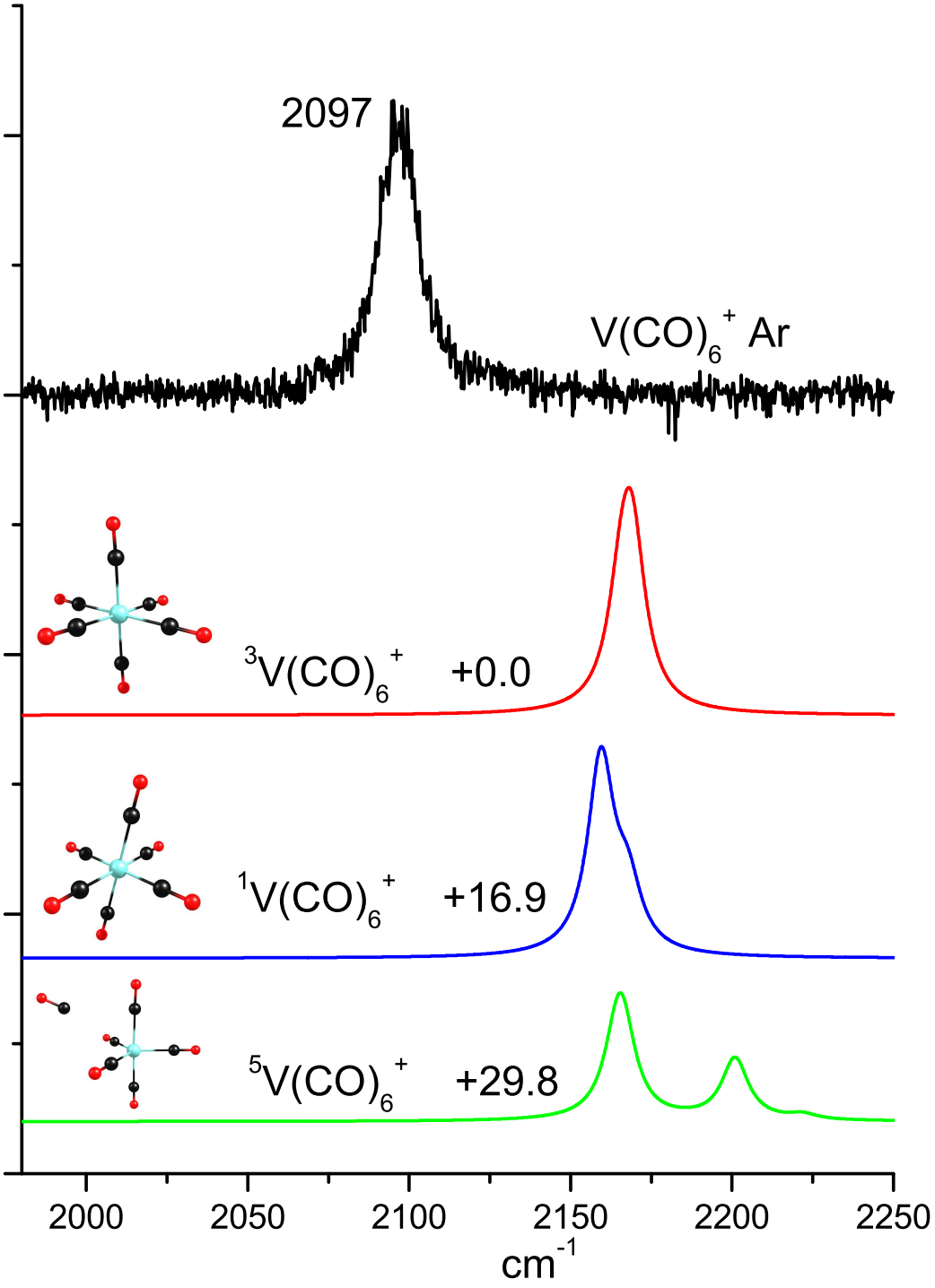

Figure 4.6: Infrared spectrum of the $V(CO)_6^+$ ion obtained using argon tagging. The calculated spectra are unscaled and given a 10 cm^{-1} FWHM Lorentzian lineshape. Calculated relative energetics of the isomers is given in kcal/mol.

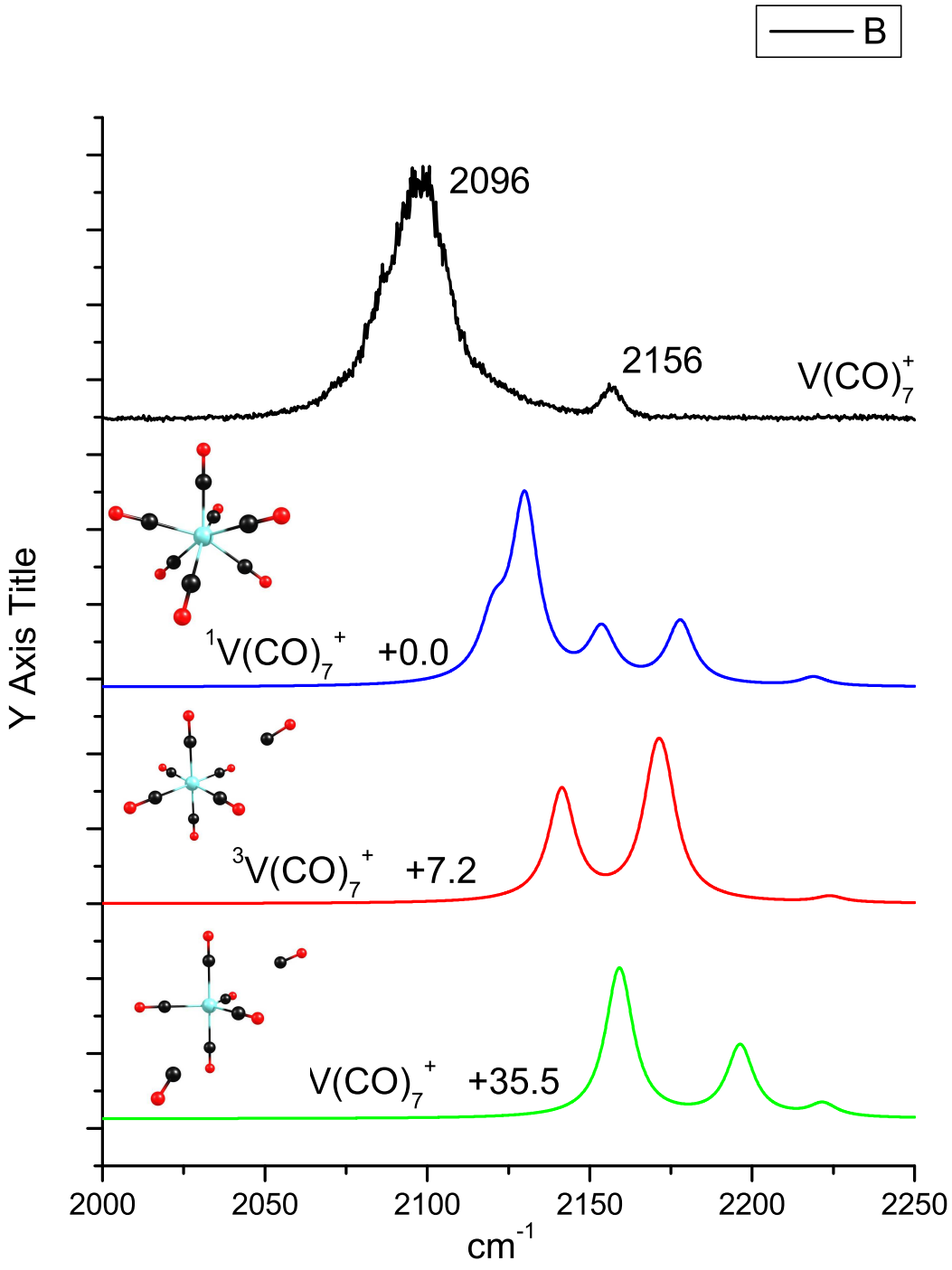

Figure 4.7: Infrared spectrum of the $V(CO)_7^+$ ion obtained via elimination of a single CO molecule. $V(CO)_7^+Ar$ was found to fragment by elimination of CO and Ar. The calculated spectra are unscaled and given a 10 cm^{-1} FWHM Lorentzian lineshape. Calculated relative energetics of the isomers is given in kcal/mol.

Chapter 5

Niobium Carbonyl Complexes

Niobium is one row below vanadium on the periodic table, therefore the two elements are isovalent and their cations have four valence electrons. However, there are some differences between the two metals, notably the size of the Nb^+ is larger than V^+ so it may be better able to accommodate seven carbonyl ligands to form the 18-electron complex we were not able to observe in the vanadium system. The quintet Nb^+ ion has been experimentally determined to be 15.9 kcal/mol smaller in energy than the triplet isomer (see Table 5.1), lower than the 24.6 kcal/mol difference measured for the vanadium ion (Table 4.1). Like the vanadium system there has been no previous spectroscopic work on cationic niobium carbonyl complexes. Presented here is a study of these ions beginning with one CO and proceeding up to and beyond the first coordination sphere. In support of this work Density Functional Theory (DFT) calculations were performed using the B3LYP functional as implemented in the pcGAMESS computational suite. The def2-qzvp basis set was used for niobium, the DZP basis for oxygen and carbon and the 6-311G(d) basis for argon and neon.

The infrared spectrum of the $Nb(CO)_1^+$ ion is shown in Figure 5.1. Tagging with three argon atoms was required before efficient fragmentation was observed. Similar to $V(CO)_1^+$, only a single peak is observed and all calculated spectra also consist of a single peak. Therefore we can only tentatively assign this spectrum to the quintet state based on the calculated relative energetics shown in Table 5.2.

The infrared spectrum of the $Nb(CO)_2^+$ ion was obtained using single, double and triple argon tagging and is shown in Figure 5.2. The $Nb(CO)_2^+Ar$ spectrum consists of two peaks when only one is calculated, similar to what was observed for the $V(CO)_2^+$ ion. The peak at

2088 cm^{-1} is assigned to the triplet isomer and the 2120 band to the quintet. The calculated relative energetics of the quintet, triplet and singlet states of $Nb(CO)_2^+$ are shown in Table 5.3. The triplet isomer is calculated to be 14.9 kcal/mol higher in energy than the quintet isomer, but when a single argon atom is added this energy difference drops to 7 kcal/mol.

When a second argon atom is added to $Nb(CO)_2^+$ the two main peaks are preserved and only slightly shifted ($\sim$3 cm^{-1}), but the relative intensities are much different and a third peak is observed at 2044 cm^{-1}. This is a puzzling result and it is possible that there are multiple isomers that differ in the argon binding site. If the first argon atom were to bind to the metal center and the second on a CO ligand the reduction in symmetry would lead to two CO stretches, a red shifted band corresponding to the carbonyl with an argon attached to it and a higher frequency band with no argon coordinated to it. However, calculations with an argon atom on a carbonyl ligand show these structures are not minima on the potential energy surface. It is also possible that additional argon atoms sufficiently distort the system from linearity such that two IR bands become active. This is somewhat supported by the theoretical calculations which predicts two bands for the triplet $Nb(CO)_2^+Ar_2$ ion, although the calculated relative intensity of these bands is not in line with the observations. Another possibility is generation of the singlet spin state, this assignment is in line with the calculations which predict the singlet vibrational frequency to the red of the triplet state. If this is the case it indicates that we are able to trap metastable species that are much higher in energy than the ground state by addition of an additional argon atom. A third argon atom yields a spectrum with three peaks in approximately the same position but with decidedly different intensities indicating that the relative abundance of the three spin isomers now favors formation of the singlet species. Although we are not currently able to positively identify the carriers of the bands seen in Figure 5.2 we can at least conclude that there must be multiple species present. It is hoped that future calculations at higher levels of theory might clear up the matter.

The infrared spectrum of the $Nb(CO)_3^+$ ion was obtained by tagging with one and two argon atoms and is shown in Figure 5.3. The singly tagged spectrum consists of a single intense peak at 2092 cm^{-1} with small shoulders at 2071 and 2113 cm^{-1}. The spectrum of the doubly tagged $Nb(CO)_3^+$ ion consists of a single intense peak 31 cm^{-1} to the red of that observed with a single argon and a weaker feature at 2001 cm^{-1}. The red shift of the most intense peak after addition of a second argon atom is larger than would be expected for the perturbation induced by argon tagging, therefore it is possible that both spectra are due to very different species.

The infrared spectrum of the $Nb(CO)_3^+Ar$ ion is shown at the top of Figure 5.4 along with the predicted spectra for the three spin states and their relative energetics. The triplet ion is calculated to have the lowest energy and is predicted to have two infrared active CO vibrations whose splitting is calculated to be much more than what is observed. The quintet is predicted to be 26.6 kcal/mol higher in energy, however the single intense peak predicted matches fairly well with the observed spectrum. This spectrum is therefore very difficult to assign and a definite conclusion cannot be reached with the current experimental and theoretical data.

The infrared spectrum of $Nb(CO)_3^+Ar_2$ is shown at the top of Figure 5.5 along with calculated spectra for the three spin states. The intense peak observed at 2061 cm^{-1} is similar to that in the $Nb(CO)_3^+Ar$ spectrum, however the peak observed at 2001 cm^{-1} is difficult to explain. It is much more red shifted than any other bands we have observed up until this point and its assignment remains a mystery.

The infrared spectrum of $Nb(CO)_4^+$ was obtained using argon tagging and is shown in Figure 5.6. The calculated spectra of the three spin states all have a single peak. Therefore we can only tentatively assign this band to the triplet ion based on the calculated relative energetics (see Table 5.5). For this ion there appears to be just one isomer present in contrast to many of the other systems. Structures with the argon tag were not computed because as the system size increases the metal argon interaction decreases and the computations

become more difficult. The calculated difference in energetics and vibrational frequencies for the $Nb(CO)_3^+$ with and without argon were small which makes sense because as the ion becomes fully coordinated the addition of argon atoms are less and less perturbing. Therefore no calculations of the $Nb(CO)_n^+$ n>3 with argon were preformed.

In contrast to the $Nb(CO)_4^+$ spectrum, the $Nb(CO)_5^+$ spectrum consists of one intense peak and several smaller ones. The calculated spectrum of the singlet isomer reproduces the 2064, 2077 and 2096 cm^{-1} bands and this isomer is only predicted to be 4.1 kcal/mol higher in energy than the triplet isomer. The intense peak at 2077 and shoulder at 2064 cm^{-1} are assigned to the triplet isomer, while the 2096 cm^{-1} feature is attributed to the quintet isomer. As discussed below, the singlet isomer was not observed in the $Nb(CO)_6^+$ system so it is strange that it would be present in this system.

The infrared spectrum of the $Nb(CO)_6^+$ ion was obtained by directly eliminating a CO ligand and is shown at the top of Figure 5.8. Fragmentation of this ion is much less efficient than that of the tagged ions, in line with a strongly bound complex similar to what was observed for $Co(CO)_5^+$. The spectrum of $Nb(CO)_6^+$ obtained using argon tagging is shown in Figure 5.8 and consists of a single band nine cm^{-1} to the blue of that observed for the bare complex. The red shift of the bare complex may be due to the multiphoton dissociation nature of fragmentation which is known to cause such effects.[56] The calculated spectra of the quintet and singlet isomers both have multiple peaks while that of the triplet isomer consists of a single peak, thus this spectrum is assigned to the triplet isomer which is also the lowest calculated energy species. This complex is distorted from O_h symmetry due to Jahn-Teller effects resulting in multiple infrared active CO vibrations, however the splitting is less than can be observed in the current experiment.

The $Nb(CO)_7^+$ ion was found to fragment efficiently by elimination of a single CO ligand. The spectrum is shown in Figure 5.9 and consists of an intense peak at 2098 cm^{-1}, a shoulder at 2083 and a weaker band at 2065. The efficient loss of CO indicates that the seventh CO molecule is loosely bound to the core $Nb(CO)_6^+$. This is further supported by the infrared

spectrum which shows the 2165 cm^{-1} "surface" CO band also observed in the cobalt and vanadium carbonyl systems. The intense 2098 cm^{-1} band in the $Nb(CO)_7^+$ spectrum is similar in position to the band observed in the $Nb(CO)_6^+Ar$ spectrum, however a shoulder is observed. This is due to the external CO causing a perturbation of the nearly octahedral core $Nb(CO)_6^+$ ion, splitting the infrared active bands to an extent that they can now be partially resolved. The calculated spectrum of the triplet isomer well reproduces the observed infrared spectrum, but the singlet isomer is predicted to be lowest in energy. The singlet isomer has all seven CO ligands directly coordinated to the central metal atom so presumably the $Nb(CO)_6^+$-CO bond energy is larger than a single infrared photon. Therefore if this isomer were present it would not be detected in our experiment by CO elimination. For the isovalent $V(CO)_7^+$ system this binding energy was measured to be > 4000 cm^{-1}.[25]

The $Nb(CO)_8^+$ cluster was found to efficiently lose one and two CO molecules and the spectra obtained by monitoring each loss channel (shown in Figure 5.10) are markedly different. The spectrum obtained by monitoring the loss of two carbonyls matches well with the spectrum of $Nb(CO)_6^+$ shown in Figure 5.11. Monitoring the loss of a single CO molecule yields a spectrum similar to that calculated for the seven coordinate single $Nb(CO)_7^+$ ion with exception of the peak at 2083 cm^{-1}. This result indicates that we have a mixture of spin isomers with different fragmentation yields. The seven coordinate ion with a single surface CO has one molecule that is weakly bound and can be eliminated with a single infrared photon, while the six coordinate triplet species has two surface molecules that can both be eliminated. The $Nb(CO)_7^+Ar$ ion was found to fragment by loss of argon and argon and CO. The loss of argon spectrum is shown in Figure **??** along with the spectrum obtained by monitoring loss of a single CO from $Nb(CO)_8^+$. The two spectra are very similar with the exception of the band at 2083 cm^{-1} which is not observed in the argon tagged spectrum. This band is observed in the $Nb(CO)_6^+$ spectrum obtained by monitoring loss of two CO from $Nb(CO)_8^+$ (top of Figure **??**) and is therefore assigned to the six coordinated species "contaminating" the seven coordinated spectrum by losing only one CO. This is interesting

because the 2080 band is observed as a shoulder off the much more intense peak at 2098 cm^{-1}, but this intense peak is not observed in the loss of one CO spectrum and must be due to the photodissociation dynamics of the $Nb(CO)_8^+$ complex.

In conclusion we have performed a complete survey of cationic niobium carbonyl complexes from species with a single CO up to and beyond the coordination sphere. Some of the spectra of the smaller complexes have proven difficult to assign and there appear to be marked differences when tagging with single or multiple rare gas atoms. This we have tentatively attributed to trapping of different metastable spin isomers, however more theoretical work is necessary to resolve these issues.

Table 5.1: Calculated and Experimental Energetics of Nb^+ ions. Experimental energies were retrieved from the NIST Handbook of Atomic Spectroscopic Data.

Species	Calculated Energy kcal/mol (absolute)	Experimental
$^5Nb^+$ ^5D J=0 ($3d^4$)	+0.0 (-56.5839386)	+0.0
$^3Nb^+$ ^3P J=0 ($4d^4$)	+28.7 (-56.5381357)	+15.9

Table 5.2: Calculated relative energies and IR active carbonyl stretching frequencies of $Nb(CO)_1^+$ ions

Species	Relative Energy kcal/mol (absolute)	IR frequencies cm^{-1} (int. km/mol)
$^5Nb(CO)_1^+$	+0.0 (-169.9827247)	2133(562)
$^3Nb(CO)_1^+$	+21.4 (-169.9485604)	2033(558)
$^1Nb(CO)_1^+$	+31.9 (-169.9318608)	2039(686)
$^5Nb(CO)_1^+Ar$	+0.0 (-697.5466290)	2127(651)
$^3Nb(CO)_1^+Ar$	+22.0 (-697.5116083)	2032(634)
$^1Nb(CO)_1^+Ar$	+33.0 (-697.4939728)	2037(765)

Table 5.3: Calculated relative energies and IR active carbonyl stretching frequencies of $Nb(CO)_2^+$ ions

Species	Relative Energy kcal/mol (absolute)	IR frequencies cm^{-1} (int. km/mol)
$^5Nb(CO)_2^+$	+0.0 (-283.3619760)	2152(1661)
$^3Nb(CO)_2^+$	+14.9 (-283.3381961)	2083(2113)
$^1Nb(CO)_2^+$	+21.4 (-283.3278281)	2079(1982)
$^5Nb(CO)_2^+Ar$	+0.0 (-810.9271981)	2151(1661)
$^3Nb(CO)_2^+Ar$	+7.0 (-810.9160407)	2083(2113)
$^1Nb(CO)_2^+Ar$	+19.6 (-810.8959371)	2064(2066)
$^5Nb(CO)_2^+Ar_2$	+0.0 (-1338.4912234)	2127(1699), 2175(71)
$^3Nb(CO)_2^+Ar_2$	+0.1 (-1338.4910209)	2006(2007), 2102(313)
$^1Nb(CO)_2^+Ar_2$	+25.5 (-1338.4505340)	2063(2109)
$^5Nb(CO)_2^+Ar_3$	+0.0 (-1866.0468911)	2112(1623), 2153(148)
$^3Nb(CO)_2^+Ar_3$	+14.5 (-1866.0698788)	2026(1030), 2089(434)
$^1Nb(CO)_2^+Ar_3$	+25.1 (-1866.0298263)	2038(2197)

Table 5.4: Calculated relative energies and IR active carbonyl stretching frequencies of $Nb(CO)_3^+$ ions

Species	Relative Energy kcal/mol (absolute)	IR frequencies cm^{-1} (int. km/mol)
$^5Nb(CO)_3^+$	+27.4 (-396.7317887)	2127(2451)
$^3Nb(CO)_3^+$	+0.0 (-396.7754675)	2065(2831), 2148(245)
$^1Nb(CO)_3^+$	+16.0 (-396.7499589)	2076(3169), 2158(122.5)
$^5Nb(CO)_3^+Ar$	+26.6 (-924.2975645)	2127(1699), 2175(71)
$^3Nb(CO)_3^+Ar$	+0.0 (-924.3399469)	2058(980), 2065(947), 2144(300)
$^1Nb(CO)_3^+Ar$	+13.9 (-924.3178146)	2069(3254), 2149(161)
$^5Nb(CO)_3^+Ar_2$	+16.5 (-1451.8762024)	2125(638), 2134(1496), 2181(114)
$^3Nb(CO)_3^+Ar_2$	+0.0 (-1451.9025432)	2054(972), 2060(951), 2140(338)
$^1Nb(CO)_3^+Ar_2$	+8.7 (-1451.8886685)	2056(615), 2058(1371), 2134(325)

Table 5.5: Calculated relative energies and IR active carbonyl stretching frequencies of $Nb(CO)_4^+$ ions

Species	Relative Energy kcal/mol (absolute)	IR frequencies cm^{-1} (int. km/mol)
$^5Nb(CO)_4^+$	+6.9 (-510.1360392)	2151(2873), 2164(224)
$^3Nb(CO)_4^+$	+0.0 (-510.1471752)	2129(3169)
$^1Nb(CO)_4^+$	+1.4 (-510.1449046)	2105(4099)

Table 5.6: Calculated relative energies and IR active carbonyl stretching frequencies of $Nb(CO)_5^+$ ions

Species	Relative Energy kcal/mol (absolute)	IR frequencies cm^{-1} (int. km/mol)
$^5Nb(CO)_5^+$	+19.5 (-623.5108616)	2123(2071), 2174(1001)
$^3Nb(CO)_5^+$	+0.0 (-623.5419846)	2119(663), 2131(1530), 2136(1340), 2147(165)
$^1Nb(CO)_5^+$	+4.1 (-623.5353804)	2104(507), 2114(2028), 2148(1001), 2209(82)

Table 5.7: Calculated relative energies and IR active carbonyl stretching frequencies of $Nb(CO)_6^+$ ions

Species	Relative Energy kcal/mol (absolute)	IR frequencies cm^{-1} (int. km/mol)
$^5Nb(CO)_6^+$	+48.2 (-736.8456760)	2120(2113), 2170(1014), 2119(76)
$^3Nb(CO)_6^+$	+0.0 (-736.9224882)	2143(4099)
$^1Nb(CO)_6^+$	+2.0 (-736.9192847)	2113(1263), 2116(1099), 2145(1192), 2170(634)

Table 5.8: Calculated relative energies and IR active carbonyl stretching frequencies of $Nb(CO)_7^+$ ions

Species	Relative Energy kcal/mol (absolute)	IR frequencies cm^{-1} (int. km/mol)
$^5Nb(CO)_7^+$	+74.0 (-850.1810322)	2115(2113), 2141(15), 2171(1017), 2220(27), 2221(123)
$^3Nb(CO)_7^+$	+26.1 (-850.2573681)	2130(42), 2133(190), 2137(1318), 2140(1297), 2149(1276), 2220(41), 2222(33)
$^1Nb(CO)_7^+$	+0.0 (-850.2988855)	2119(659), 2128(2409), 2147(756), 2169(870), 2225(63)

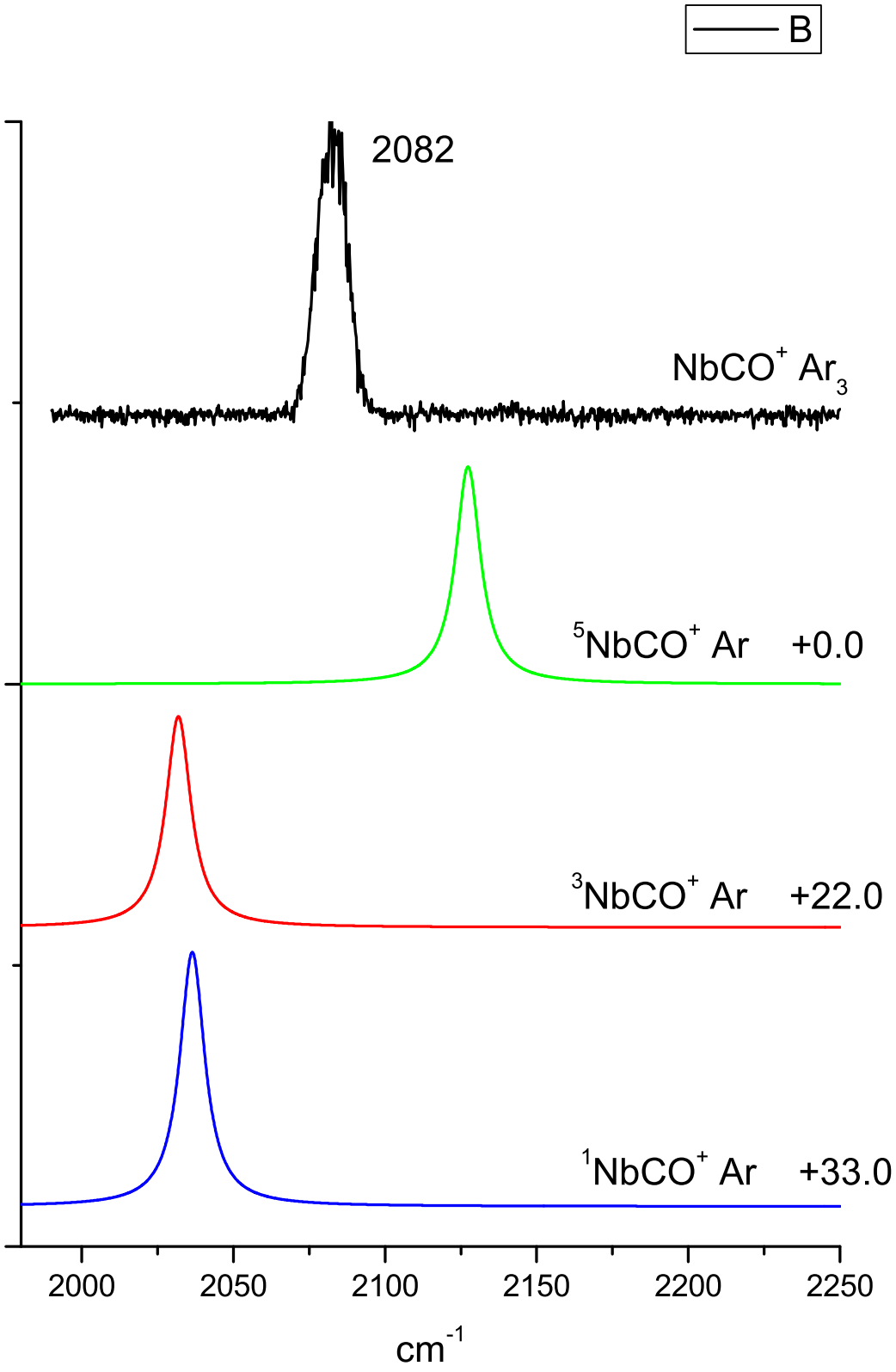

Figure 5.1: Infrared spectrum of the $Nb(CO)_1^+$ ion obtained using argon tagging.

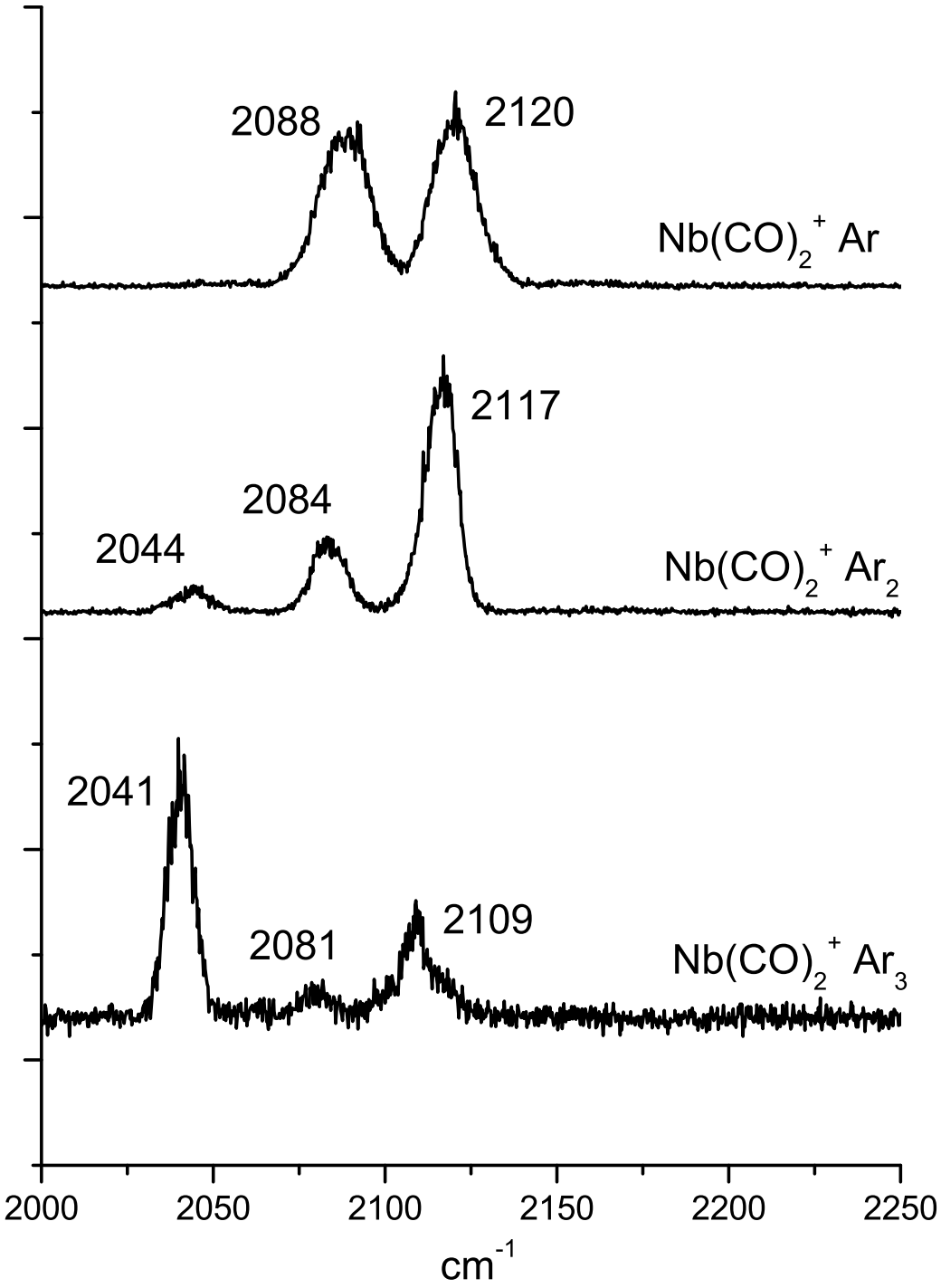

Figure 5.2: Infrared spectrum of the $Nb(CO)_2^+$ ion obtained using argon tagging.

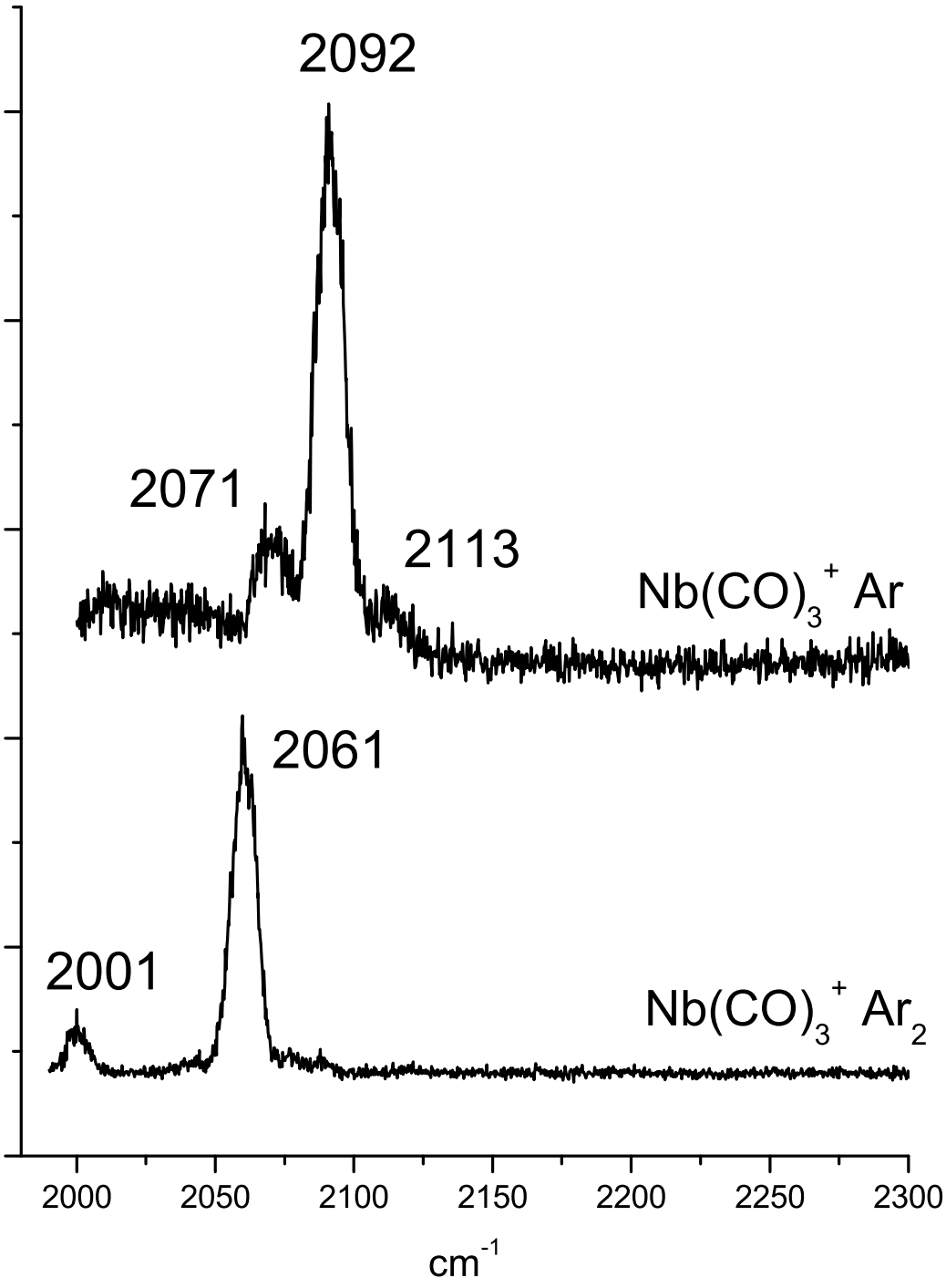

Figure 5.3: Infrared spectrum of the $Nb(CO)_3^+$ ion obtained by tagging with one and two argon atoms.

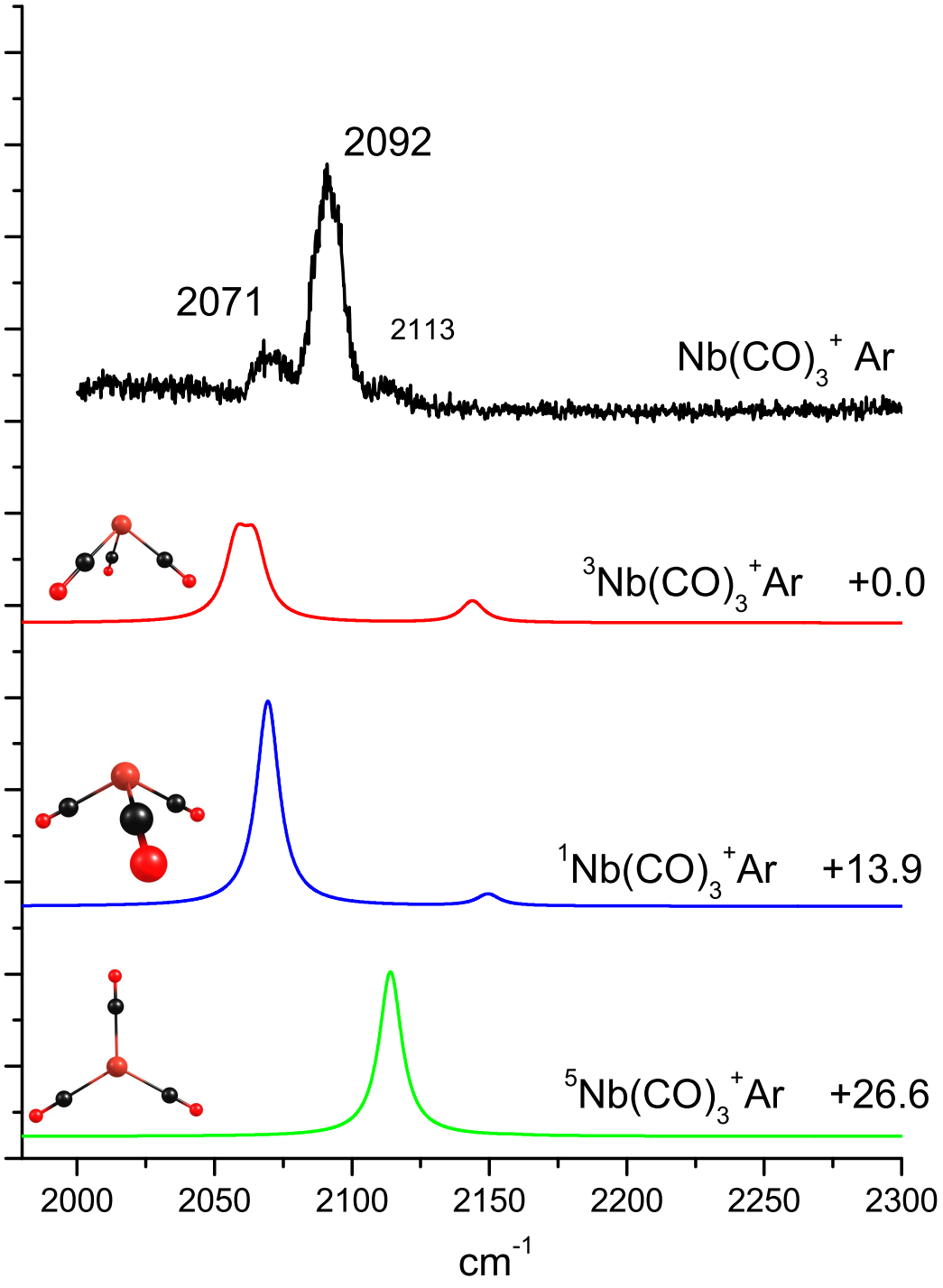

Figure 5.4: Infrared spectrum of the $Nb(CO)_3^+$ ion obtained using argon tagging along with predicted spectra. The calculated spectra are unscaled and given a 10 cm^{-1} FWHM Lorentzian lineshape. Relative energetics of the isomers is given in kcal/mol.

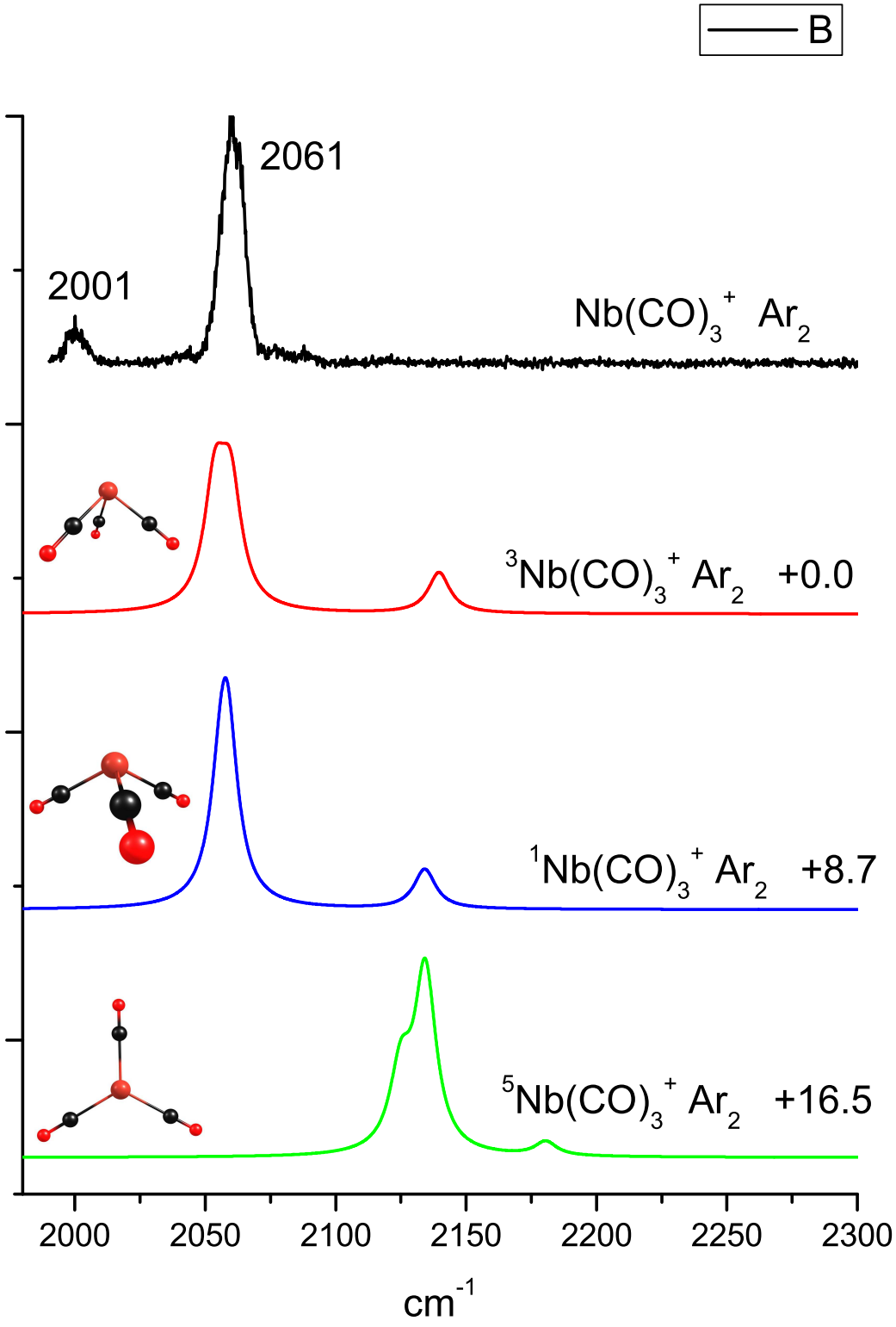

Figure 5.5: Infrared spectrum of the $Nb(CO)_3^+$ ion obtained by tagging with two argon atoms along with predicted spectra. The calculated spectra are unscaled and given a 10 cm^{-1} FWHM Lorentzian lineshape. Relative energetics of the isomers is given in kcal/mol.

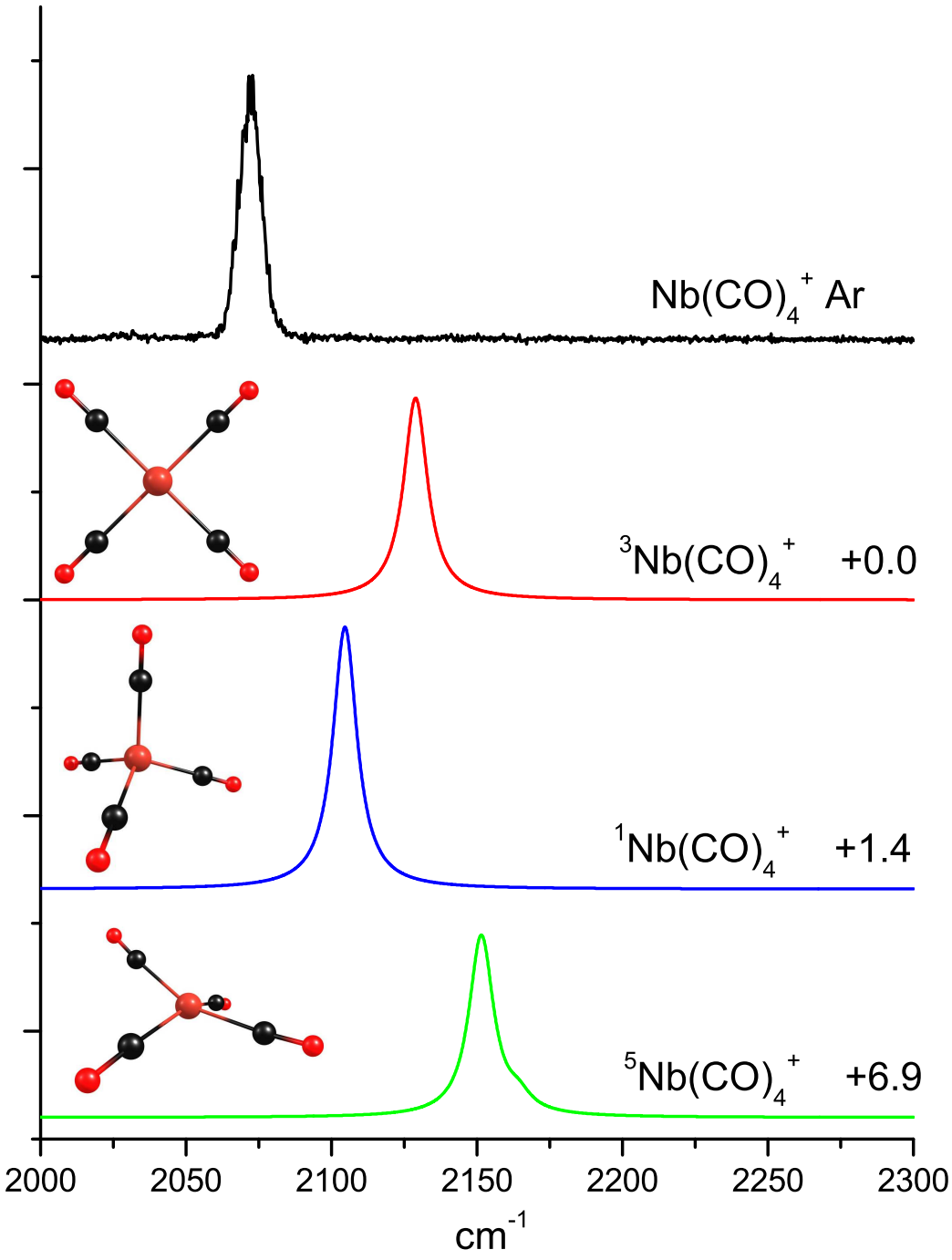

Figure 5.6: Infrared spectrum of the $Nb(CO)_4^+$ ion obtained using argon tagging. The calculated spectra are unscaled and given a 10 cm^{-1} FWHM Lorentzian lineshape. Relative energetics of the isomers is given in kcal/mol.

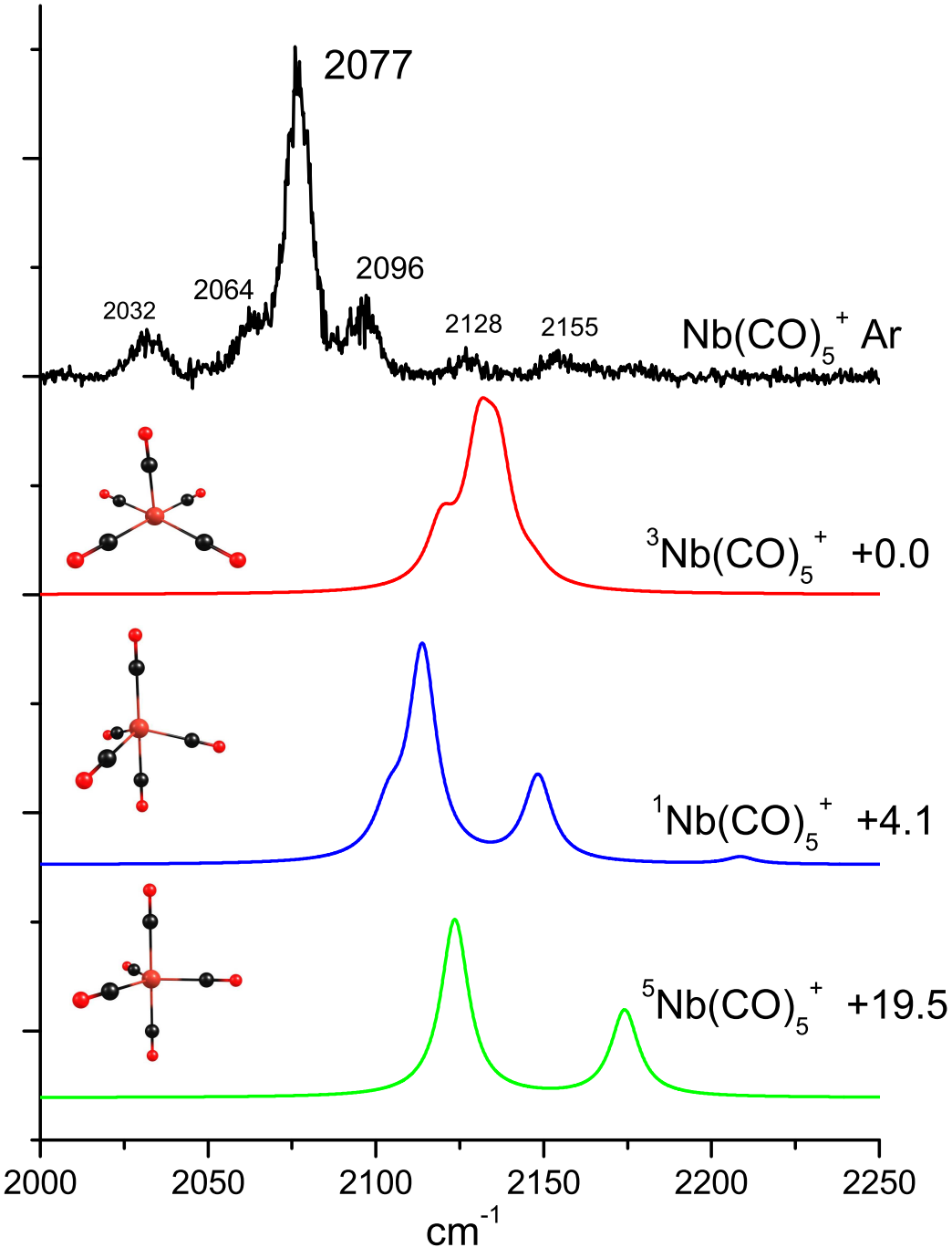

Figure 5.7: Infrared spectrum of the $Nb(CO)_5^+$ ion obtained using argon tagging. The calculated spectra are unscaled and given a 10 cm^{-1} FWHM Lorentzian lineshape. Relative energetics of the isomers is given in kcal/mol.

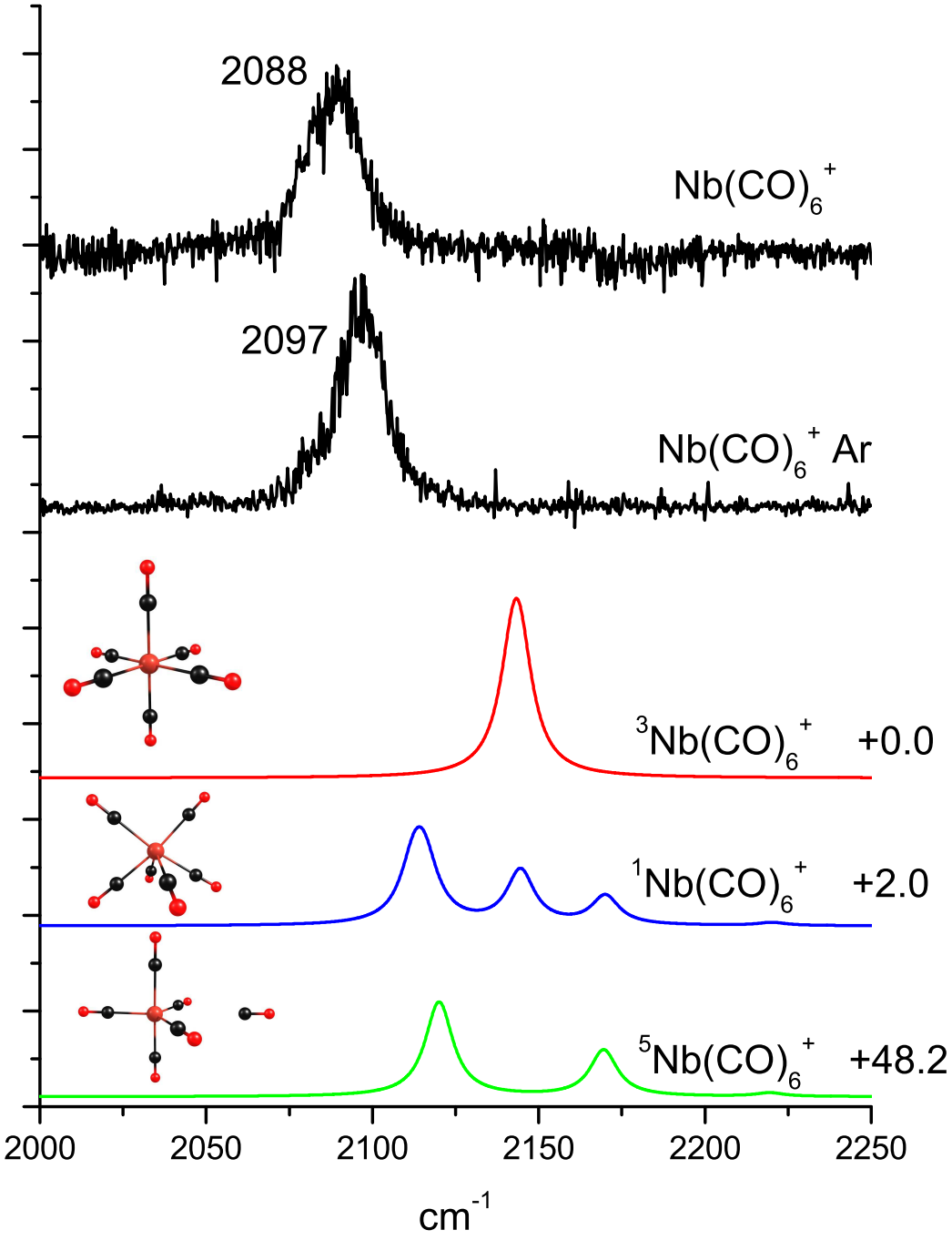

Figure 5.8: Infrared spectrum of the $Nb(CO)_6^+$ ion, the top spectrum was obtained by fragmenting CO from $Nb(CO)_6^+$ the second from top by argon tagging. The calculated spectra are unscaled and given a 10 cm^{-1} FWHM Lorentzian lineshape. Relative energetics of the isomers is given in kcal/mol.

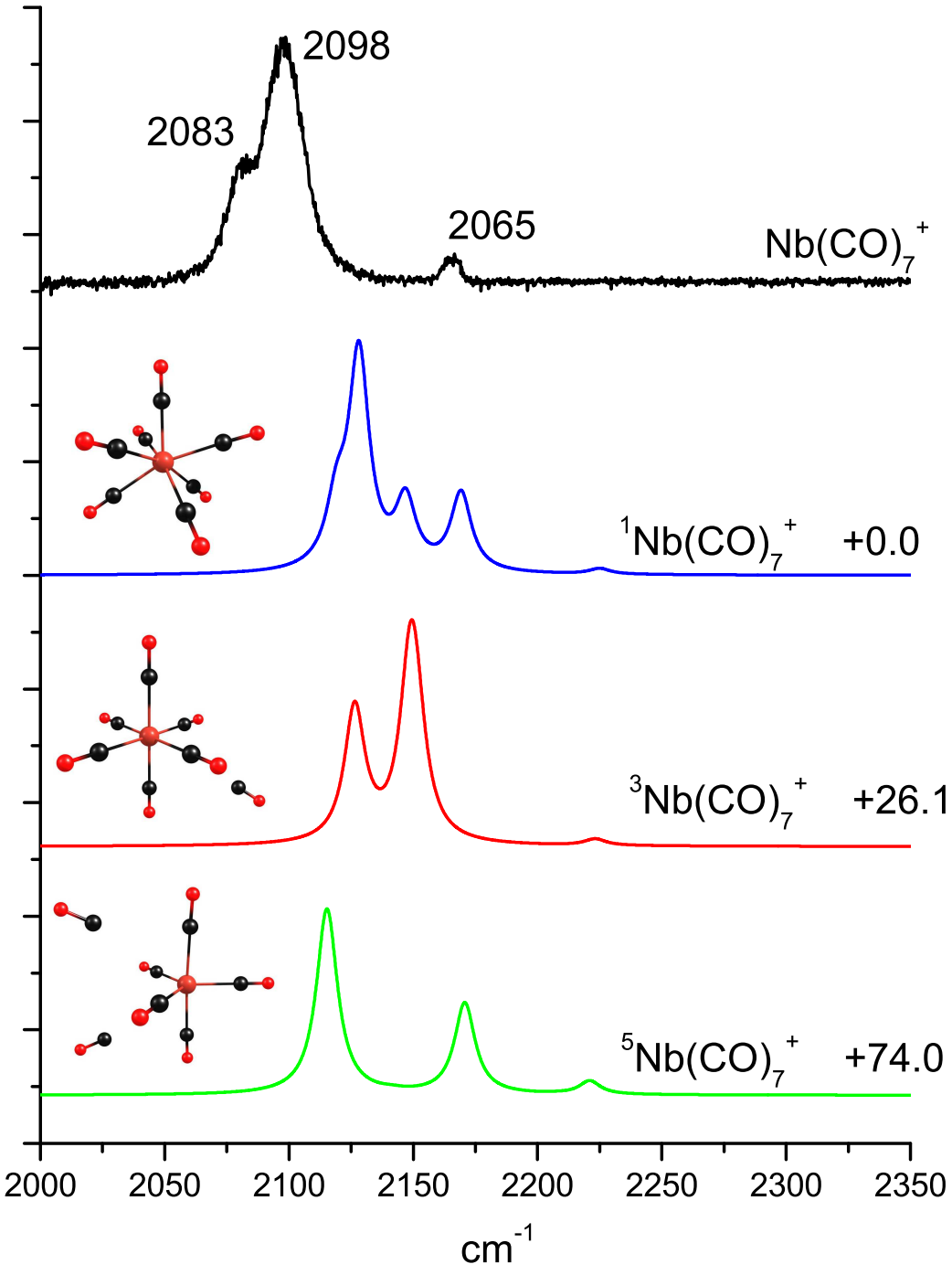

Figure 5.9: Infrared spectrum of the $Nb(CO)_7^+$ ion obtained by fragmenting CO from the complex. Calculated spectra are unscaled and given a 10 cm^{-1} FWHM Lorentzian lineshape. Relative energies are given in kcal/mol.

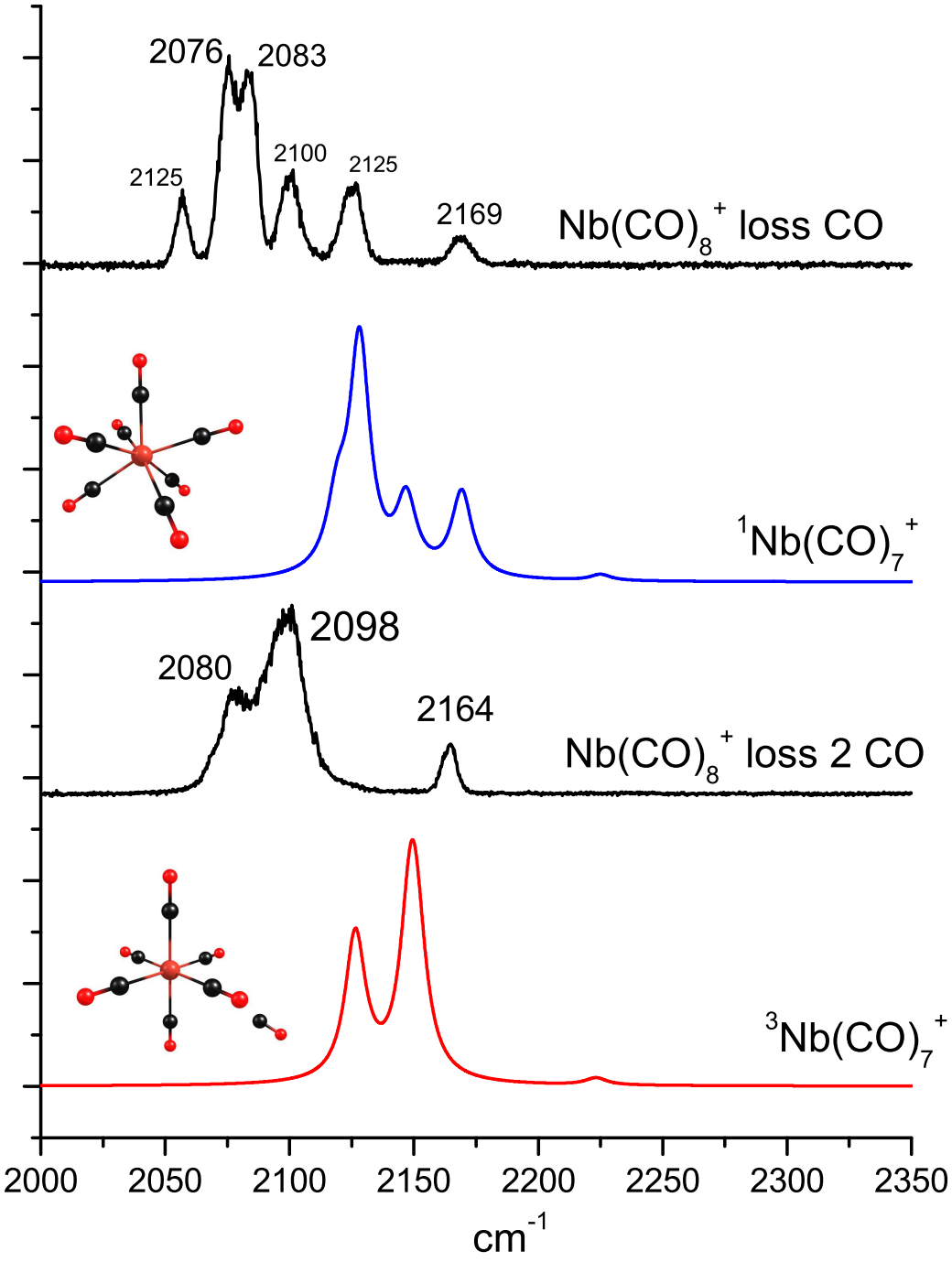

Figure 5.10: Infrared spectrum of the $Nb(CO)_8^+$ ion obtained by monitoring the loss of one CO molecule (top) and two (middle). The calculated spectra are unscaled and given a 10 cm^{-1} FWHM Lorentzian lineshape. Relative energies are in kcal/mol.

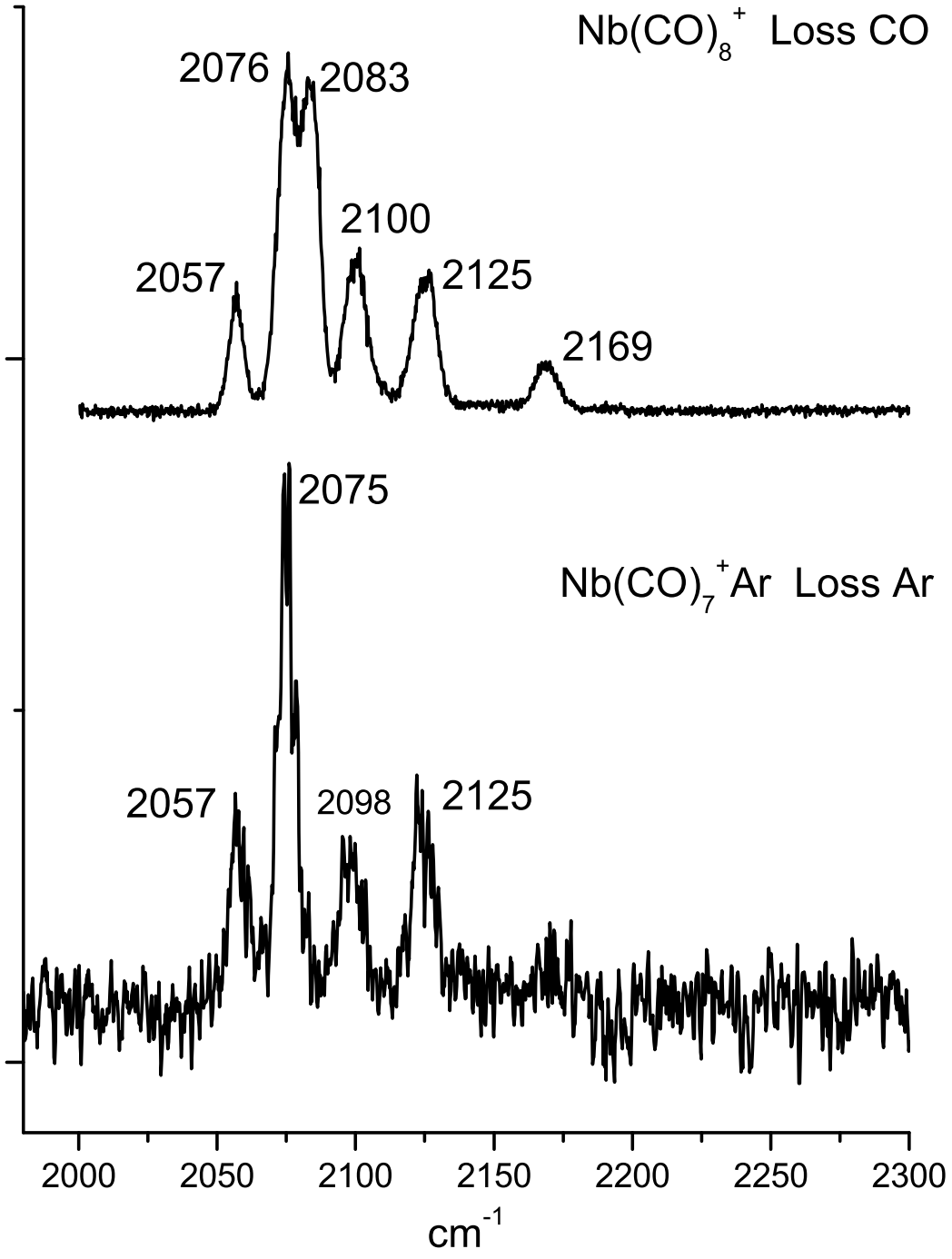

Figure 5.11: Infrared spectrum of the $Nb(CO)_7^+$ ion obtained by monitoring the loss of one CO molecule from $Nb(CO)_8^+$ (top) and by by monitoring loss of Ar from $Nb(CO)_7^+Ar$.

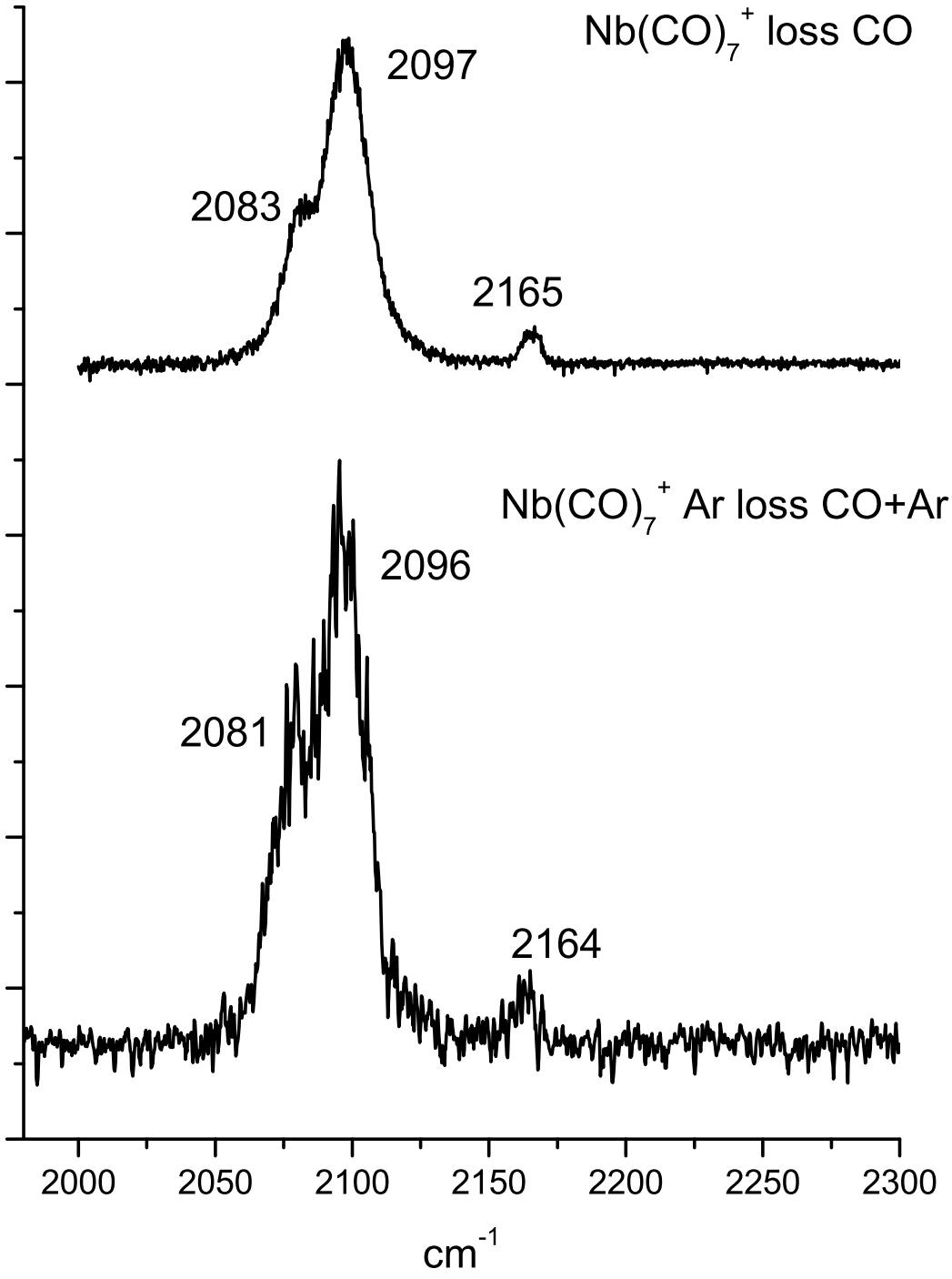

Figure 5.12: Infrared spectra of the $Nb(CO)_7^+$ ion obtained by monitoring loss of CO and $Nb(CO)_6^+Ar$ ion monitoring loss of Ar.

Chapter 6

Tantalum Carbonyl Complexes

Moving down the periodic table from vanadium we arrive at niobium which was investigated in the previous chapter. One more step down is tantalum which, like niobium, is isovalent to vanadium and has an ionic radius still larger than niobium. This metal completes our journey down the d^5 block of transition metals on the periodic table because the next element down, Dubnium, is synthetic and highly radioactive and not applicable to our laboratory studies.

This chapter demonstrates the first systematic study of cationic tantalum carbonyl complexes. In support of this work Density Funcational Theory calculations were performed using the B3LYP functional as implemented in the pcGAMESS code.[48] The def2-tzvp Effective Core Potential basis set was used for the tantalum atom, the DZP basis set for carbon and oxygen and the 6-311G(d) basis set for neon and argon. In certain cases the unscaled calculated vibrational frequencies are given a 10 cm^{-1} FWHM for comparison to experimental spectra.

The infrared spectrum of the $Ta(CO)_1^+$ ion was obtained by tagging with two neon atoms. Fragmentation was not observed using single neon tagging and the doubly tagged ion was found to fragment via elimination of both neon atoms. This fact tells us that the binding energy of a single neon atom to the $Ta(CO)_1^+$ ion is less than the energy of the infrared photon but there is too low a density of vibrational states for Intramolecular Vibrational Energy Redistribution (IVR) to be efficient enough such that fragmentation is observed on the timescale of the experiment. When the carbonyl stretch is excited rapid IVR couples the vibrational energy to other normal modes of the molecule. When enough energy reaches

the dissociation coordinate, in this case the metal neon bond, fragmentation occurs. The efficiency of this process depends on the binding energy of the neon atom and the coupling between the carbonyl stretch and the neon metal stretching mode. This is most efficient when there is a large density of vibrational states present, and for a four atom system like $Ta(CO)_1^+$ the density of vibrational states is fairly small. Addition of a second neon atom increases the vibrational state density, in this case sufficiently enough to allow fragmentation of the neon atoms on the experimental timescale ($\sim 1\mu$s).

Two peaks are observed in the $Ta(CO)_1^+Ne_2$ spectrum (shown in Figure 6.1) at 2005 and 2059 cm^{-1}. Calculated relative energetics of the various spin states is shown in Table 6.1 and predict the triplet as the lowest energy state. When two neon atoms are added the quintet becomes lowest. It is most likely that the quintet state is lowest in all cases in agreement with the previous work on vanadium and niobium, and this result is most likely an artifact of the calculation. Based on the calculated relative energetics and frequencies, the peak at 2005 cm^{-1} is tentatively assigned to the triplet state and that at 2059 to the quintet state.

Efficient fragmentation of the $Ta(CO)_2^+Ne$ ion was observed and its infrared spectrum is shown in Figure 6.2. In contrast to the niobium and vanadium systems, this spectrum consists of a single peak at 2008 cm^{-1} which is indicates the presence of one isomeric species. The observed band is just slightly to the blue of the weak peak observed at 2005 cm^{-1} in the $Ta(CO)_1^+Ne_2$ spectrum. That band was assigned to the triplet isomer, therefore this band is tentatively assigned to the triplet state. This result is in contrast to the $V(CO)_2^+$ and $Nb(CO)_2^+$ in which both the triplet and quintet states were observed.

The infrared spectrum of the $Ta(CO)_3^+$ ion obtained using neon tagging is shown at the top of Figure 6.3 along with the calculated spectra of the quintet, triplet and singlet isomers. The experimental spectrum consists of two peaks at 1973 and 2074 cm^{-1} similar to those calculated for the triplet and singlet isomers. The quintet isomer is predicted to have a planar D_{3h} structure which gives rise to a single infrared active CO band and this isomer can be eliminated from consideration. The singlet isomer is calculated to be substantially

higher in energy than the triplet isomer (see Table 6.3) and therefore the observed spectrum is assigned to the triplet state.

Each spin isomer of the $Ta(CO)_4^+$ is predicted to have a single infrared active CO band while the infrared spectrum of this ion obtained using neon tagging has three peaks as shown in Figure 6.4. This is similar to what was observed for the $Nb(CO)_2^+$ ion which was assigned to three distinct spin states. The best assignment we can make based on the current data is to assign each peak to a different spin state. It is unclear why we would observe one spin state for the $Ta(CO)_3^+$ system and multiple isomers in the $Ta(CO)_4^+$ system.

The infrared spectrum of the $Ta(CO)_5^+Ne$ ion is shown at the top of Figure 6.5 and consists of three peaks at 2023, 2061 and 2080 cm^{-1}. The calculated spectrum of the triplet isomer (red trace) matches this, having two bands with similar intensity to the 2061 and 2023 cm^{-1} bands but with slightly smaller splitting than observed. The shoulder at 2080 cm^{-1} could be due to the quintet isomer or an anharmonic effect such as a Fermi Resonance. The calculations were preformed without the neon tag atom which might account for the discrepancy between the observed and calculated splitting.

The $Ta(CO)_6^+Ne$ complex was not generated in sufficient abundance for our studies, so argon tagging was used and the spectrum shown in Figure 6.6 was obtained. It consists of a single intense peak at 2081 cm^{-1} with a weaker feature at 2046 cm^{-1}. The 2081 cm^{-1} feature is similar to that observed for the $V(CO)_6^+$ and $Nb(CO)_6^+$ ions (Figures 4.6 and 5.8) both of which were assigned to the triplet spin state. The $V(CO)_6^+$ and $Nb(CO)_7^+$ ions both had a peak at 2097 cm^{-1}, 16 cm^{-1} to the blue of the band observed for $Ta(CO)_6^+$ so there is the possibility that the shift is caused by the presence of the singlet isomer in the tantalum system. As will be subsequently discussed, the $Ta(CO)_7^+Ar$ system exhibited two distinct isomers similar to what was observed for $Nb(CO)_7^+Ar$ which are assigned to the triplet and singlet isomers. The spectrum assigned to the triplet isomer has a band at 2081 cm^{-1}, the same position as the band observed here. Therefore this spectrum is assigned to

the triplet isomer, the 16 cm^{-1} shift is due to differences carbonyl binding in the tantalum and vanadium and niobium ions.

In contrast to the niobium and vanadium systems, we were unable to fragment the $Ta(CO)_7^+$ ion. The $Ta(CO)_8^+$ ion was found to efficiently fragment via elimination of a single CO and the infrared spectrum is shown in Figure 6.7. This spectrum is similar to that observed for the $Nb(CO)_8^+$ ion with the exception of the band assigned to the triplet isomer in the niobium system. The experimental spectrum matches well with that calculated for the singlet seven coordinate species. This indicates that the $Ta(CO)_7^+$ ion consists of only the single seven coordinate species.

Similar to the $Nb(CO)_7^+Ar$ system, the $Ta(CO)_7^+Ar$ ion was found to fragment via elimination of argon and argon and CO. The spectrum observed monitoring the argon loss channel is shown at the bottom of Figure 6.8 and matches well with the spectrum of $Ta(CO)_8^+$. Monitoring loss of argon and CO gives a spectrum similar to that observed for the $Ta(CO)_6^+$ ion (Figure **??**), therefore this spectrum is assigned to the triplet isomer. The band at 2063 cm^{-1} in this spectrum is assigned to a surface carbonyl while the band at 2046 cm^{-1} in the $Ta(CO)_6^+Ar$ spectrum is not observed. This lends credence to our previous assignment of this band to a different isomer. It is interesting that in the $Ta(CO)_8^+$ system only the singlet seven coordinate isomer was observed but both isomers were observed in the $Ta(CO)_7^+Ar$ system. Argon binding to a fully coordinated ion is a very weak interaction, therefore argon complexes are only formed under very cold formation conditions. If there is a barrier to form the seven coordinate species the argon tagged complex might not have enough internal energy to overcome it. This might be why the triplet isomer is observed when in the $Ta(CO)_7^+Ar$ system.

In conclusion we have generated tantalum carbonyl cations beginning with one CO ligand and up though the coordination sphere which we have determined to be seven carbonyls for the singlet isomer and six for the triplet. The singlet six coordinate species was only observed when an argon was complexed with the $Ta(CO)_7^+$ ion.

Table 6.1: Energetics and Vibrational Frequencies of $Ta(CO)_1^+$ ions

Species	Relative Energy kcal/mol (absolute)	IR frequencies cm^{-1} (int. km/mol)
$^5Ta(CO)_1^+$	+1.1 (-169.9530385)	2090(634)
$^3Ta(CO)_1^+$	+0.0 (-169.9548307)	2045(634)
$^1Ta(CO)_1^+$	+26.4 (-169.9128176)	2026(735)
$^5Ta(CO)_1^+Ne_2$	+0.0 (-427.9168319)	
$^3Ta(CO)_1^+Ne_2$	+24.9 (-427.8770861)	
$^1Ta(CO)_1^+Ne_2$	+34.8 (-427.8614170)	

Table 6.2: Energetics and Vibrational Frequencies of $Ta(CO)_2^+$ ions

Species	Relative Energy kcal/mol (absolute)	IR frequencies cm^{-1} (int. km/mol)
$^5Ta(CO)_2^+$	+0.0 (-283.3732800)	2144(1765)
$^3Ta(CO)_2^+$	+15.4 (-283.3486825)	2093(1948)
$^1Ta(CO)_2^+$	+33.1 (-283.3205838)	2059(2147)
$^5Ta(CO)_2^+Ne$	+0.0 (-412.3355706)	2143(1771)
$^3Ta(CO)_2^+Ne$	+20.3 (-412.3031283)	2066(2240)
$^1Ta(CO)_2^+Ne$	+29.9 (-412.2879076)	2056(2159)

Table 6.3: Energetics and Vibrational Frequencies of $Ta(CO)_3^+$ ions

Species	Relative Energy kcal/mol (absolute)	IR frequencies cm^{-1} (int. km/mol)
$^5Ta(CO)_3^+$	+16.1 (-396.7659345)	2097(761), 2144(1779)
$^3Ta(CO)_3^+$	+0.0 (-396.7915296)	2056(896), 2058(1631), 2149(216)
$^1Ta(CO)_3^+$	+20.3 (-396.7591893)	2052(2958), 2145(139)
$^5Ta(CO)_3^+Ne$	+37.3 (-525.7025515)	2085(2578)
$^3Ta(CO)_3^+Ne$	+0.0 (-525.7620547)	2049(1008), 2053(989), 2138(266)
$^1Ta(CO)_3^+Ne$	+25.4 (-525.7215883)	2058(2789), 2145(135)

Table 6.4: Energetics and Vibrational Frequencies of $Ta(CO)_4^+$ ions

Species	Relative Energy kcal/mol (absolute)	IR frequencies cm^{-1} (int. km/mol)
$^5Ta(CO)_4^+$	+8.1 (-510.1502108)	2120(3338), 2125(507)
$^3Ta(CO)_4^+$	+4.2 (-510.1563806)	2110(3592)
$^1Ta(CO)_4^+$	+0.0 (-510.1631161)	2088(4526)

Table 6.5: Energetics and Vibrational Frequencies of $Ta(CO)_5^+$ ions

Species	Relative Energy kcal/mol (absolute)	IR frequencies cm^{-1} (int. km/mol)
$^5Ta(CO)_5^+$	+18.5 (-623.5490361)	2107(2282), 2165(1145)
$^3Ta(CO)_5^+$	+0.0 (-623.5784572)	2110(735), 2139(1682), 2133(1576), 2147(80.2)
$^1Ta(CO)_5^+$	+12.8 (-623.5579930)	2098(520), 2104(2704), 2132(1238), 2202(35)

Table 6.6: Energetics and Vibrational Frequencies of $Ta(CO)_6^+$ ions

Species	Relative Energy kcal/mol (absolute)	IR frequencies cm^{-1} (int. km/mol)
$^5Ta(CO)_6^+$	+53.3 (-736.8688180)	2093(2324), 2153(1149), 2223(80)
$^3Ta(CO)_6^+$	+3.7 (-736.9479306)	2130(4564)
$^1Ta(CO)_6^+$	+0.0 (-736.9538286)	2139(3465), 2144(1001)

Table 6.7: Energetics and Vibrational Frequencies of $Ta(CO)_7^+$ ions

Species	Relative Energy kcal/mol (absolute)	IR frequencies cm^{-1} (int. km/mol)
$^5Ta(CO)_7^+$	+78.3 (-850.2038229)	2090(2282), 2121(33), 2152(1162), 2220(51), 2222(106)
$^3Ta(CO)_7^+$	+28.6 (-850.2830329)	2116(1656), 2134(2873), 2140(51), 2224(76)
$^1Ta(CO)_7^+$	+0.0 (-850.3285419)	2155(706), 2123(2620), 2139(841), 2158(465), 2161(461), 2223(50)

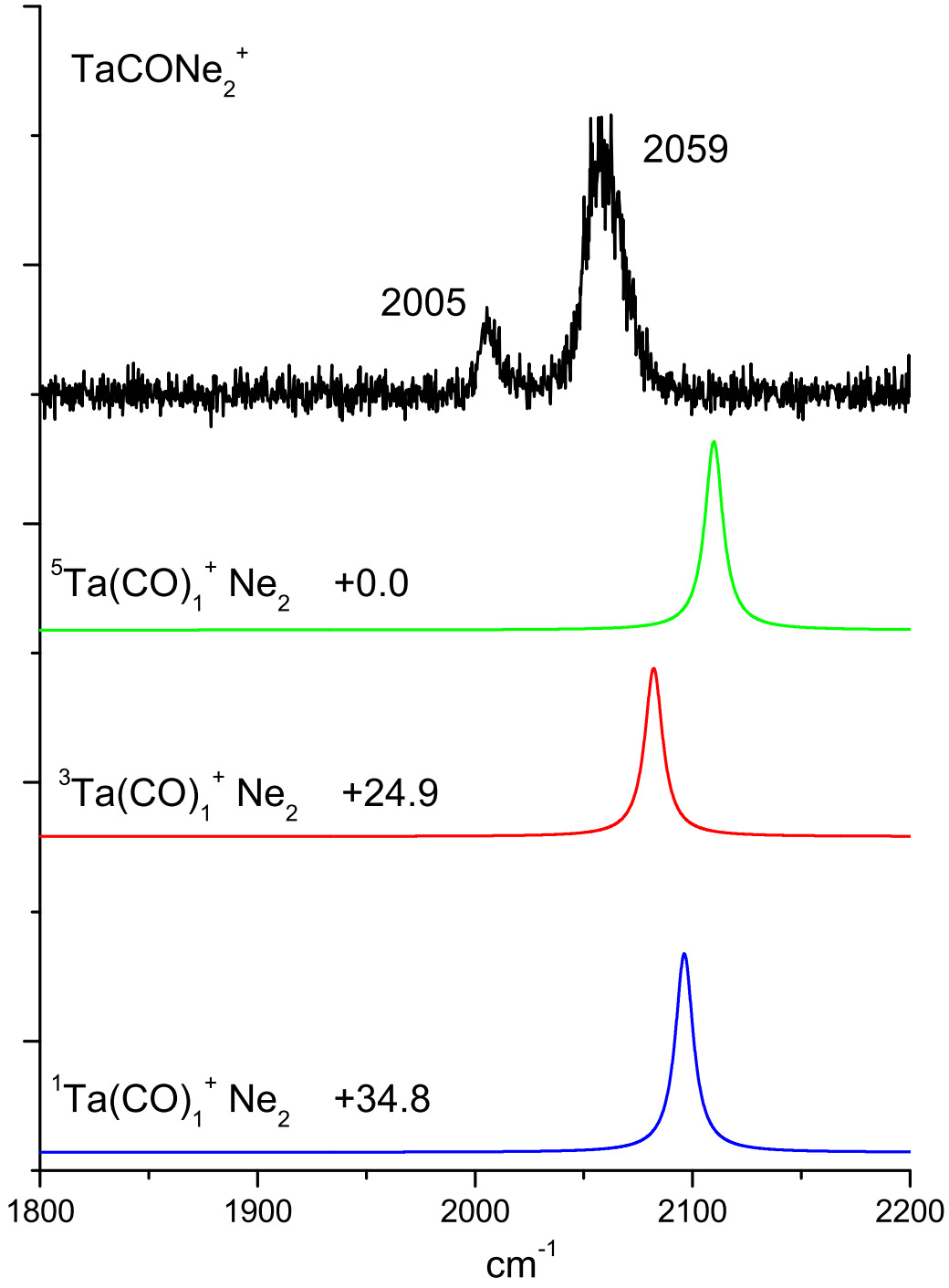

Figure 6.1: infrared spectrum of the $TaCO^+$ ion obtained using neon tagging. The calculated spectra are unscaled and given a 10 cm^{-1} FWHM Lorentzian lineshape. Relative energetics are in kcal/mol.

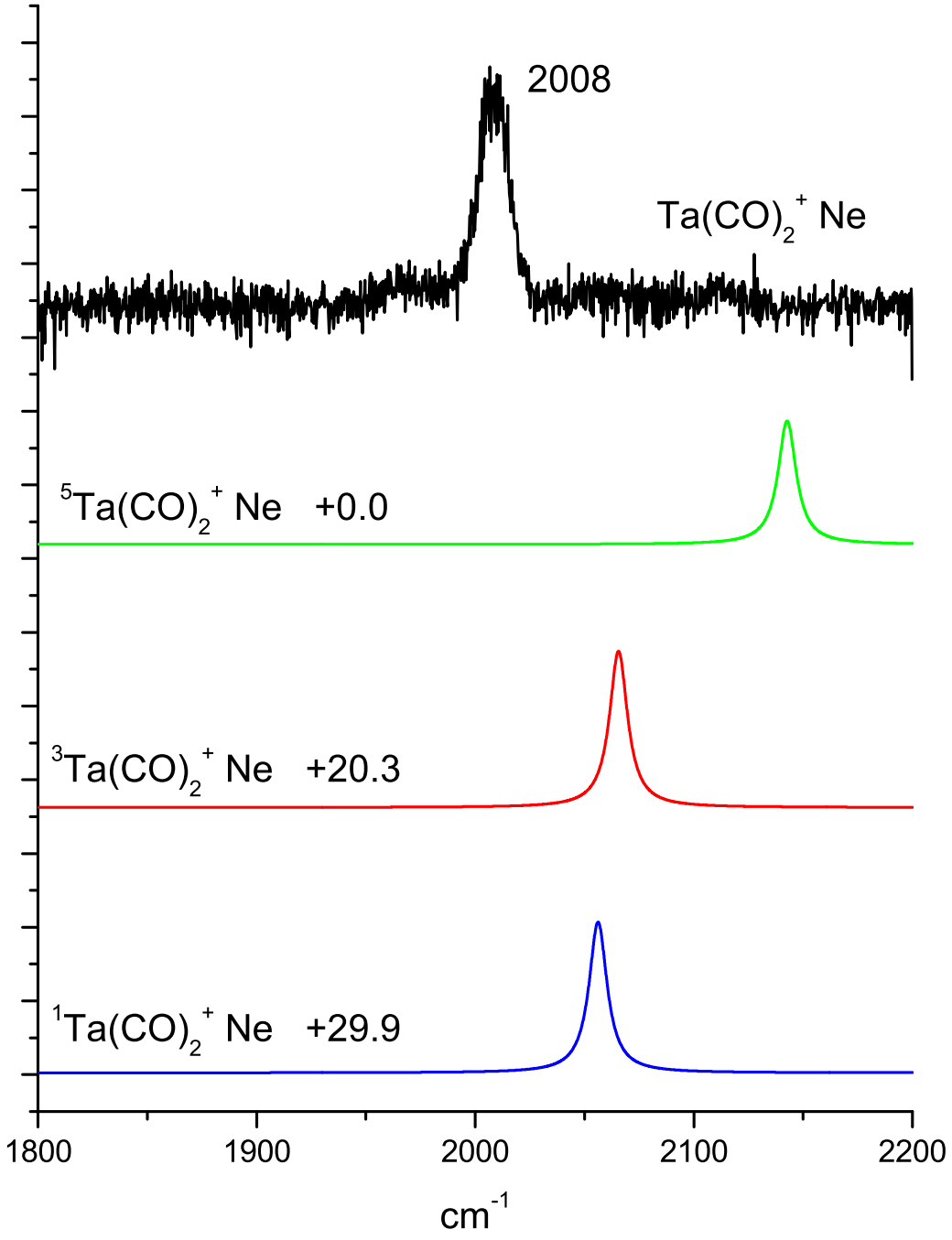

Figure 6.2: infrared spectrum of the $Ta(CO)_2^+$ ion obtained using neon tagging. The calculated spectra are unscaled and given a 10 cm^{-1} FWHM Lorentzian lineshape. Relative energetics are in kcal/mol.

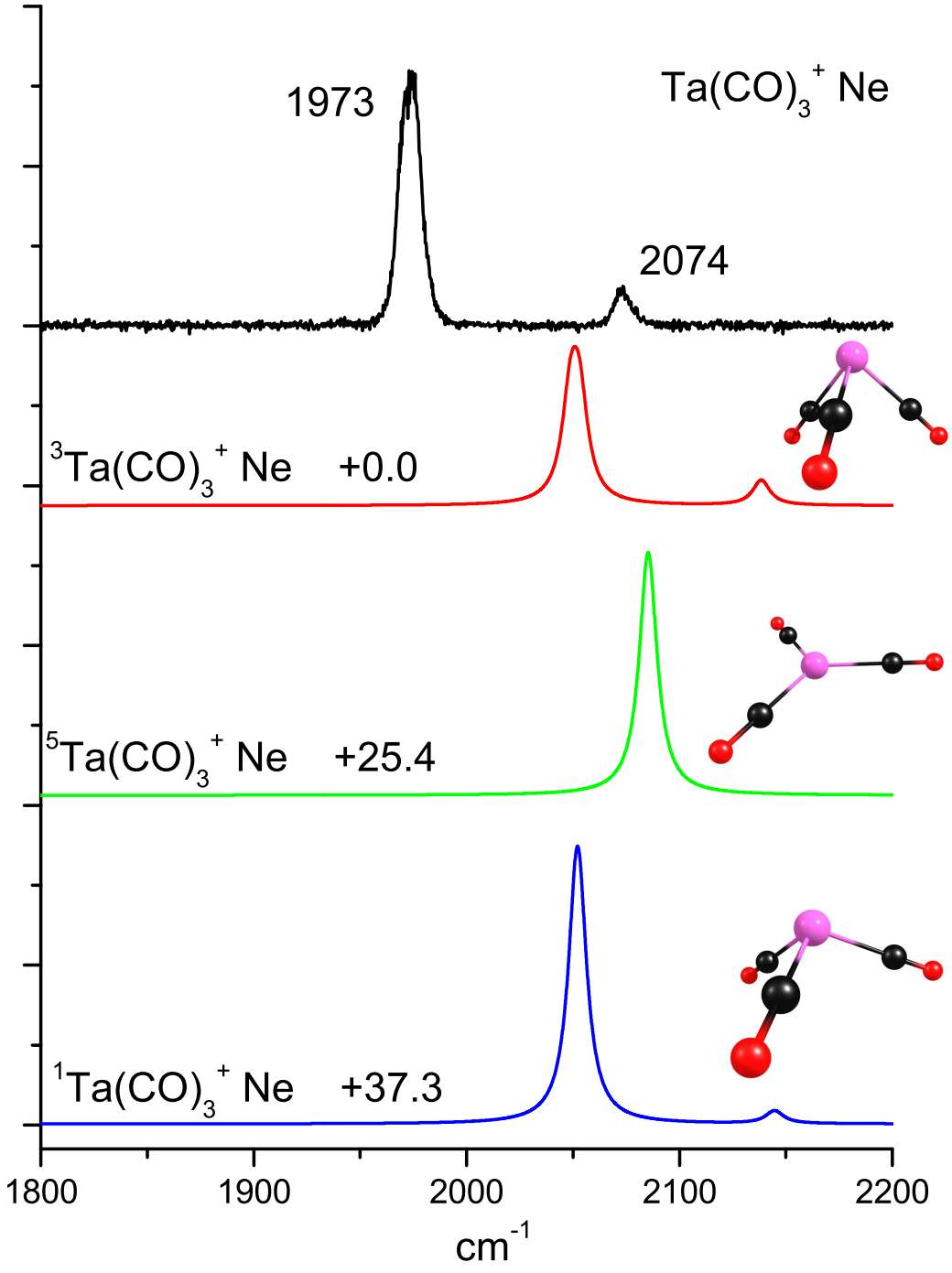

Figure 6.3: infrared spectrum of the $Ta(CO)_3^+$ ion obtained using neon tagging. The calculated spectra are unscaled and given a 10 cm^{-1} FWHM Lorentzian lineshape. Relative energetics are in kcal/mol.

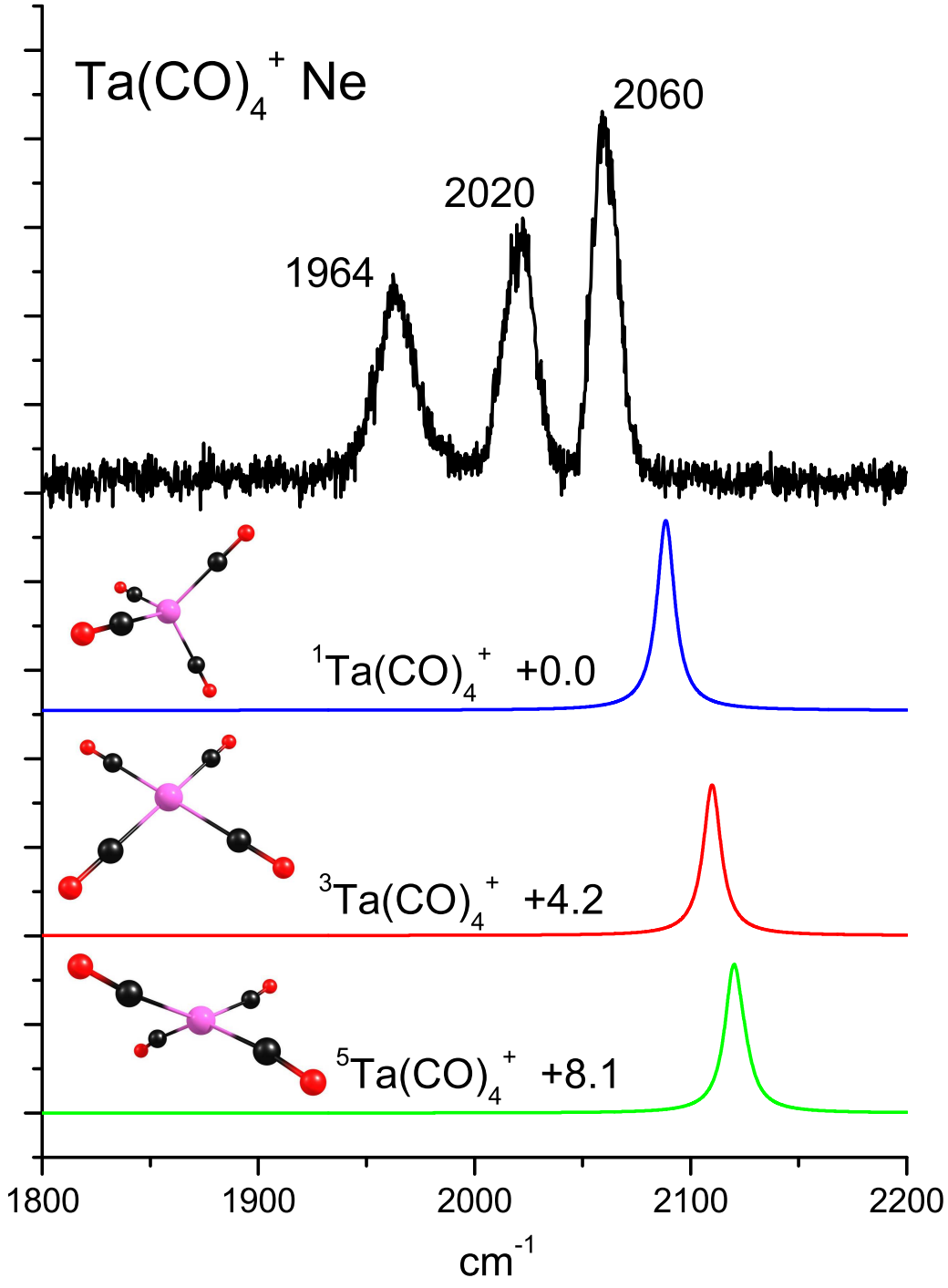

Figure 6.4: Infrared spectrum of the $Ta(CO)_4^+$ ion obtained using neon tagging. The calculated spectra are unscaled and given a 10 cm^{-1} FWHM Lorentzian lineshape. Relative energetics are in kcal/mol.

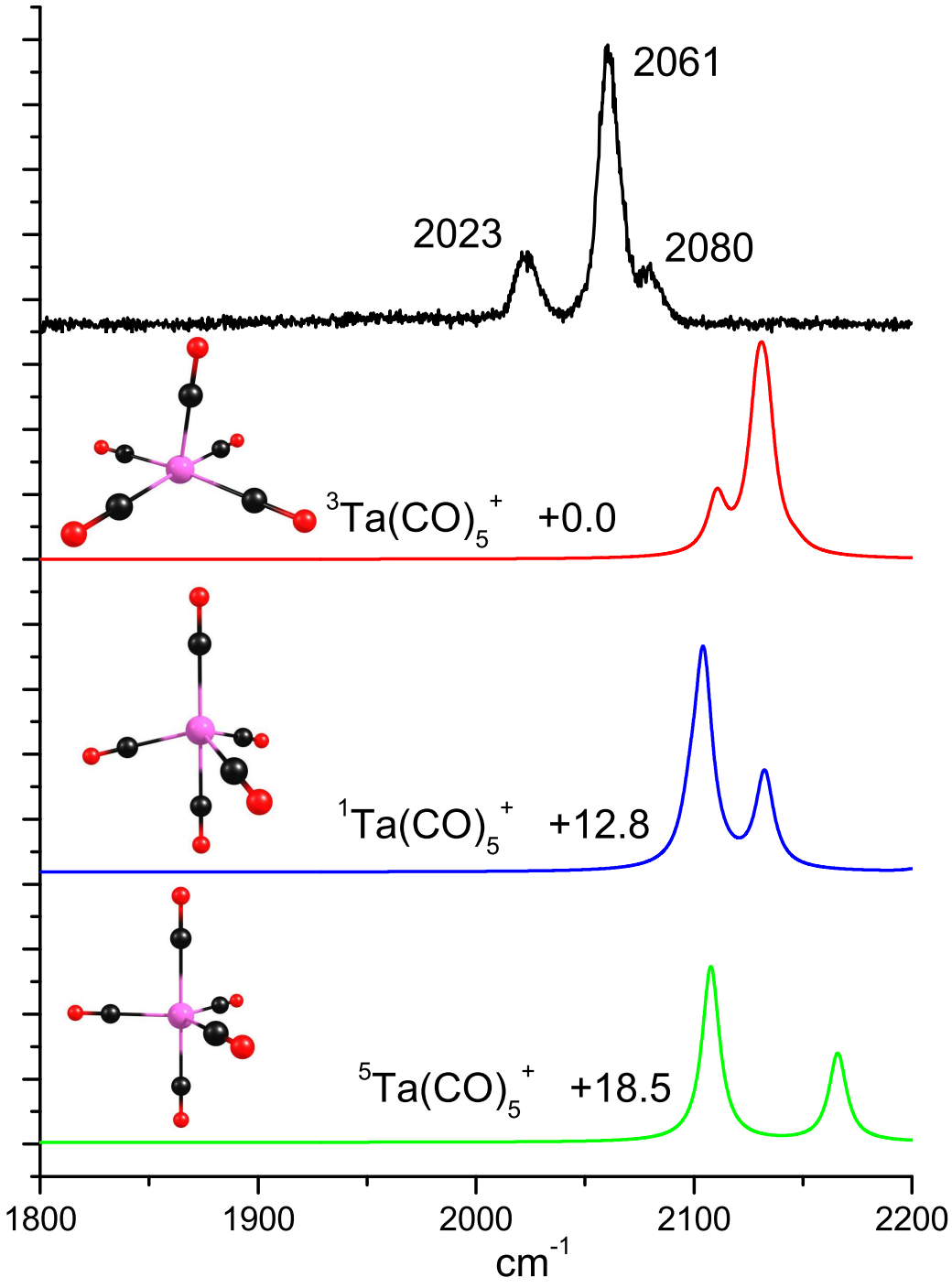

Figure 6.5: Infrared spectrum of the $Ta(CO)_5^+$ ion obtained using neon tagging. The calculated spectra are unscaled and given a 10 cm^{-1} FWHM Lorentzian lineshape. Relative energetics are in kcal/mol.

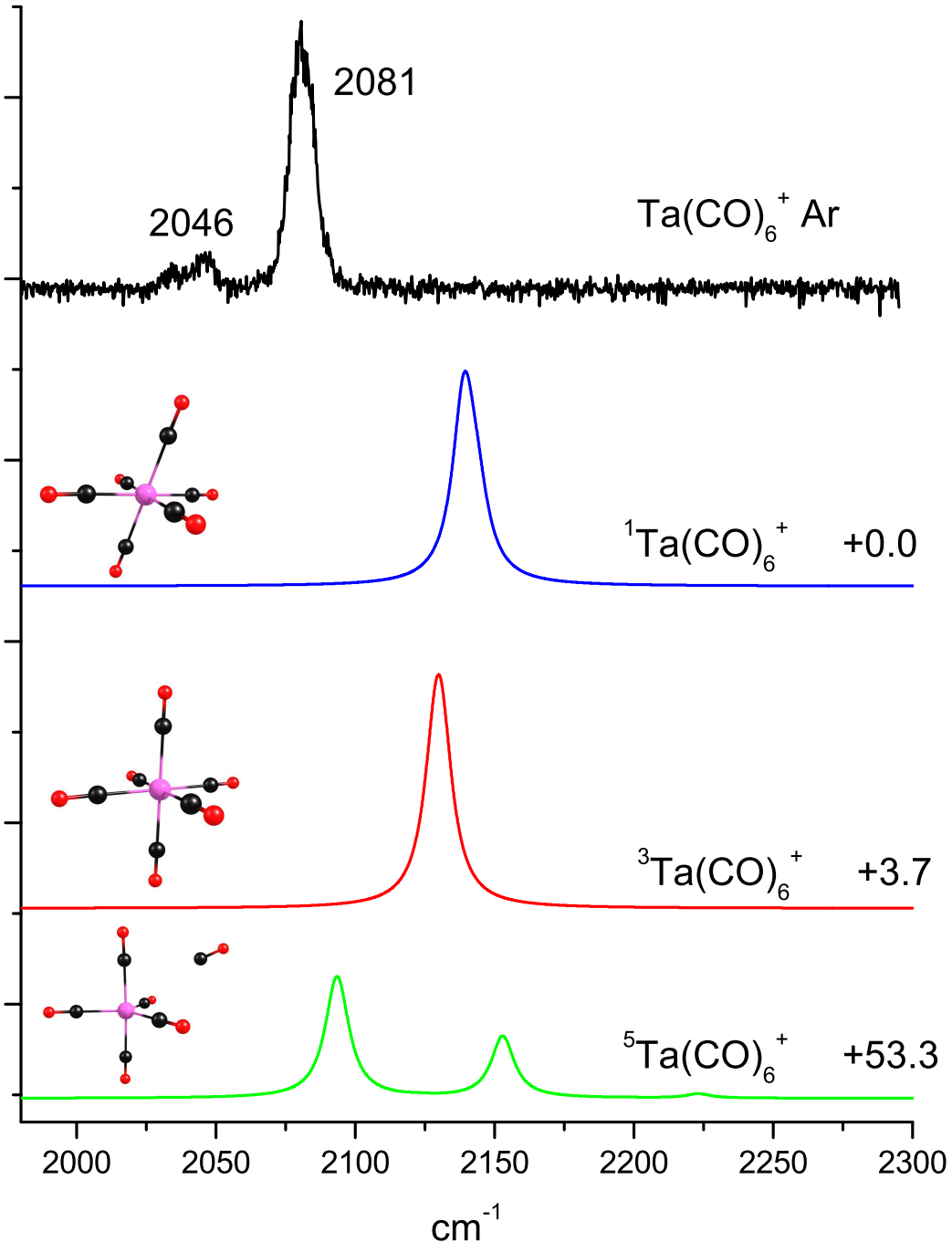

Figure 6.6: Infrared spectrum of the $Ta(CO)_6^+$ ion obtained using argon tagging. The calculated spectra are unscaled and given a 10 cm^{-1} FWHM Lorentzian lineshape. Relative energetics are in kcal/mol.

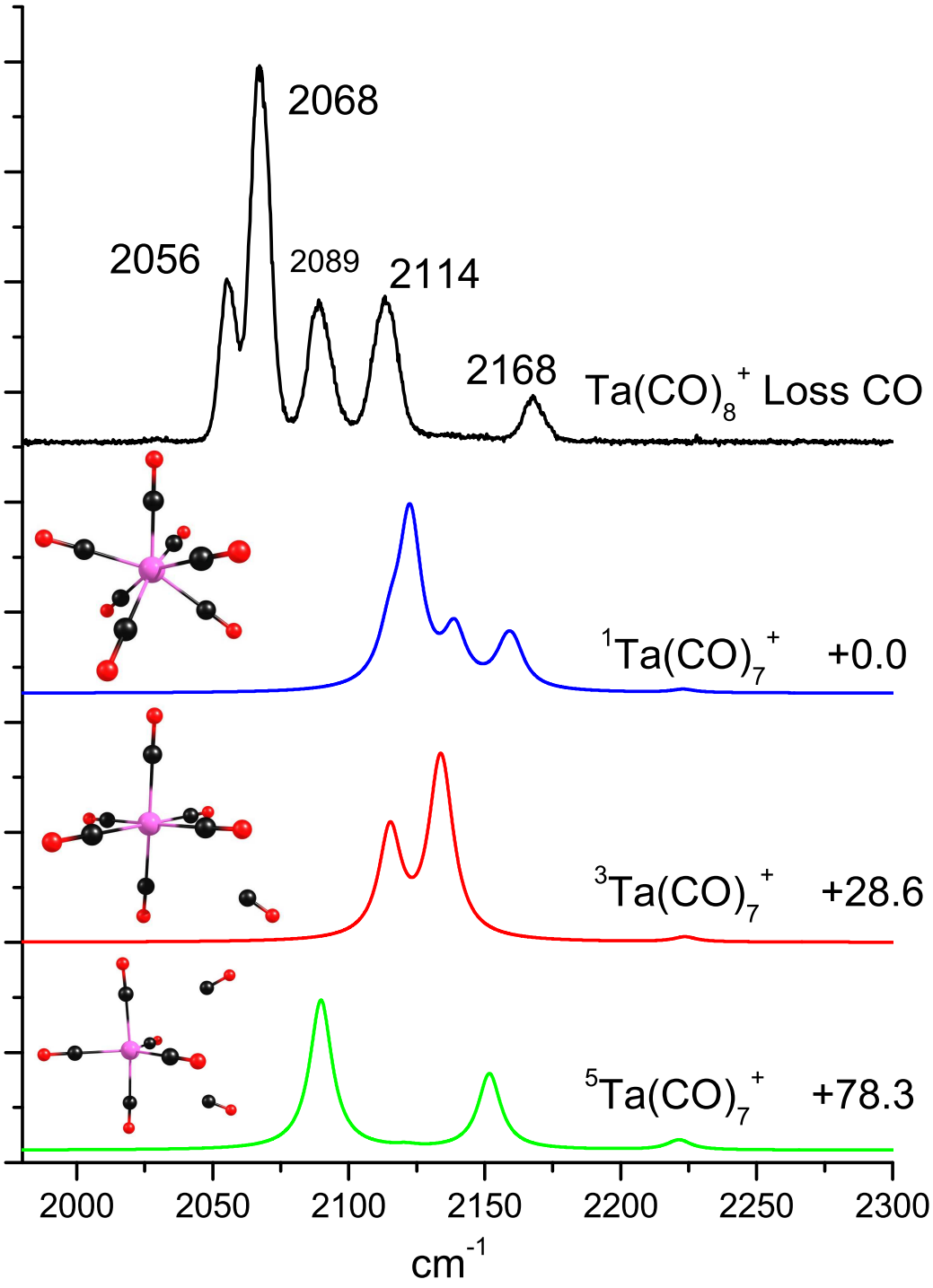

Figure 6.7: Infrared spectrum of the $Ta(CO)_8^+$ ion by monitoring elimination of a single CO. The calculated spectra are unscaled and given a 10 cm^{-1} FWHM Lorentzian lineshape. Relative energetics are in kcal/mol.

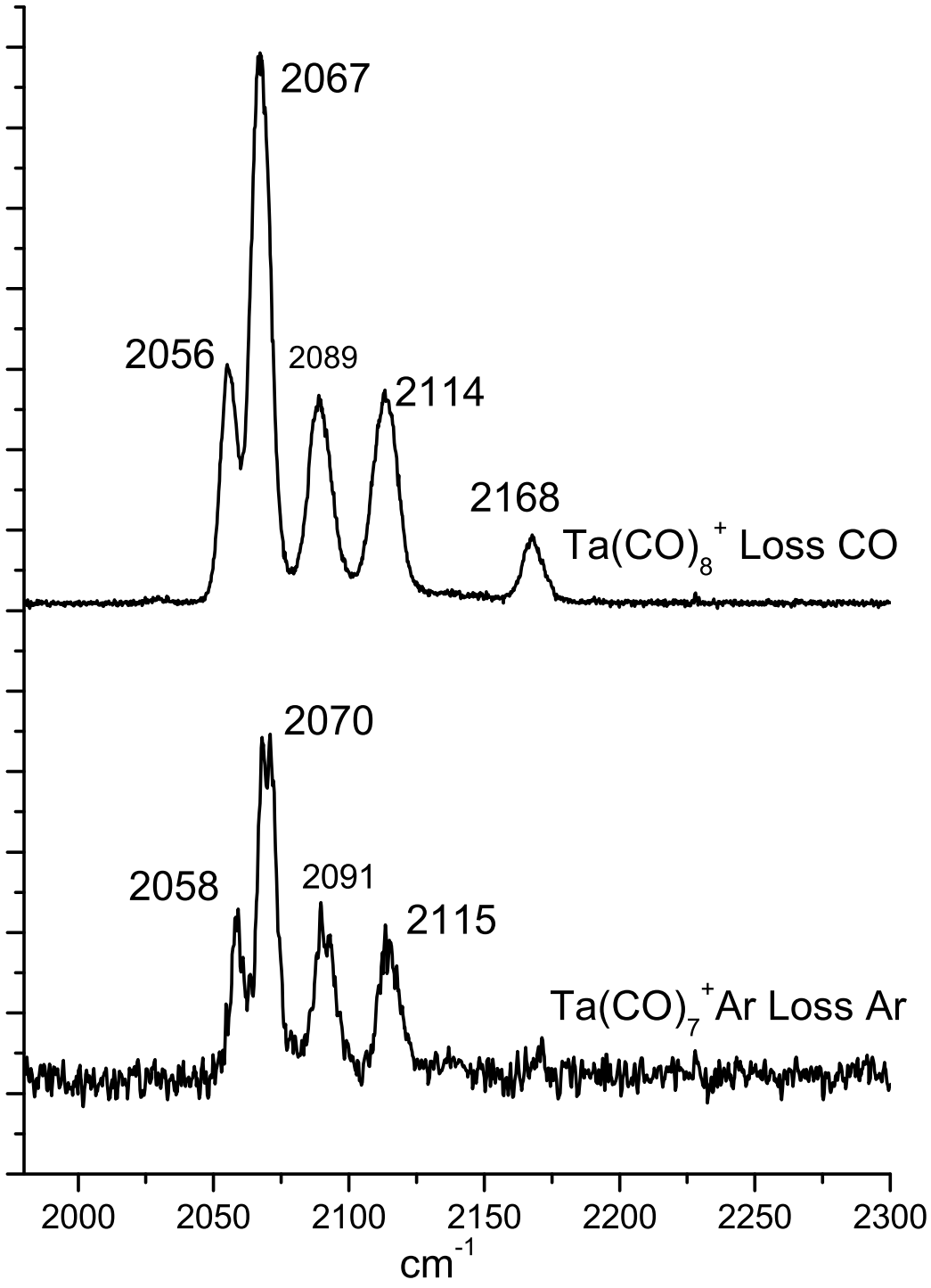

Figure 6.8: Infrared spectra of the $Ta(CO)_8^+$ $Ta(CO)_7^+Ar$ ions. The top spectrum was obtained by monitoring elimination of CO, the bottom spectrum by monitoring loss of Ar.

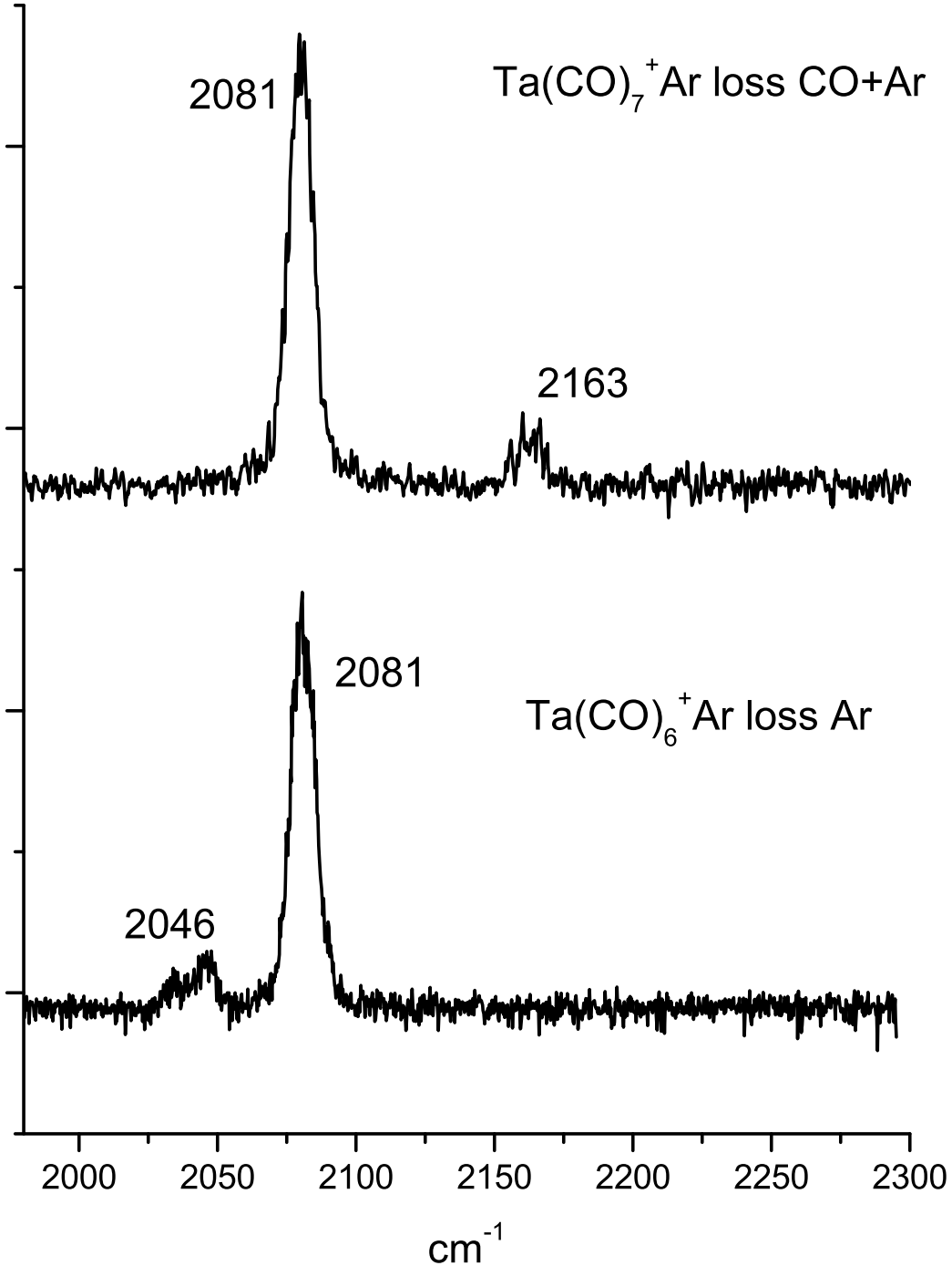

Figure 6.9: Infrared spectra of the $Ta(CO)_7^+Ar$ and $Ta(CO)_6^+Ar$ ions. The top spectrum was obtained by monitoring loss of CO and Ar from $Ta(CO)_7^+Ar$, the bottom loss of Ar from $Ta(CO)_6^+Ar$

Chapter 7

Uranium and Uranium Oxide Carbonyl Complexes

The structure of solvated uranium ions is an active area of research due to uranium use in power generation and concerns over its environmental impact.[64] In aqueous environments uranium commonly exists as the UO_2^{2+} ion which is known to have a closed shell $^1\Sigma_g^+$ electronic structure.[65] Extended X-ray Absorption Fine Structure measurements of UO_2^{2+} cations in aqueous condensed phase solutions reveal D_{5h} pentagonal bipyramidal $UO_2(H_2O)_5^{2+}$ structures;[66,67] reduction of the uranium generates eight-coordinate $U(H_2O)_8^{4+}$ ions. Recently singly charged UO_2^+ ions have been studied in the gas phase using a combination of mass spectrometric and spectroscopic techniques.[68,69,70,71] This work has led to the conclusion that the ground state is $^2\Phi(5/2_u)$.[71] Infrared spectroscopic work has been done on UO_2^+ with various ligands attached using a Free Electron Laser and Infrared Multiphoton Dissociation but the resulting spectra were very broad and definite structural assignments were tenuous at best. Although there has been significant previous work on structure and spectroscopy of coordinated uranium ions there have been no gas phase studies of uranium carbonyl complexes and almost no studies of coordination to the bare U^+ ion. In the present study we report the first IR spectra of U^+ and UO_2^+ carbonyl complexes.

In traditional inorganic chemistry the structure and bonding of transition metal complexes is usually dictated by the 18-electron rule, this being the number required to give the metal a $s^2p^6d^{10}$ noble gas configuration. The previous chapters have investigated carbonyl systems where this rule plays an important role in determining the structure of the fully coordinated ion, even if it requires coordination up to seven carbonyl molecules. For members of the actinide and lanthanide series, where the f orbitals become accessible, a $s^2p^6d^{10}f^{14}$ noble

gas configuration would require 32 electrons. Steric effects preclude coordination numbers sufficient to achieve this configuration. The d orbitals in actinide elements are sufficiently high in energy that they do not participate in bonding, therefore stable actinide complexes generally have 22 electron configurations such as (η^8-C_8H_8)$_2$U diooctatetraenyluranium.[72] The uranium cation has five valence electrons so it cannot form the 22-electron complex with carbonyl ligands, although it could possibly form the 21 or 23-electron complex which would also be expected to be stable. To extend the previous work into coordination of carbonyls we have investigated the binding of carbonyl ligands to the U^+ and UO_2^+ cations and found that both form highly symmetric complexes.

A mass spectrum typical for this experiment is shown in Figure 7.1. There is a clear preference for formation of $U(CO)_8^+$ over other cluster sizes. The inset at the top of Figure 7.1 shows so-called infrared breakdown spectrum of the mass selected $U(CO)_{10}^+$ obtained by subtracting a mass spectrum with the fragmentation infrared laser off from one with it on. There again is a clear preference for formation of the $U(CO)_8^+$ ion, another indication of its inherent stability. Breakdown spectra of still larger clusters show a similar preference for $U(CO)_8^+$. The mass spectrum shown at the bottom of Figure 7.1 shows mainly a progression of $UO_2(CO)_n^+$ ions and indicates a preference for $UO_2(CO)_5^+$ formation. The breakdown spectrum of $UO_2(CO)_7^+$ (inset) supports this.

The infrared spectra of the $U(CO)_8^+$ and $UO_2(CO)_5^+$ ions were obtained by monitoring loss of CO from the parent ion and are shown in Figure 7.2 along with predicted structures and spectra. The spectrum of the $U(CO)_8^+$ ion shows a single peak which is indicative of a high symmetry structure which suggests an eight-coordinate doublet D_{4d} structure. The single peak is shifted 43 cm^{-1} to the red of the gas phase carbon monoxide stretch, an indication of significant π donation from the uranium ion weakening the CO bond. The spectrum of the $UO_2(CO)_5^+$ ion also consists of a single peak again indicative of a high symmetry structure. The proposed D_{5h} ion has a similar structure to that calculated for the $UO_2(CO)_5^{2+}$ ion[73] as well as to that observed[67] and predicted[74] for the $UO_2(H_2O)_5^{2+}$ in aqueous solution. The CO

stretch is observed 51 cm^{-1} to the blue from the gas phase carbon monoxide stretch and 114 cm^{-1} from the $U(CO)_8^+$ ion. This indicates a lack of π interaction between the metal atom and the CO ligands, consistent with the high oxidation state of uranium ion. The large blue shift is therefore attributed to a purely electrostatic interaction between the core ion and the carbonyl ligands similar to what we have observed previously.[75]

Much of the previous work on uranium complexes has involved uranium in a high oxidation state, usually +4 and +6.[76] The current study of the $U(CO)_8^+$ ion provides a unique opportunity to study a uranium with formal +1 oxidation state in an inorganic complex. Binding of ligands to f-block elements provides a contrast to transitional metal interactions because there is a 60° angle between lobes in f orbitals compared to 90° in d orbitals.[77] Interestingly the CO vibration in $U(CO)_8^+$ occurs at a frequency similar to what we have observed in transition metal carbonyl complexes.[75,78]

While conducting this work we were able to generate a large array of uranium oxide carbonyl complexes, a compilation of the infrared spectra of these larger complexes is shown in Figure 7.3. The top frame shows the infrared spectrum of $U(CO)_{10}^+$ which is similar to that for $U(CO)_8^+$ in Figure 7.2 with the exception of the band at 2060 cm^{-1} which is assigned to second sphere carbonyl ligands. The spectrum of $UO(CO)9^+$ has a band at 832 cm^{-1} which is the UO stretch previously observed at 911.9 cm^{-1} for the ion in a rare gas matrix.[79] The carbonyl stretching region is much more congested indicating this ion is lower symmetry those previously investigated and a definite structural assignment is not currently possible. The bands in this spectral region are on top of a broad underlying continuum which we have assigned to an electronic transition, the apparent dips in this continuum around 2350 cm^{-1} are due to atmospheric CO_2 absorption affecting the laser power.

The spectrum of the $UO_2(CO)_7^+$ ion (third from top in Figure 7.3 has a band at 2096 cm^{-1} similar in position to that observed for the $UO_2(CO)_5^+$ ion (Figure 7.2 with an additional band at 2158 cm^{-1} which is assigned to second sphere CO ligands. The feature at 939 cm^{-1} is assigned to the asymmetric O-U-O stretch of the core UO_2^+ which was previously identified

at 980 cm^{-1} in a neon matrix.[68] The spectrum of the $UO_4(CO)_6^+$ ion shown at the bottom of Figure 7.3 is similar to that of $UO_2(CO)_7$ in the carbonyl region and is assigned similarly. The O-U-O asymmetric stretch is observed at 981 cm^{-1} and there is an equally intense feature at 1181 cm^{-1} which is near the O-O stretching band of the O_2^- anion (1084 cm^{-1}).[80] There are also weaker features observed at 898 cm^{-1} and 1870 cm^{-1}. The 898 cm^{-1} band is assigned to the normally IR inactive O-U-O symmetric stretch previously observed at 921 cm^{-1} in the gas phase using photoelectron spectroscopy.[71] The 1870 cm^{-1} feature is attributed to a combination between the asymmetric and symmetric stretches. The appearance of the normally IR inactive symmetric stretch indicates that this ion is distorted from linearity and the appearance of the O_2^- anionic band indicates that the additional O_2 is strongly bound and carries a formal negative charge.

A recent DFT study of the UO_4^+ cation concluded that O_2 binds to the uranium atom in the linear UO_2^+ ion in an η^2 fashion to form a superperoxo ion.[77] We studied this ion using argon tagging and spectra of the $UO_4Ar_2^+$ and $UO_6Ar_2^+$ ions are shown in Figure 7.4. The spectrum of the $UO_4Ar_2^+$ ion is similar to that of $UO_4(CO)_6^+$ with the bands being slightly blue shifted and matches well with the calculated bands (vertical bars) for the η^2 structure.[77] The 1013 and 1169 cm^{-1} bands in the $UO_6Ar_2^+$ spectrum are similar to those observed for $UO_4Ar_2^+$, however we do not observe the 930 cm^{-1} symmetric O-U-O stretching feature. This indicates that the O-U-O core has become more linear and the IR activity of this mode has decreased to the extent that we can no longer observe it. The feature 1554 cm^{-1} is near the free O_2 stretching frequency of 1580 cm^{-1}. This all indicates that O_2 binds to UO_4^+ end on in an η^1 fashion causing the O-U-O core to become more linear and giving the O_2 stretch weak IR intensity.

This work presents the first gas phase measurements of U^+ and UO_2^+ carbonyl complexes. The $UO_2(CO)_5^+$ ion was found to have a D_{5h} structure similar to that of $UO_2(H_2O)_5^{2+}$ observed in aqueous solution. A novel eight-coordinate 21-electron $U(CO)_8^+$ complex was found to have high symmetry in agreement with theoretical calculations. The UO_4^+ superoxo

cation was identified spectroscopically for the first time and shown that the coordinating O_2 ligand carries a formal negative charge. The UO_6^+ ion was found to consist of a strongly bound UO_4^+ core with a weakly coordinating O_2 ligand.

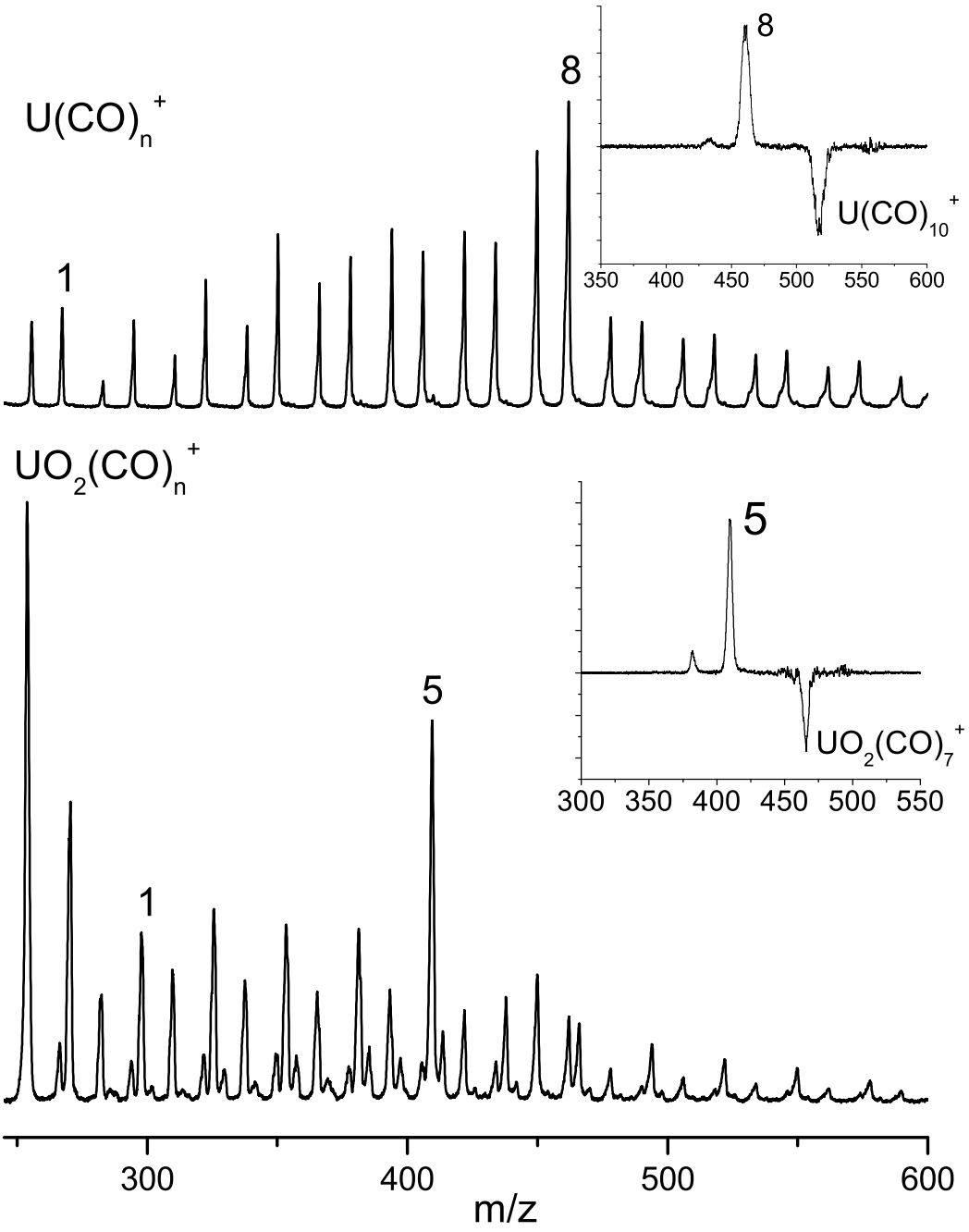

Figure 7.1: Mass spectrum of uranium carbonyl and uranium oxide carbonyl ions. The mass spectrum at top shows a progression of $U(CO)_n^+$ with the peaks in between being $UO(CO)_n^+$. The bottom mass spectrum shows predominantly $UO_2(CO)_n^+$ ions with $UO(CO)_n^+$ and $UO_n(CO)_n^+$ ions also present. The insets show infrared breakdown spectra for the $U(CO)_{10}^+$ and $UO_2(CO)_7^+$ ions.

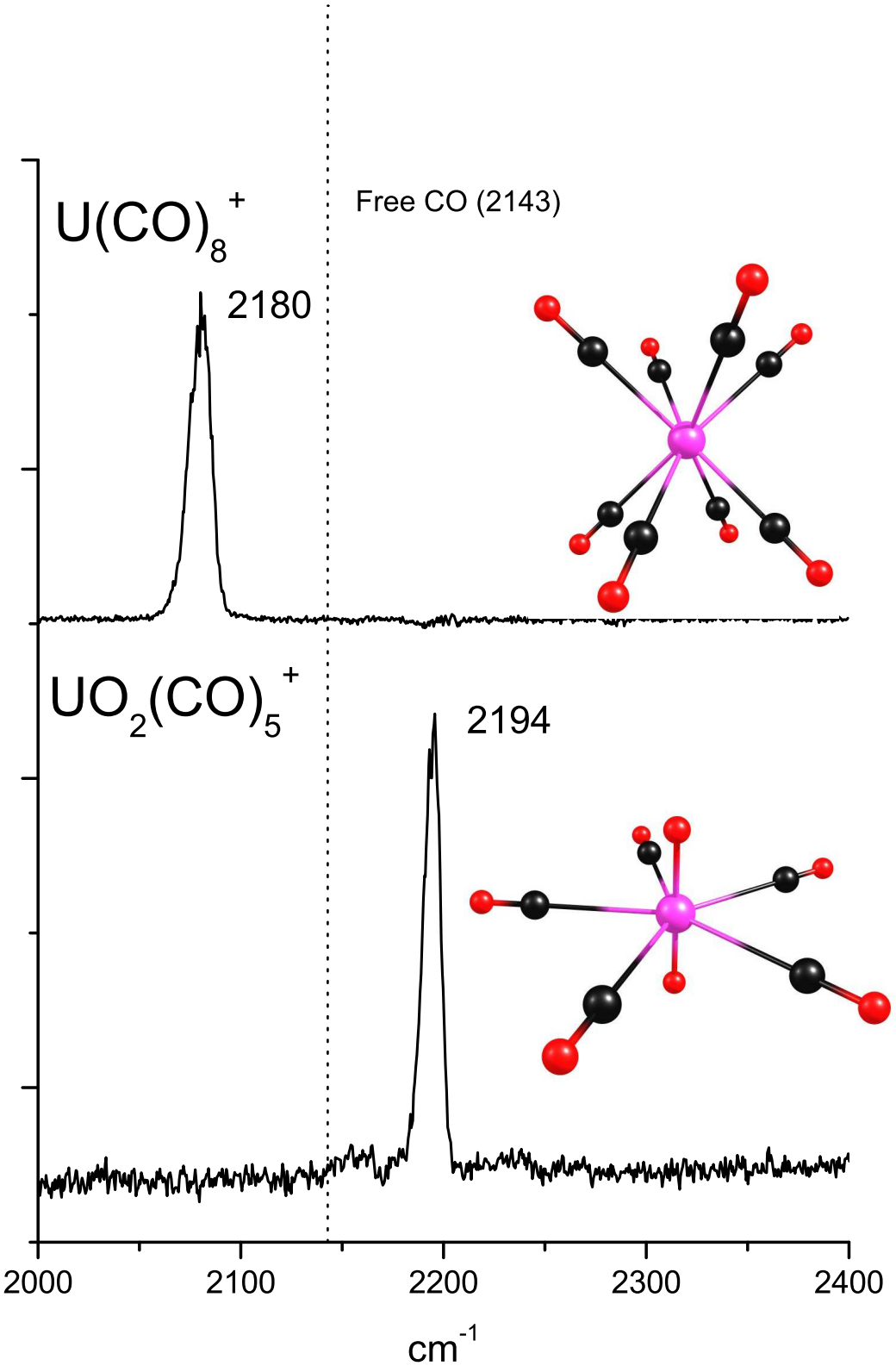

Figure 7.2: Infrared spectra of the $U(CO)_8^+$ and $UO_2(CO)_5^+$ ions along with proposed high symmetry structures.

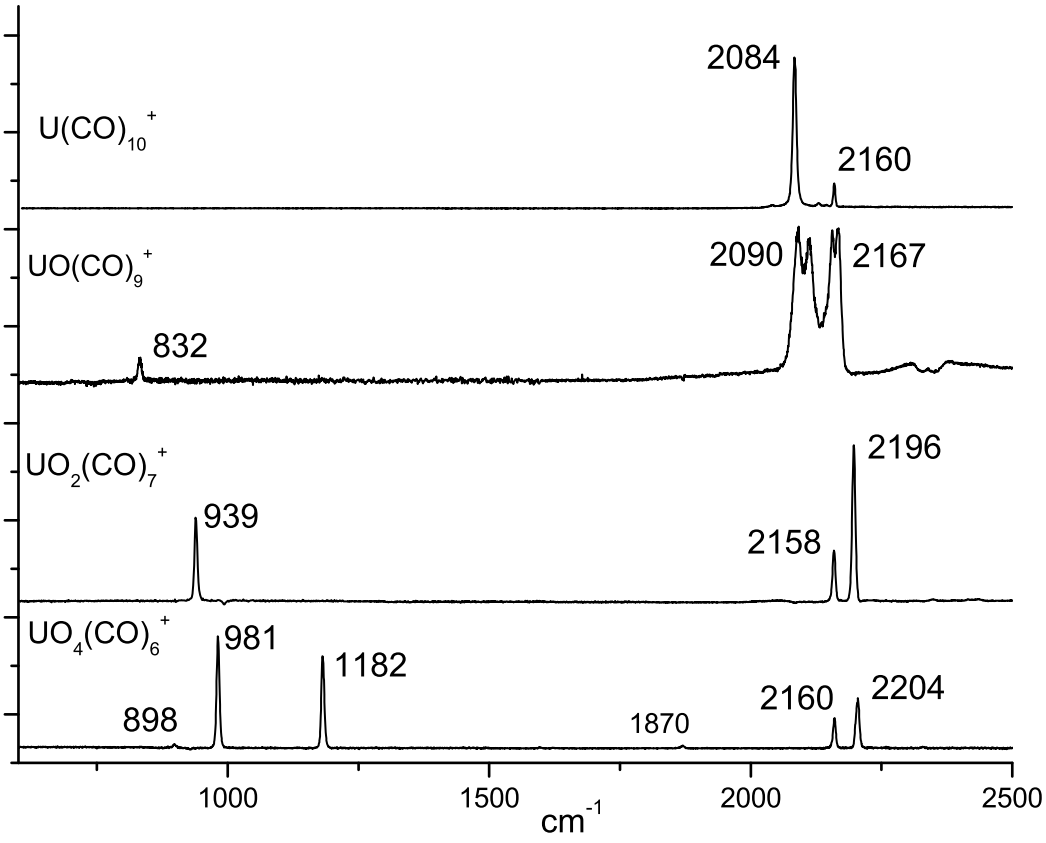

Figure 7.3: The infrared spectra of larger uranium and uranium oxide carbonyl cations.

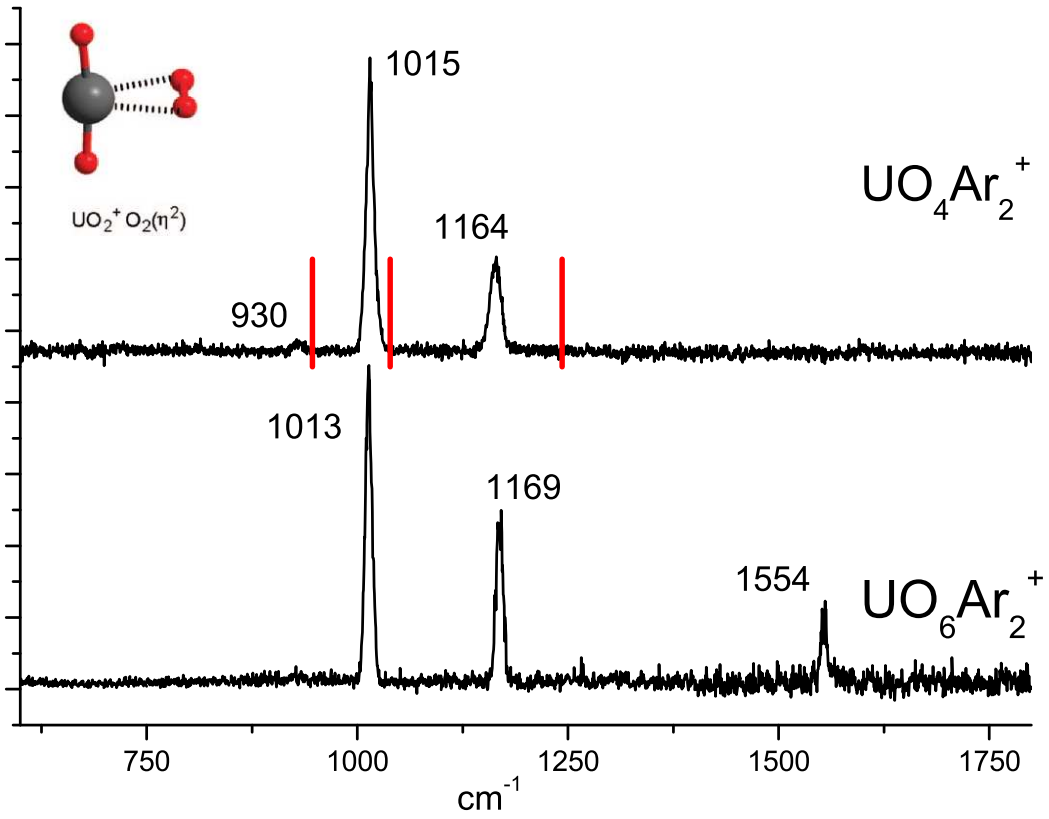

Figure 7.4: The infrared spectra of the $UO_4Ar_2^+$ and $UO_6Ar_2^+$ ions. The inset shows the structure of the η^2 UO_4^+ cation and the vertical bars are the calculated frequencies of this ion. Structure and frequencies taken from reference [77].

Chapter 8

Bibliography

Bibliography

1. F. A. Cotton, *Advanced Inorganic Chemistry 6th ed* (John Wiley and Sons, Inc., New York, 1999).

2. J. E. Huheey, E. A. Keiter, and R. L. Keiter, *Inorganic Chemistry Principles of Structure and Reactivity* (Harper Collins, New York, 1993).

3. M. Wrighton, "The Photochemistry of Metal Carbonyls", Chem. Rev. **74**, 401 (1974).

4. I. Bertini, H. B. Gray, E. I. Stifel, and J. S. Valentine, *Biological Inorganic Chemistry Structure and Reactivity* (University Science Books, Sausolito California, 2007).

5. G. L. Gutsev, L. Andrews, and C. W. Bauschlicher Jr., "3d-Metal monocarbonyls MCO, MCO^+ and MCO^- (M=Sc to Cu): comparative bond strengths and catalytic ability to produce CO_2 in reactions with CO ", Chem. Phys. **290**, 47 (2003).

6. G. A. Somorjai, *Introduction to Surface Chemistry and Catalysis* (John Wiley and Sons, Inc., New York, 1994).

7. H. Stammerich, K. Kawai, Y. Tavares, P. Krumholz, J. Behmoiras, and S. Bril, "infrared spectra of $Fe(CO)_4^{2-}$ in aqueous solution (not real title)", J. Chem. Phys. **32**, 1482 (1960).

8. E. W. Abel, A. N. McLean, S. P. Tyfield, P. S. Braterman, A. P. Walker, and P. J. Hendra, "infrared spectra of $V(CO)_6^-$ and $Re(CO)_6^+$ in CH_3CN solution (not real title)", J. Mol. Spec. **30**, 29 (1969).

9. W. F. Edgell and J. I. Lyford, "infrared spectra of $Co(CO)_4^-$ in DMF solution (not real title)", J. Chem. Phys. **52**, 4329 (1970).

10. G. Boquet and M. Birgone, "infrared spectra of $Ni(CO)_4$ in gas phase (not real title)", Spectrochim. Acta. **27A**, 139 (1971).

11. R. A. N. McLean, "infrared and raman spectra of $Mn(CO)_6^+$ CH_3CN solution and solid (not real title)", Can. J. Chem. **52**, 213 (1974).

12. M. F. O'Dwyer, "Infrared Spectra and Normal Coordinate Analysis of Iron Pentacarbonyl", J. Molec. Spectroscopy **2**, 144 (1958).

13. B. Beagley and D. G. Schmidling, A Re-Evaluation of the molecular structure of iron pentacarbonyl, J. Molec. Struct. **22**, 5466 (1974).

14. L. H. Jones, R. S. McDowell, and M. Goldblatt, "infrared spectra of $Cr(CO)_6$, $Mo(CO)_6$ and $W(CO)_6$ Gas phase (not real title)", Inorg. Chem. **28**, 2349 (1969).

15. P. C. Engelking and W. C. Lineberger, "Laser Photoelectron spectrometry of the negative ions of iron and iron carbonyls. Electron affinity determination for the series $Fe(CO)_n$ n=0,1,2,3,4", J. Am. Chem. Soc. **101**, 5579 (1979).

16. P. W. Villalta and D. G. Leopold, "A study of the FeCO and the σ and σ states of FeCO by negative ion photoelectron spectroscopy", J. Chem. Phys. **98**, 7730 (1993).

17. A. A. Bengali, S. M. Casey, C. L. Cheng, J. P. Dick, P. T. Fenn, P. W. Villalta, and D. G. Leopold, "Negative ion photoelectron spectroscopy of the coordinatively unsaturated Group VI metal carbonyls of chromium, molybdenum and tungsten", J. Am. Chem. Soc. **114**, 5257 (1992).

18. P. C. Butcher, B. F. G. Johnson, J. S. McIndoe, X. Yang, X. B. Wang, and L. S. Wang, "Collision-Induced Dissociation and Photodetachment of Singly and Doubly Charged Anionic Polynuclear Transition Metal Carbolyl Clusters $Ru_3CO(CO)_{13}^-$, $Ru_6CO(CO)_{16}^{2-}$, $Ru_6CO(CO)_{18}^{2-}$", J. Chem. Phys. **116**, 6560 (2002).

19. K. Nakamoto, *Infrared and Raman Spectra of Inorganic and Coordination Compounds* (John Wiley, New York, 1997).

20. A. S. Goldman and K. Krogh-Jespersen, "Why do cationic carbon monoxide complexes have high CO stretching force constants and short CO bonds? Electrostatic effects, not σ bonding ", J. Am. Chem. Soc. **118**, 12159 (1996).

21. A. J. Lupinetti, S. Fau, G. Frenking, and S. H. Strauss, "Theoretical Analysis of the Bonding between CO and Positively Charged Atoms", J. Phys. Chem. **101**, 9551 (1997).

22. T. A. Albright, J. K. Burdett, and M. H. Whangbo, *Orbital Interactions in Chemistry* (Wiley, New York, 1985).

23. R. L. DeKock, A. C. Sarapu, and R. F. Fenske, "CO homo antibonding (not real title)", Inorg. Chem. **10**, 38 (1971).

24. F. A. Khan, D. E. Clemmer, R. H. Schultz, and P. B. Armentrout, "Sequential bond energies of chromium carbonyls ($Cr(CO)_x^+$, x=1-6)", J. Phys. Chem. **97**, 7978 (1993).

25. M. R. Sievers and P. B. Armentrout, " Collision-Induced Dissociation Studies of $V(CO)_x^+$, x=1-7: Sequential Bond Energies and the Heat of formation of $V(CO)_6$", J. Phys. Chem. **99**, 8135 (1995).

26. F. Meyer, Y. M. Chen, and A. P. B., "Sequential Bond Energies of $Cu(CO)_x^+$ and $Ag(CO)_x^+$ (x=1-4)", J. Am. Chem. Soc. **117**, 4071 (1995).

27. F. Meyer and P. B. Armentrout, "Sequential bond energies of $Ti(CO)_x^+$, x= 1-7", Mol. Phys. **88**, 187 (1996).

28. X. G. Zhang and P. B. Armentrout, "Sequential Bond Energies of $Pt^+(CO)_x$ (x=1-4) Determined by Collision-Induced Dissociation," ", Organometallics **20**, 4266 (2001).

29. A. Fielicke, G. v. Helden, G. Meijer, D. B. Pedersen, B. Simard, and D. M. Rayner, "Size and Charge Effects on Binding of CO to Small Isolated Rhodium Clusters", J. Phys. Chem. B. **108**, 14591 (2004).

30. D. T. Moore, J. Oomens, J. R. Eyler, G. Meijer, G. v. Helden, and D. P. Ridge, "Gas-Phase IR Spectroscopy of Anionic Iron Carbonyl Clusters", J. Am. Chem. Soc. **126**, 14726 (2004).

31. A. Fielicke, G. v. Helden, G. Meijer, B. Simard, and D. M. Rayner, "Gold Cluster Carbonyls: Vibrational Spectroscopy of the Anions and the Effects of Cluster Size, Charge, and Coverage on the CO Stretching Frequency", J. Phys. Chem. B. **109**, 23935 (2005).

32. A. Fielicke, G. v. Helden, G. Meijer, D. B. Pedersen, B. Simard, and D. M. Rayner, "Size and charge effects on the binding of CO to late transition metal clusters ", J. Chem. Phys **124**, 194305 (2006).

33. M. Zhou and L. Andrews, " Infrared Spectra of $RhCO^+$, RhCO, and $RhCO^-$ in solid neon: a scale for charge support in catalyst systems", J. Am. Chem. Soc. **121**, 9171 (1999).

34. M. Zhou and L. Andrews, " Infrared Spectra and density functional calculations of $CuCO_n^+$(n=1-4),$CuCO_n$(n=1-3), and $CuCO_n^-$(n=1-3), in solid neon ", J. Chem. Phys. **111**, 4548 (1999).

35. M. Zhou and L. Andrews, " Infrared Spectra and density functional calculations of $RuCO^+$, $OsCO^+$,$RuCO_x$, $OsCO_x$, $RuCO_x^-$, and $OsCO_x^-$ (x=1-4) in solid neon ", J. Phys. Chem. A. **103**, 6956 (1999).

36. M. Zhou and L. Andrews, " Reactions of laser-ablated iron atoms and cations with carbon monoxide: Infrared spectra of '$FeCO^+$, $Fe(CO)_2^+$, $Fe(CO)_x$ and $Fe(CO)_x^-$ (x=1-4) in solid neon ", J. Chem. Phys. **110**, 10370 (1999).

37. M. Zhou and L. Andrews, " Matrix infrared spectra and density functional calculations of ScCO, $ScCO^-$, and $ScCO^+$ ", J. Phys. Chem. A. **103**, 2964 (1999).

38. M. Zhou and L. Andrews, "Infrared spectra and density functional calculations for OMCO, and OM-(η^2-CO^-), $OMCO^+$ and $OMOC^+$ (M=V, Ti) in solid argon ", J. Phys. Chem. A. **103**, 2964 (1999).

39. B. Liang and L. Andrews, "Reactions of Laser-Ablated Ag and Au atoms with carbon monixide: Matrix Infrared Spectra and Density Functional Calculations on $Au(CO)_n$ (n=2,3), $Au(CO)_n^-$(n=1,2), and $M(CO)_n^+$ (n=1-4), (M=Ag, Au)", J. Phys. Chem. A **104**, 9156 (2000).

40. B. Liang, M. Zhou, and L. Andrews, "Reactions of Laser-Ablated Ni, Pd, and Pt atoms with carbon monixide: Matrix Infrared Spectra and Density Functional Calculations on $M(CO)_n$ (n=1-4), $M(CO)_n^-$(n=1-3), and $M(CO)_n^+$ (n=1-2), (M=Ni, Pd, Pt)", J. Phys. Chem. A **104**, 3905 (2000).

41. E. J. Bieske and O. Dopfer, "High-Resolution Spectroscopy of Cluster Ions", Chem. Rev. **100**, 3063 (2000).

42. M. A. Duncan, "Infrared spectroscopy to probe structure and dynamics in metal ion-molecule complexes", Intl. Rev. Phys. Chem. **22**, 407 (2003).

43. N. R. Walker, R. S. Walters, and M. A. Duncan, "Frontiers in the infrared spectroscopy of gas phase metal ion complexes", New J. Chem. **29**, 1495 (2005).

44. J. V. III and M. A. Duncan, "IR Photodissociation Spectroscopy of Gas Phase $Pt^+(CO)_n$ (n=4-6)", J. Chem. Phys. **461**, 28 (2008).

45. J. V. III, B. Njegic, M. S. Gordon, and M. A. Duncan, "IR Photodissociation Spectroscopy and Theory of $Au^+(CO)_n$ Complexes: Nonclassical Carbonyls in the Gas Phase", J. Phys. Chem. A. **112**, 1907 (2008).

46. T. G. Dietz, M. A. Duncan, and R. E. Smalley, "Laser Production of Supersonic Metal Cluster Beams", J. Chem. Phys. **74**, 6511 (1981).

47. W. C. Wiley and I. H. McLaren, "Time-of-Flight Mass Spectrometer With Improved Resolution", Rev. Sci. Instr. **26**, 1150 (1955).

48. A. V. Nemukhin, B. L. Grigorenko, and A. A. Granovsky, Molecular modeling by using the PC GAMESS program: From diatomic molecules to enzymes, Moscow University Chemistry Bulletin **45**, 75 (2004).

49. E. Bernhardt, M. Finze, H. Willner, C. W. Lehman, and F. Aubke, "Salts of the Cobalt(I) Complexes $[Co(CO)_5]^+$ and $[Co(CO)_2(NO)_2]^+$and the Lewis Acid-Base Adduct $[Co_2(CO)_7CO\text{-}B(CF_3)_3]$", Chem. Eur. J. **12**, 8276 (2006).

50. S. Goebel, C. L. Haynes, F. A. Khan, and P. B. Armentrout, "Collision-Induced Dissociation Studies of $Co(CO)_x^+$, x=1-5: Sequential Bond Energis and Heats of Formation of $Co(CO)_4$", J. Am. Chem. Soc. **117**, 6994 (1995).

51. A. D. Becke, Becke 3 term correlation functional (part of b3lyp), J. Chem. Phys. **98**, 5648 (1993).

52. C. Lee, W. Yang, and R. G. Parr, Lee Yang Parr exchange functional (part of b3lyp), Phys. Rev. B. **98**, 5648 (1998).

53. A. J. H. Watchers, Watchers basis set, J. Chem. Phys. **52**, 1033 (1970).

54. T. H. D. Jr., DZP basis set, J. Chem. Phys. **53**, 2823 (1970).

55. J. H. Jang, G. J. Lee, H. Lee, Y. Xie, and F. I. Schaefer, Henry, "Molecular Structures and Vibrational Frequencies of Iron Carbonyls: $Fe(CO)_5$, $Fe_2(CO)_9$, and $Fe_3(CO)_{12}$", J. Phys. Chem. A. **102**, 5298 (1998).

56. J. Oomens, A. G. G. M. Tielens, B. G. Sartakov, G. v. Helden, and G. Meijer, "Laboratory Infrared Spectroscopy of Cationic Polycyclic Aromatic Hydrocarbon Molecules ", Astrophys. J. **591**, 968 (1999).

57. A. P. Scott and L. Radom, "Harmonic Vibrational Frquencies: An Evaluation of Hartree-Fock, Moller-Plesset, Quadratic Configuration Interaction, Density Functional Theory, and Semiempirical Scale Factors", J. Chem. Phys. **100**, 16502 (1996).

58. R. S. Walters, N. R. Brinkmann, H. F. Schaefer, and M. A. Duncan, "Infrared Photodissociation Spectroscopy of Mass-Selected $Al^+(CO_2)_n$ and $Al^+(CO_2)_nAr$ Clusters", J. Phys. Chem. **38**, 7396 (2003).

59. V. Kasalova, W. D. Allen, H. F. S. III, E. D. Pillai, and M. A. Duncan, "Model Systems for Probing Metal Cation Hydration: The V^+(H2O) and ArV^+(H2O) Complexes", J. Phys. Chem. A **111**, 7599 (2007).

60. E. D. Pillai, T. D. Jaeger, and M. A. Duncan, "IR Spectroscopy and Density Functional Theory of Small $V^+(N_2)_n$ Complexes", J. Phys. Chem. A **109**, 3521 (2005).

61. K. S. Molek, Z. D. Reed, and A. M. Ricks, "Photodissociation of chromium oxide cluster cations ", J. Phys. Chem. A **112**, 12355 (2008).

62. J. W. Dicke, N. J. Stibrich, and H. F. SchaeferIII, "$V(CO)_7^+$: A Capped Octahedral Structure Completes the 18-electron Rule", J. Chem. Phys. **456**, 13 (2008).

63. Y. Ibrahim, E. Alshareah, R. Mabrouki, P. Momoh, E. Xie, and M. S. El-Shall, "Ion Mobility of Ground and Excited States of Laser-Generated Transition Metal Cations", J. Phys. Chem. A **112**, 1112 (2008).

64. G. R. Choppin, "Actinide Science: Fundamental and Environmental Aspects", J. Nuclear Radiochemical Sciences **6**, 1 (2005).

65. D. Majumdar, K. Balasubramanian, and H. Nitsche, "A comparative theoretical study of bonding in UO_2^{++}, UO_2^{+}, UO_2, UO_2^{-} OUCO, $O_2U(CO)_2$ and UO_2CO_3 ", Chem. Phys. Lett. **361**, 143 (2003).

66. C. Hennig, J. Tutschku, A. Rossberg, G. Bernhard, and A. C. Scheinost, "Comparative EXAFS Investigation of Uranium(VI) and-(IV) Aquo Chloro Complexes in Solution Using a Newly Developed Spectrochemical Cell", Inorg. Chem. **44**, 6655 (2005).

67. S. Pocev and G. Johansson, "An X-Ray Investigation of the Coordination and the Hydrolysis of the Uranium(IV) Ion in Aqueous Perchlorate Solutions", Acta Chem. Scand. **27**, 2146 (1973).

68. M. Zhou, L. Andrews, N. Ismail, and C. Marsden, "Infrared Spectra UO_2, UO_2^{+}, and UO_2^{+} in Solid Neon", J. Phys. Chem. A **104**, 5495 (2000).

69. G. S. Groenwold, K. C. Cossel, G. L. Gresham, A. K. Gianotto, A. D. Appelhans, J. E. Olson, M. J. V. Stipdonk, and W. Chien, "Binding of Molecular O_2 to Di- and Triligated $[UO_2]^{+}$", J. Am. Chem. Soc. **128**, 3075 (2006).

70. G. S. Groenwold, M. J. V. Stipdonk, W. A. de Jong, J. Oomens, G. L. Gresham, M. E. Mcilwain, D. Gao, B. Siboulet, L. Visscher, M. Kullman, et al., "Infrared Spectroscopy(sic) of Dioxouranium(V) Complexes with Solvent Molecules: Effect of Reduction", Chem. Phys. Chem. **9**, 1278 (2008).

71. J. M. Merritt, J. Han, and M. C. Heaven, "Spectroscopy of the UO_2^{+} cation and the delayed ionization of UO_2", J. Chem. Phys. **128**, 084304 (2008).

72. N. J. Long, *Metallocenes: An Introduction to Sandwich Complexes* (Blackwell Sciences Ltd., Oxford England, 1998).

73. J. L. Sonnenberg, P. J. Hay, R. L. Martin, and B. E. Bursten, "Theoretical Investigations of Uranyl-Ligand Bonding: Four- and Five-Coordinate Uranyl Cyanide, Isocyanide, Carbonyl and Hydroxide Complexes", Inorg. Chem. **44**, 2255 (2005).

74. P. Nichols, E. J. Bylaska, G. K. Schenter, and W. de Jong, "Equatorial and apical solvent shells of the UO_2^{2+} ion ", J. Chem. Phys. **128**, 124507 (2008).

75. A. M. Ricks, J. M. Bakker, G. E. Douberly, and M. A. Duncan, "Infrared Spectroscopy and Structures of Cobalt Carbonyl Cations, $Co(CO)_n^+$ (n=1-9) ", J. Phys. Chem. A. **113**, 4701 (2009).

76. S. Cotton, *Lanthanide and Actinide Chemistry* (Wiley, West Sussex England, 2007).

77. V. S. Bryanstev, W. A. de Jong, K. C. Cossel, M. S. Dialo, W. A. G. III, G. S. Groenwold, W. Chien, and M. J. V. Stipdonk, "Two-Electron Three-Centered Bond in Side-On (η^2) Uranyl(V) Superoxo Complexes", J. Phys. Chem. A **112**, 5777 (2008).

78. A. M. Ricks and Z. D. Reed, "Seven-Coordinate Homoleptic Metal Carbonyls in the Gas Phase", J. Am. Chem. Soc. **131**, 9176 (2009).

79. V. Goncharov, L. A. Kaledin, and M. C. Heaven, "Probing the electronic structure of UO^+ with high-resolution photoelectron spectroscopy", J. Chem. Phys. **125**, 133202 (2006).

80. C. G. Bailey, D. J. Lavrich, D. Serxner, and M. A. Johnson, "Autodetachment from vibrational levels of the O_2^- A $^2\Pi_u$ resonance across its dissociation limit by photoexcitation from O_2^- X $^2\Pi_g$", J. Chem. Phys. **105**, 1807 (1996).